Master's thesis

NTNU
Norwegian University of Science and Technology
Faculty of Information Technology and Electrical Engineering
Department of Engineering Cybernetics

Ludvig Vik Løite

Simulation-Based, Risk-Influenced Path Planning Framework for Marine Surface Vessels

Master's thesis in Cybernetics and Robotics
Supervisor: Børge Rokseth
June 2023

NTNU
Norwegian University of
Science and Technology

Ludvig Vik Løite

Simulation-Based, Risk-Influenced Path Planning Framework for Marine Surface Vessels

Master's thesis in Cybernetics and Robotics
Supervisor: Børge Rokseth
June 2023

Norwegian University of Science and Technology
Faculty of Information Technology and Electrical Engineering
Department of Engineering Cybernetics

NTNU
Norwegian University of
Science and Technology

Preface

This Master's thesis was written at the Department of Engineering Cybernetics at the Norwegian University of Science and Technology during the spring of 2023.

The work conducted in this thesis is a continuation of the work done in the author's specialization project (Løite (2022)). Certain sections are significantly influenced by the findings of that report. Particularly, Chapters 1 and 2, which provide the background and theoretical underpinnings of this study, draw extensively from the aforementioned report. Sections 1.1, 1.3, 2.1, 2.2, 2.3, 2.4 and 2.8 are particularly influenced by the research presented in Løite (2022).

The software developed in this thesis has been made available on Github (Løite (2023)). For researchers interested in leveraging this framework for their own investigations, I am happy to assist, both in the form of in-depth information about the framework, as well as guidance on how to effectively set it up for use.

I would like to extend my deepest gratitude to my supervisor, PhD Børge Rokseth. Your unwavering optimism, profound knowledge, ready availability, and flexible approach have been immensely valuable throughout this journey. You have fostered an environment where no question is considered too trivial, encouraging open and enriching discussions. Your grounded and pragmatic demeanor has led to many insightful conversations. The quality of your mentorship has surpassed my expectations in every possible way.

Trondheim, 26.06.2023

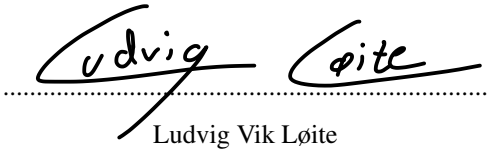

Ludvig Vik Løite

Abstract

The maritime industry is currently experiencing significant transformations, particularly in the domain of vessel autonomy. A fundamental component of this advancement is the determination of the optimal navigational route. This Master's thesis seeks to contribute to the field of marine cybernetics by proposing a simulation-based path-planning framework for marine surface vessels. The framework incorporates a cost function that combines grounding risk, fuel consumption, and cost of time usage to determine the optimal path among a predefined set of options.

The grounding risk analysis component of the framework has received particular attention. In order to assess the grounding risk of a specific path, simulations of propulsion loss are conducted at regular intervals throughout the entire trajectory of the route. If the vessel is simulated to experience grounding, the risk is defined by considering both the likelihood of propulsion loss and the consequence of the grounding incident. The likelihood of experiencing propulsion loss is estimated by utilizing a Bayesian Network that incorporates theoretical statistics related to propulsion loss. The consequences of grounding are further assessed in terms of their environmental, social, and economic impacts. These values are determined based on vessel characteristics and a predicted damage state resulting from the grounding incident. This damage state is determined using another Bayesian Network that incorporates vessel speed, weather conditions at the grounding site, and the type of material on which the ship has grounded. The grounding risk of a given path is defined as the combined risks of the propulsion loss simulations for all time steps, which is then combined with fuel consumption and the cost of time usage to form a cost function. Minimizing this cost function enables the identification of the optimal path.

The path-planning framework is designed for flexibility, and implementing specific vessel and environmental data should be straightforward. Furthermore, various weighting parameters are included to enable operators to make prioritization choices according to their specific needs.

Sammendrag

Sjøfartssektoren står overfor betydelig utvikling, spesielt når det gjelder autonome fartøy. En viktig oppgave i denne utviklingen er å identifisere den optimale ruten et fartøy kan følge i en gitt situasjon. Formålet med denne masteroppgaven er å bidra innenfor marin kybernetikk ved å foreslå et rammeverk for ruteplanlegging for maritime overflatefartøy. Rammeverket bruker en kostnadsfunksjon som kombinerer risiko for grunnstøting, drivstofforbruk, og tidsforbruk for å beregne den mest optimale ruten blant et forhåndsbestemt utvalg av alternativer.

Rammeverket legger spesiell vekt på risikoen for grunnstøting. For å vurdere grunnstøtingsrisikoen for en gitt rute, utføres regelmessige simuleringer av tap av fremdriftskraft langs hele ruten. Hvis et fartøy blir simulert til å grunnstøte, defineres risikoen ved å vurdere både sannsynligheten for tap av fremdriftskraft og konsekvensene av grunnstøtingen. Sannsynligheten for tap av fremdriftskraft estimeres ved å hjelp av et bayesiansk nettverk som bruker statistisk teori knyttet til tap av fremdriftskraft. De potensielle konsekvensene av grunnstøting vurderes med tanke på miljømessige, sosiale og økonomiske konsekvenser. Disse konsekvensene fastsettes basert på informasjon om fartøyet og en estimert skadetilstand på skipet som har grunnstøtt. Skadetilstanden bestemmes ved hjelp av et bayesiansk nettverk som tar hensyn til fartøyets hastighet, værforholdene og grunnforholdene på stedet hvor grunnstøtingen er simulert til å ha skjedd. Den totale risikoen for grunnstøting for en gitt rute defineres som den samlede risikoen fra alle simuleringene, som deretter kombineres med kostnaden for drivstoff og tidsbruk for å beregne verdien til en kostnadsfunksjon. Ruten som simuleres til å ha lavest verdi på denne kostnadsfunksjonen defineres som den optimale ruten.

I utviklingen av ruteplanleggingsrammeverket har fleksibilitet blitt høyt prioritert. Målet er å gjøre det enkelt å integrere spesifikke fartøysdata og informasjon om omstendighetene. Rammeverket implementerer også forskjellige vektingsparametere som operatører kan bruke til å bestemme hvilke faktorer de ønsker å prioritere.

Table of Contents

List of Tables

List of Figures

Abbreviations

Abbreviation	Description
COLREG	Convention on the International Regulations for Preventing Collisions at Sea
GNSS	Global Navigation Satellite Systems
RADAR	Radio Detection and Ranging
LIDAR	Light Detection and Ranging
AIS	Automatic Identification System
FTA	Fault Tree Analysis
DP	Dynamic Positioning
OCA	Online Consequence Analysis
BN	Bayesian Network
BBN	Bayesian Belief Network
CPT	Conditional Probability Table
RIF	Risk Influencing Factor
PSC	Port State Control
NMA	Norwegian Maritime Authority
FM	Failure Mode
DOF	Degree of Freedom
ECI	Earth-centered Inertial frame
ECEF	Earth-centered Earth-fixed frame
NED	North, East, Down coordinate frame
BO	Blackout
FOB	Frquency of blackout
LOS	Line Of Sight
DWT	Deadweight Tonnage
VSL	Value of Statistical Life
TCE	Time Charter Equivalent

1

Introduction

The following thesis presents a simulation based path-planning optimization framework for marine surface vessels. The essence of the framework is to identify the optimal path in which a vessel should sail. This is determined based on an estimated risk as well as fuel consumption and time usage. The central focus of this study is on risk estimation, particularly the risk associated with grounding as a result of loss of propulsion. Throughout this thesis, the term *blackout* is also used to denote the loss of propulsion. Other hazards, such as fire, explosion, capsizing, powered grounding, or collision with other vessels, are not included in this study.

The proposed path-planning optimization framework holds potential to be used both in the planning phase of a voyage and as an online risk model, continuously reassessing and determining the optimal path throughout a voyage.

1.1 Background and Motivation

Autonomous and unmanned vehicles are relatively new concepts that will change the way we think about transport. In 2009, Google launched its self-driving car project. Five years later, they announced that the cars had driven 300 000 miles without any accidents (The Atlantic (2014)). The maritime industry is also undergoing substantial changes with regards to autonomy. In the later years, important steps has been done in order to realize autonomous marine vessels. Massterly is the world's first dedicated company operating autonomous vessels (Wilhelmsen (2023)). It was established in 2018 as a joint venture between Kongsberg Maritime and Wilhelmsen, both pioneers within development of technical solution for the maritime industry. This joint venture was formed in the wake of the announcement of another milestone project. Yara, Kongsberg Maritime and Massterly teamed up to build the world's first autonomous and zero-emission container vessel, removing 40 000 diesel-powered trucks every year (Yara (2023)). *Yara Birkeland* was put

into commercial operation in the spring of 2022, expecting full autonomous sailing in 2023.

Another milestone for autonomous marine vessels is the Autoferry project at NTNU. The concept is to put small autonomous passenger ferries in urban areas as a flexible, cost-effective and environmentally-friendly alternative to bridges or manned ferries (NTNU (2023)). This initiative has led to the development of the fully autonomous ferry *milliAmpere 2*, which was launched for trial with passengers in Trondheim in 2022 (Norwegian SciTech News (2022)).

The objectives of the systems above are very similar. They all attempt to perform a complex task with very little information from human operators, in a safe and effective manner. They attempt to replace processes that today are ineffective, unsafe, or both. A ferry travelling across waterways can replace building an expensive bridge. Making it autonomous potentially reduces the cost of operation drastically. The autonomous container vessel *Yara Birkeland* will replace 40 000 diesel-powered trucks annually, making the roads safer and reducing air pollution.

(a) MilliAmpere 2 **(b)** Yara Birkeland

Figure 1.1: Autonomous vessels

Increasing autonomy in marine vessels may reduce accidents by avoiding what we call ”human errors”. Fields (2012) estimates that 75% to 96% of all marine accidents can be attributed to human errors. While autonomous vessels hold promise in addressing this issue, their implementation is not without challenges and complexities.

On April 15, 1912, the *Titanic*, a passenger ship on its maiden voyage from Southampton, England to New York City, experienced a tragic accident when it collided with an iceberg and subsequently sank. The sinking of the Titanic has been attributed to a variety of factors, but it is generally believed that human error played a role. The ship was traveling at a high speed in an area known to have icebergs, and the crew did not receive sufficient warning about their presence. A reason for this may be that the captain was informed that the Titanic was unsinkable.

An interesting question emerges when considering if the introduction of an autonomous operator would have avoided the Titanic accident, given the same information as the captain. Why would it spend lots of fuel on avoiding an iceberg that could do no damage to the vessel? And what about the scheduled arrival time in New York? This anecdote is meant as a reflection around whether it is possible to completely avoid so called ”human

errors". It is clear, however, that increased autonomy leads to the introduction of new errors and the removal of others. Well-designed autonomous systems have the potential to make drastically safer and more effective solutions than the manual systems we use today.

In 2019, the passenger vessel *Viking Sky* departed its harbour despite quite harsh weather. The vessel had a blackout and lost its propulsion power at the worst possible time. Hustadvika, situated in Møre and Romsdal county, Norway, is known for its numerous awash rocks and history with accidents, and now a passenger vessel with 1373 people onboard was left in this area, without propulsion power. The wind and current left the vessel drifting straight towards the shore. Viking Sky dropped its two anchors, which only stuck with the sea floor after drifting for over 30 minutes. The accident investigation concluded that Viking Sky was less than a ship length away from grounding (Norwegian Directorate for Civil Protection (2020)).

With waves too high to deploy rescue boats, six rescue helicopters used 19 hours to transfer the passengers to land. Although passengers were injured, including things like bruising, trauma, and broken bones, and approximately a dozen were hospitalized, there were no fatalities (Norwegian Directorate for Civil Protection (2020)). Other recent blackout situations include the cruise ships *Carnival Triumph*(2013), *Vasco da Gama*(2017), *Vision of the Sea*(2018), and *Coral Princess*(2019) (Ibrion et al. (2021)).

These cases serves as examples of the exact thing the framework presented in this report want to prevent. Although ship grounding accidents may be considered infrequent and rare, statistical findings from Eliopoulou et al. (2016) have shown an increase in such incidents over the past decade, despite advancements in navigation technology. Consequently, it is crucial to maintain ongoing investigations into the safety of maritime waterways in order to mitigate the risk of grounding hazards.

The proposed framework is intended to serve as a valuable tool for ship operators, whether they are manned or unmanned, to optimize their routes based on risk, fuel consumption, and time usage. The ultimate goal is to minimize the occurrence of accidents in the future while still taking into account the economic considerations of fuel consumption and the efficient utilization of time. By incorporating these factors into the decision-making process, the framework aims to enhance safety and operational efficiency in maritime navigation.

Conseptualizing using the proposed framework in the case of the Hustadvika-accident, the simulation of a blackout in that exact area should be estimated to result in a grounding with quite high consequence. This should lead the path-planning tool to suggest sailing farther from land, despite increased fuel cost and time usage.

The motivation for this thesis is to contribute within the field of marine cybernetics, by proposing a framework for path planning of marine surface vessels using a simulation based risk analysis. The framework will only consider risk of grounding, but the extension to include other events would require minimal effort. The properties of the ship, area of voyage, local environmental conditions and consequence metrics are examples on factors that may be modified based on the need.

1.2 Problem Description

The problem description for this report is the following:

The development of autonomous ships necessitates the assurance of dependable guidance and navigation systems. These can potentially be achieved by creating risk-based guidance and navigation control systems that incorporate risk models into their decision-making processes. The primary objective of this master's thesis is to design a path-planning optimization framework that identifies the most optimal navigation route for marine surface vessels, taking various metrics into account, including grounding risk.

An essential aspect of the path-planning framework that requires particular attention is the development of a grounding risk model. By incorporating the risk model into the path-planning optimization process, it becomes possible to conduct a comprehensive risk assessment of different route alternatives. This integration significantly enhances the versatility and application potential of the framework.

Ultimately, this path-planning framework should be integrated with a ship simulator. The functionality and robustness of the framework should then be tested through various case studies.

In other words, the main objectives of this thesis are:

- Develop a grounding risk model for marine surface vessels
- Combine this grounding risk model with other relevant metrics to develop a path-planning framework
- Implement the path-planning framework into a simulation environment, allowing for rigorous evaluation and refinement to ensure real-world applicability
- Develop several case studies to demonstrate and evaluate the proposed framework.

1.3 Delimitations

When developing the risk analysis, numerous factors related to risk must be considered. The risk model used in this report only examines the risk of grounding due to loss of propulsion on the vessel. Other types of hazards, such as fire, capsizing, collision with other vessels, and damage to the cargo, are not included in the model. Additionally, the risk of powered grounding, which can be viewed as a problem of avoiding obstacles, is not addressed in this report.

It is also important to note that the risk model and simulations presented in this report do not take into account any COLREG rules, which may result in some of the suggested routes being in violation of these regulations. It is also assumed that the sea depth data used is accurate and that all areas have been sufficiently mapped.

In the event of a loss of propulsion, one common safety measure is to drop anchors to prevent the vessel from grounding. However, this report does not consider the use of anchors as a possible option.

Recovery of the ship after the vessel has re-initiated engine function is hard to simulate. The suggested framework assumes that the vessel will be able to survive if it regains engine function before any groundings.

2

Background Material

The purpose of the following chapter is to provide the necessary background information for creating a simulation-based analysis of the risk of grounding for marine vessels. The chapter begins with a discussion on the concept of risk and Bayesian belief network, followed by a review of the literature on grounding risk modelling. A discussion on marine accidents and its causes are then provided, before presenting the backbone for the risk analysis and optimization framework. Lastly, the mathematical foundation for the vessel simulated is presented

2.1 Risk

The proposed path planning framework includes evaluating the risk of grounding for a given route. With this in mind, a discussion about the concept of risk is necessary.

There are numerous definitions of risk. Thieme et al. (2021) describe risk as a "*combination of scenarios, consequences, and the associated uncertainty*". This general idea of risk is widely accepted and forms the basis for many definitions of risk. Varde et al. (2018) defines the quantitative measure of risk as

$$R = \sum_i p_i C_i \tag{2.1}$$

where p_i is the probability of occurrence of a scenario i and C_i is the corresponding measure of consequence (Varde et al. (2018)). The scenario i might for instance be a blackout, and the corresponding consequence measure may for example represent the resulting damage to the vessel, passengers, and environment.

Using a single number to represent risk can be inadequate and lead to confusion. A well-developed risk analysis should include additional information. The issue is exemplified using the situations A and B. While scenario A may involve frequent events with low consequences and scenario B may involve rare events with high consequences, their risk as calculated by the product of probability and consequence may be the same. The two situations do, however, differ substantially, and should be treated differently in the decision making. Additionally, the greater frequency of events in scenario A suggests that background knowledge of this scenario may be more extensive. This knowledge affect the amount of uncertainty associated with the scenarios (Mazaheri et al. (2014)).

Aven (2013) implements this information by representing the risk related to an hazardous event e_i by the triplet

$$r = \{e_i, c_i, q\}|k \tag{2.2}$$

Here c_i is the consequence of the event e_i, q is a measure of the uncertainty involved, and k is the background knowledge used for determining the mentioned variables. Including the background knowledge in the equation is an interesting approach especially for Bayesian modeling of risk. Events associated with weak background knowledge will be given less weight when making a decision, compared to events associated with stronger background knowledge (Bremnes et al. (2020)).

Further information on risk and risk analyses can be retrieved from Kaplan and Garrick (1981), Aven (2010), Rausand (2013) or Aven (2012).

2.2 Bayesian Belief Networks

Bayesian belief networks will be used in the framework presented in this thesis. A brief introduction to the concept is given.

Bayesian networks (BNs) are graphical models for probabilistic reasoning under uncertainty that represent uncertain variables as nodes and causal dependencies as directed arcs. Each node has a conditional probability table (CPT) that specifies the probability distribution of a child node based on the states of its parent nodes (Bremnes et al. (2020)). BNs are directed acyclic graphs, meaning that there are no cycles in the relationships between the nodes. BNs have been used for risk assessments in various domains (e.g. Bremnes et al. (2020), Brito and Griffiths (2016), Hegde et al. (2018), Thieme and Utne (2017)).

One of the benefits of Bayesian networks are their ability to be used in decision making. Decision networks are a type of Bayesian network that includes additional nodes for decisions and utilities. According to Russel and Norvig (2012), decision nodes represent the options available for action, while utility nodes represent the level of satisfaction or benefit achieved with respect to a specific objective. By combining these elements, decision networks allow for the incorporation of decision-making considerations into Bayesian network analysis.

2.3 Modelling of Grounding Risk - Literature Study

Many scholars have tried to model grounding accidents in order to estimate the likelihood of grounding given a set of criteria (see e.g. Fuji et al. (1974), MacDuff (1974), Fowler and Sørgård (2000), Otto et al. (2002), Fossdal (2018), Rasmussen (2019), Sakar et al. (2021)). This section will try to give a brief understanding of the previous work that has been done in the segment of grounding risk modelling, from the analytical model of MacDuff (1974), to the simulation based, probabilistic model of Rasmussen (2019).

MacDuff (1974) and Fuji et al. (1974) are both analytical models, meaning the estimations are obtained based on a geometrical understanding of the event. The reports introduced the idea that grounding accident probability could be divided into geometrical (P_G) and causation probabilities (P_C). Geometrical probability of grounding gives the likelihood for grounding given no grounding preventing maneuvers are performed. Causation probability expresses the likelihood that the ship heading a ground will not evade it due to a variety of reasons (Mazaheri et al. (2014)).

MacDuff (1974) estimated the geometrical probability of grounding (P_G) based on the width of the waterway (C) and the stopping distance (T), according to Equation (2.3). Fuji et al. (1974) estimates the number of groundings (N_G) as a function of causation probability (P_C), the width of the shoal (D), the traffic density (ρ), and the speed of the ship (V). The function is presented in Equation (2.4).

$$P_G = \frac{4T}{\pi C} \tag{2.3}$$

$$N_G = P_C D \rho V \tag{2.4}$$

According to the functions presented, the factors that can impact the probability of grounding are all either location-based or based on ship properties. In practise, most of these factors prove very hard to modify. The factors affecting the causation probabilities implemented in the models are unknown, and the model cannot recommend any feasible methods of reducing the risk. Moreover, since the models are not scenario oriented, they do not provide any knowledge regarding the possible triggering causes of the accident (Mazaheri et al. (2014)).

Despite its limitations, the methodology described above has been adopted and developed by Pedersen et al. (1995), and later Simonsen (1997), to the function presented in Equation (2.5).

$$N_{\mathrm{G}} = \sum_{\text{Ship class } i}^{n \text{ class}} P_{C,i} Q_i e^{-d/a_i} \int_{Z_{\min}}^{Z_{\max}} f_i(z) \mathrm{d}z \tag{2.5}$$

The models were extended to also include the ship class, the annual number of transshipment (Q), the average time interval between position checks by the navigator (a) and the

width of the waterfall. The traffic density metric is more detailed, using the actual traffic distribution of ships (f) through the transverse coordinates of the obstacle (z). The causation probability (P_C) is estimated using fault tree analysis (FTA). These models provide more information that are helpful in a consequence analysis, like the type and size of the ship.

The same methodology is used by Fowler and Sørgård (2000), which estimates the frequency of powered (f_{pg}) and drift groundings (f_{dg}) separately. The causation probability P_C is extended by estimating causation probabilities both for good(P_c) and bad(P_f) visibilities. Instead of including a density function for the ship traffic, the report has defined critical situations, utilizing expert consultation. The critical situation for powered grounding, defined as n_{pg}, is when the vessel is on a grounding coarse and within 20 minutes from impact. For drift grounding, the definition of the critical situation is more complex, and can be further studied in Fowler and Sørgård (2000).

The functions are provided in Equations (2.6) and (2.7).

$$f_{\mathrm{pg}} = n_{\mathrm{pg}} \left(P_{\mathrm{c}} p_{\mathrm{pg,c}} + P_{\mathrm{f}} p_{\mathrm{pg,f}} \right) \tag{2.6}$$

$$f_{\mathrm{dg}} = \sum_{\mathrm{l}} f_{\mathrm{p,1}} p_{\mathrm{d}} \sum_{\mathrm{w}} p_{\mathrm{w}} \left[\left(1 - p_{\mathrm{sr,w}}\right) \left(1 - p_{\mathrm{t,w}}\right) \left(1 - p_{\mathrm{a,w}}\right) \right] \tag{2.7}$$

Eide et al. (2007) use the same procedure as Fowler and Sørgård (2000), but with the advantage of utilizing dynamic meteorological data, such as wind, current and waves. The method also acknowledge the dynamic nature of ship conditions like position and speed. All these properties affect both frequency, F, and consequence, C, of drift grounding. The method is summarized mathematically in Equations (2.8) and (2.9).

$$\mathrm{Risk}(x, y, t) = F(x, y, t) \times C(x, y, t) \tag{2.8}$$

$$F(x, y, t) = F_{\text{drift}} \times P_{\text{grounding|drift}} \left(x, y, t\right) \tag{2.9}$$

The frequency of drifting is estimated based on historical failure rates of steering and propulsion for specific ship types. Judgement from experts have been utilized for slight modifications. The probability of grounding given drift is based on the dynamic condition of the environment as well as control regaining options, like self-repair and tug assistance.

Eide et al. (2007) models oil tankers, and the consequence of grounding is defined as size of oil spill. This is dependant on ship size, loading condition, hull structure, sensitivity of the location and type of spilled oil. The risk of grounding is then estimated based on frequency of grounding and consequence of grounding. The model is therefore capable of providing the required knowledge for post-accident consequence analysis, which makes it more suitable for risk management.

In recent years, research has been done regarding consequence analyses for vessels equipped with Dynamic Positioning (DP) systems. Such vessels are often used in the oil and gas

industry, where it is required to have a consequence analysis embedded into the control system. This analysis should be able to simulate the worst case failure mode of the system and trigger an alarm if the vessel is unable to maintain its position in the current weather conditions (DNV GL (2014)).

Bø et al. (2016) developed a dynamic consequence analysis for vessels during DP operation. The method is presented in figure 2.1. One key finding from this study was that the static consequence analyses commonly used in the marine industry may overestimate the ability of the system to withstand adverse weather conditions. This is because the analysis does not take into account the vessel's behavior during transitions, when it may not be able to maintain its position despite being able to do so before and after a fault occurs. It is advised to implement a more dynamic consequence analysis, like the one developed in Bø et al. (2016),

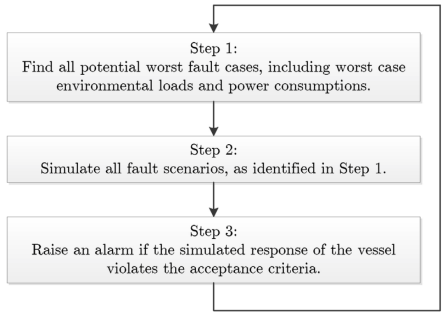

Figure 2.1: Steps in the dynamic consequence analysis presented in Bø et al. (2016)

Fossdal (2018) expanded upon previous research on consequence analysis for DP systems to create a method that can be applied to vessels in transit. The thesis presents an online consequence analysis (OCA) for situational awareness for autonomous vehicles. It involves simulating the dynamics of the vessel during different failure modes in specific weather conditions. The failure modes covered in the thesis are listed in Table 2.1.

Table 2.1: Failure modes presented in Fossdal (2018)

FM_1	Full power blackout for a specified duration of time
FM_2	80% power loss for a specified duration of time
FM_3	50% power loss for a specified duration of time
FM_4	Rudder freeze for a specified duration of time

After the failure modes have been simulated, the results are evaluated with respect to the vessel's minimum distance to obstacles during the simulations. Based on these distances, a consequence level for each failure mode is calculated. A risk indicator is calculated based on a quantitative measure of total risk defined by Varde et al. (2018):

$$R := \sum_i P(FM_i) CL_{FM_{i,\max}} \tag{2.10}$$

where the probability of the different failure modes occurring is not determined through statistical methods, but rather assigned arbitrarily.

The framework presented in Fossdal (2018) is promising, being able to capture transient effects and the overall increase in risk when maneuvering in confined waters. The framework serves as a building block in the relatively underdeveloped segment of online consequence analyses for vessels in transit.

There are, however, several ways in which the OCA framework could be improved. One potential improvement is to more accurately determine the probability of occurrence of the different failure modes using statistical methods such as fault tree analysis or Bayesian networks. Additionally, the OCA only initiates failure mode simulations every 15 seconds, which means that events occurring between these time instances are not considered. This could result in the risk related to smaller obstacles being overlooked.

The purpose of the framework presented in Fossdal (2018) is to calculate a risk indicator for the different segments of a pre-defined route. This risk indicator could be used to adjust the vessel's planned behavior, such as reducing speed or changing route, if the risk exceeds a certain threshold. However, the OCA does not outline how this risk threshold should be determined or how the vessel's behavior should be modified in response to the risk indicator. This would need to be implemented outside of the OCA framework.

Rasmussen (2019) presents a functionality that to a large degree is an extension of the online consequence analysis (OCA) presented in Fossdal (2018). Instead of arbitrarily choosing failure mode probabilities, Rasmussen (2019) integrates a Bayesian network, shown in Figure 2.2. The failure modes are the same as presented in Fossdal (2018), given in Table 2.1. The failure mode probabilities may be modified dynamically with changing environmental conditions. The consequence levels are determined in a similar manner to Fossdal (2018), using the minimum distance between vessel and object.

For each time step, a risk indicator is generated and utilized as input for an A* path planner. This path planner is activated to generate an alternative path when the risk indicator exceeds a specified threshold. However, due to the significant amount of computer memory required to execute the simulations mentioned in Rasmussen (2019), the failure modes were initiated every 20 seconds, lasting only 15 seconds. Consequently, it is possible that certain hazardous areas are not fully taken into account. Particularly, smaller objects may not be adequately covered by the simulations, leading to potentially inaccurate risk estimations.

In the grounding risk analysis presented by Løite (2022), the methodology builds upon the groundwork laid by Fossdal (2018) and Rasmussen (2019). To address the necessity of accounting for small obstacles, the analysis in Løite (2022) is enhanced by the simulation of specific failure modes twice per second. The recorded outcomes from these simulations are then utilized to establish a consequence metric. Furthermore, a Bayesian Network is

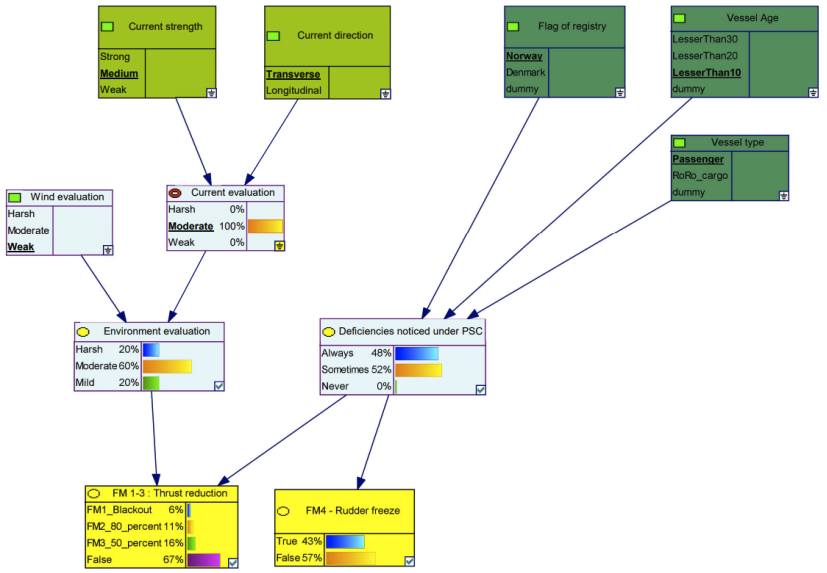

Figure 2.2: Bayesian Network from Rasmussen (2019)

used to estimate the probability of each potential failure. These measures are integrated to derive a risk estimation for a specific path. Unlike the frameworks in Fossdal (2018) and Rasmussen (2019) which provide risk indicators for predefined waypoints at discrete time periods, Løite (2022) goes a step further by enabling a risk comparison across possible paths circumventing obstacles.

2.4 Marine Accidents and Causes

To accurately simulate risk scenarios in the risk analysis, it is necessary to consider the most common causes of accidents. In this section, a brief investigation of marine accidents is conducted. The results of this investigation will be used to inform the calculation of accident probabilities in Section 3.3.

Rausand (2013) classifies the causes and contributing factors contributing to accidents as the following:

- Direct causes are the causes that lead immediately to accident effects. Direct causes are also called immediate causes or proximate causes, as they usually result from other, lower-level causes.
- Root causes are the most basic causes of an accident. The process used to identify and evaluate root causes is called root cause analysis.
- Risk-influencing factors (RIFs) are background factors that influence the causes and/or the development of an accident.

In an analysis focusing on the reduction of marine accidents in general, it can be argued that the most important of the three to consider are risk-influencing factors (RIFs). For example, if multiple accidents are caused by a lack of proper maintenance, addressing the risk influencing factor of inadequate maintenance can help to prevent future accidents, regardless of the specific direct cause or root cause of each individual accident. By addressing risk influencing factors, it is possible to address the underlying issues that contribute to the risk of accidents and take a proactive approach to accident prevention.

The term is further elaborated by Rausand (2013): ”a RIF is not an isolated event but an enduring condition that influences the occurrence of hazardous events and the performance of the barriers”. Risk-influencing factors represent, in other words, something lasting that affect the rate of which accidents happen.

Analysis of Norwegian Maritime Authority (NMA) Incident Database

Stornes (2015) is an exploratory statistical analysis of the incident database of the Norwegian Maritime Authority(NMA), with the objective of exploring possible RIFs in Norwegian maritime traffic. It use data on vessel accidents reported from 1981 through 2014 on groundings, collisions, allisions, fires/explosions and capsizing. The report propose the following main risk influencing factors (Stornes (2015)):

- For **fires/explosions**, fishing vessels appear at high risk. Large gross tonnages increase risk of fires, as well as longer vessels. The risk of fires is high at the quayside, while weather appears to be little influential.
- For **groundings**, cargo vessels (work and service vessels in particular) appear at higher risk. Vessels of low gross tonnage and longer length appear at higher risk. Narrow coastal waters increase the relative risk of groundings substantially.
- For **collisions**, small break bulk vessels appear at higher risk. Travelling in no visibility increases the relative risk of a collision considerably. Outer coastal waters increases the risk of a collision considerably.
- For **allisions**, high speed craft of medium gross tonnage and longer lengths appear at higher risk of allisions. Allisions are closely tied to the harbour area.

Figure 2.3 shows other interesting results from Stornes (2015). These tables must be interpreted with a good amount of scepticism. The data used in these tables is taken from an accident database, meaning that it does not include information about voyages without accidents or the relationship between different states. For example, Figure 2.3c may lead someone to conclude that a calm sea is a risk factor, as it appears that 54.6% of accidents occur when the sea is calm. However, this interpretation is misleading because the sea is much more likely to be classified as calm than the other states.

Observations from Port State Control Inspections

Cariou et al. (2008) includes observations from port state control (PSC) inspections done by the Swedish Maritime Administration in the years 1996-2001. The probabilities for

Ship Age	Accident type					
	Fire/expl.	*Grounding*	*Capsizing*	*Collision*	*Allision*	*Total*
0-5	12,2%	12,1%	7,9%	11,0%	17,7%	12,6%
6-15	23,3%	24,2%	24,5%	26,9%	24,1%	24,5%
16-25	20,8%	24,3%	25,9%	27,5%	22,8%	24,3%
25+	41,0%	36,2%	37,4%	30,9%	30,2%	35,2%
Unknown	2,6%	3,2%	4,3%	3,7%	5,2%	3,5%
	100,0%	100,0%	100,0%	100,0%	100,0%	100,0%
Total N	**614**	**3607**	**139**	**865**	**772**	**5997**

(a) Table 7.1.9: Distribution of vessel age within accident types

Vessel type	Accident type					
	Fire/expl.	*Grounding*	*Capsizing*	*Collision*	*Allision*	*Total*
Fishing <15m	39,9%	15,8%	31,7%	25,0%	2,8%	18,3%
Fishing >15m	24,9%	21,8%	14,4%	18,8%	5,8%	19,5%
Ferries	4,4%	11,6%	2,9%	9,2%	48,8%	15,1%
Passenger/cruise	5,2%	5,9%	1,4%	7,7%	8,9%	6,4%
High-speed	1,5%	2,1%	0,0%	2,3%	7,0%	2,6%
Other passenger	3,9%	2,6%	0,7%	2,9%	1,2%	2,6%
Work and service	4,2%	4,8%	23,0%	3,5%	3,1%	4,7%
Offshore service	2,0%	1,2%	0,0%	1,4%	3,6%	1,6%
Wellboats	0,7%	2,4%	0,0%	0,8%	0,6%	1,7%
Tanker	1,3%	2,7%	1,4%	2,3%	2,2%	2,4%
Bulk	1,6%	3,9%	2,9%	3,5%	3,2%	3,5%
Goods (Godsfartøy)	10,4%	25,2%	21,6%	22,5%	12,6%	21,6%
	100,0%	100,0%	100,0%	100,0%	100,0%	100,0%
Total N	**614**	**3607**	**139**	**865**	**772**	**5997**

(b) Table 7.1.2: Distribution of vessel types within accident types

Sea state	Accident type					
	Fire/expl.	*Grounding*	*Capsizing*	*Collision*	*Allision*	*Total*
Calm seas	43,8%	56,0%	29,5%	62,7%	52,6%	54,6%
Slight/moderate seas	11,2%	14,4%	22,3%	12,3%	5,3%	12,8%
High seas	0,8%	2,8%	12,2%	1,4%	1,6%	2,5%
Unknown	44,1%	26,8%	36,0%	23,7%	40,5%	30,1%
	100,0%	100,0%	100,0%	100,0%	100,0%	100,0%
Total N	**614**	**3607**	**139**	**865**	**772**	**5997**

(c) Table 7.3.2: Distribution of sea states within accident types

Figure 2.3: Tables retrieved from Stornes (2015)

deficiencies detected during these inspections are shown in Figure 2.4. All of the ships included in the study were inspected at least twice. If the ship did not have any deficiencies during any of the inspection, it was labelled as "never deficient". Vessels which alternatively exhibited no or some deficiencies during PSC inspections was labelled "sometimes deficient". If at least one deficiency was noted for all PSC inspections, the ship was labelled "always deficient". The table suggests that factors such as vessel age, type of ship, and flag of registry have a significant impact on the likelihood of deficiencies being detected. Overall, the data may be summarized as follows:

- Vessels aged 25-30 years has the highest rate of always being deficient, with 28.8%. What is interesting is that vessels aged more than 30 years have a lower deficiency rate. Cariou et al. (2008) suggests the reason for this might be "a selection effect that implies that only extremely well maintained vessels older than 30 years still remain in operation".
- Passenger ships has the (marginally) highest rate of always being deficient, with 17%. Passenger ships are very rarely "never deficient". One explanation of this might be that passenger ships have more systems that needs to work compared to, for example, container ships. Air condition, life jackets and life boats for all passengers are some of them.
- Ships registered in Norway has the highest rate of always being deficient, with 26.5%. Norwegian ships does not, however, have the lowest rate of never being deficient. Ships registered on Bahamas are never deficient 12.2%, compared to 20.7% for Norwegian ships.

Study on the Frequency of Accidents

This section has so far discussed potential risk-influencing factors (RIFs). For later use, it also proves interesting to conduct a study on the expected frequency of ship failures, more specifically the frequency of blackouts.

Friis-Hansen et al. (2008) suggest that "*most ships experiences of the order of one black out of the main engine per year. The number of any blackout for a given ship will typically lie in the interval from 0.1 to 2 blackouts per year*". The study argues that passenger vessels, which often have a high level of built-in redundancy in the engine room with two to four propulsion units, tend to have a lower frequency of blackouts than other vessels. The blackout frequencies presented in Table 2.2 are selected by Friis-Hansen et al. (2008) as base values.

Table 2.2: Blackout frequencies retrived from Friis-Hansen et al. (2008)

Vessel Type	Annual Frequency	Hourly Frequency
Passenger / Ro-Ro	$0.1y^{-1}$	$1.15 \cdot 10^{-5}h^{-1}$
Other vessels	$0.75y^{-1}$	$8.56 \cdot 10^{-5}h^{-1}$

Bolbot et al. (2021) compares blackout frequencies in different operating phases. The results are shown in Table 2.3, where FOB stands for *frequency of blackout*. The study

Ship-level analysis of deficiency trajectory

Number of deficiencies	Never deficient	Sometimes deficient	Always deficient	Number of observations	Chi^2 (prob.)
Vessel age at time of PSC (%)					
[0; 5[	43.8	52.3	3.8	130	54.99
[5; 10[	28.5	62.6	8.9	123	(0.000)
[10; 15[	24.8	62.0	13.2	121	
[15; 20[	24.7	63.3	12.0	158	
[20; 25[	24.2	56.8	18.9	132	
[25; 30[	15.3	55.9	28.8	111	
[30; ∞[	26.6	54.7	18.7	64	
Compliance with ISM Code in 1998 (%)					
No	29.4	54.6	16.0	469	7.31
Yes	24.0	63.8	12.2	370	(0.026)
Type of ship (%)					
General cargo	27.0	57.1	15.8	366	53.02
Bulk carrier	21.7	64.3	13.9	230	(0.000)
Passenger	7.5	75.5	17.0	53	
Ro-ro passenger	15.0	75.0	10.0	20	
Chemical tanker	54.0	37.8	8.1	37	
Ro-ro cargo	52.6	31.6	15.8	38	
Oil tanker	37.5	58.3	4.2	24	
Refrigerated cargo carrier	46.7	40.0	13.3	15	
Container	38.9	55.6	5.6	18	
Others	21.0	63.2	15.8	38	
Flag (%)					
Antigua and Barbuda	23.1	61.5	15.4	52	60.39
Bahamas	12.2	70.7	17.1	41	(0.000)
Cyprus	22.2	66.7	11.1	36	
Denmark	41.2	51.5	7.3	68	
Finland	20.9	72.1	7.0	43	
Germany	44.3	53.4	2.3	88	
Malta	24.0	64.0	12.0	25	
Netherlands	37.5	55.0	7.5	80	
Norway	20.7	53.7	25.6	82	
Russia	19.1	60.3	20.6	141	
Others	25.1	57.4	17.5	183	
All (%)	27.1	58.6	14.3	839	–

Source: Swedish Maritime Administration (SMA) 1996–2001.

Figure 2.4: Deficiencies noted under PSC (Cariou et al. (2008))

concludes that the overall blackout frequency is approximately 0.4 per ship per year across all operating phases.

Table 2.3: Table 6 in Bolbot et al. (2021): Comparison of λ^B in different operating phases

Operation Phases	$\boldsymbol{\lambda^B(h^{-1})}$	FOB($\frac{events}{ship-year}$)
General (100%)	$4.515 \cdot 10^{-5}$	0.3955
Harbour(ship at berth) (28%)	$1.691 \cdot 10^{-4}$	1.481
Sailing (69%)	$3.225 \cdot 10^{-7}$	0.003
Manoeuvring (3%)	$3.646 \cdot 10^{-5}$	0.319

2.5 Consequence of Grounding

Numerous studies have examined the impact of grounding accidents, exploring various methods and data sources for assessing their consequences.

For instance, Otto et al. (2002) introduced damage criteria that establish a connection be-

tween the calculated distribution of damage size and location to monetary units. However, this study did not consider factors such as loss of human life and reputation.

Another study by Yamada (2009) proposed a methodology to estimate the costs associated with oil spills from ships. This approach utilized regression analysis based on historical oil spill data. Nevertheless, the current models used to evaluate the consequences of ship grounding incidents do not provide a comprehensive assessment of the overall damages incurred in such events.

This thesis draws inspiration from the works of Dong and Frangopol (2015) and Liu and Frangopol (2018) to establish the consequences of ship grounding incidents in terms of their environmental, economic, and social implications. Severe grounding incidents can have significant environmental consequences. An example is the Exxon Valdez grounding, which led to a massive oil spill and caused severe and long-lasting environmental impacts, as documented by Peterson et al. (2003). Furthermore, ship grounding incidents can result in structural damages to the ship, leading to an extensive cost repair cost as well as other costs. Finally, severe grounding accidents pose a high risk of causing fatalities and injuries to crew and passengers onboard.

The consequence analysis starts by evaluating the structural damage to the ship, which serves as the foundation for assessing the environmental, economic, and social consequences. Additional factors are also considered in the consequence analysis, such as vessel type, value of cargo and environmental fragility of the location of the grounding. The framework is highly adaptable, allowing for the inclusion of additional factors as needed. This flexibility ensures that the framework can accommodate and account for a wide range of variables to provide a comprehensive evaluation of the consequences associated with ship grounding incidents.

In the study conducted by Liu and Frangopol (2018), the estimation of structural damage is carried out by analyzing the geometric characteristics of the damage. The researchers utilize five physical damage metrics, among others longitudinal and vertical extent of the damage. These are used to estimate a corresponding damage state. This estimation process results in a scale ranging from 1 to 6, where each damage state represents a different level of severity or extent of damage. Table 2.4 provides detailed information on the specific damage states assigned to a grounded oil tanker based on their research findings.

Table 2.4: Damage states of grounded tanker presented in Liu and Frangopol (2018)

Damage state(DS_i)	Damage Extent(DE_i)	Result
1	Limited plane damage	No oil spillage
2	Large plane damage	No oil spillage
3	One tank penetrated	Spillage of one tank of oil
4	Two tanks penetrated	Spillage of two tanks of oil
5	Three tanks penetrated	Spillage of three tanks of oil
6	Multiple tanks (≥ 4) penetrated	Spillage of four tanks of oil

In the study conducted by Liu and Frangopol (2018), a Monte Carlo simulation approach was employed to generate probabilistic damage characteristic variables. This simulation

involved collecting and classifying a large number of damage samples. A representative AFRAMAX type oil tanker was used as the basis for the simulation.

The resulting probabilities for different damage states are presented in Table 2.5. This table serves as a valuable reference, as it provides insights into the probabilities associated with different damage states in the study conducted by Liu and Frangopol (2018). The implementation of damage state prediction developed in this thesis should aim to approximate these values to enhance the applicability and relevance of the metrics derived from the study by Liu and Frangopol (2018) within the context of this thesis.

Table 2.5: Probability of AFRAMAX damage states presented in Liu and Frangopol (2018)

Damage state (DS_i)	1	2	3	4	5	6
Damage state probability (P_{DS_i})	40.8%	37%	11.5%	7.6%	0.9%	2.2%

2.5.1 Environmental Consequence

Grounding accidents can have a significant environmental impact, particularly when they involve the spillage of hazardous substances like oil. Such spills have devastating effects on marine ecosystems, and the cleanup process can be extremely costly. It has been established that grounding incidents are the major cause of oil spills (Huijer (2005)).

This thesis focuses on two factors associated with environmental consequences. The first factor is the environmental damage resulting from the impact of the ship itself, while the second factor is the environmental damage caused by the spillage of hazardous chemicals.

Consequence from Impact of Ship

Let us first consider the environmental damage resulting from the impact of the ship itself. A notable incident occurred in 2012 when the USS Guardian, a minesweeper ship, ran aground on the Tubbataha National Marine Park in The Philippines, which is home to one of the world's most diverse coral reefs (Haribon (2016)).

Determining a monetary value of environmental damage is a complex and contentious task, primarily due to the unique nature of ecosystems and the diverse human perspectives on nature and its value.

One practical approach for estimating the cost of environmental harm is to consider the fines imposed on shipping companies following grounding accidents. Regulatory bodies often impose fines on responsible parties to ensure accountability and to work deterrent. These fines, intended to partially reflect the environmental losses, can serve as a useful indicator for approximating the monetary value of the damage.

However, it is important to note that such fines may not fully capture the complete cost of environmental harm. It is important to consider indirect effects, such as impacts on tourism or local fisheries, as well as intangible factors like biodiversity loss or aesthetic degradation. Furthermore, the restoration and recovery of damaged ecosystems can take years or even decades, making accurate damage assessment more challenging.

According to Rosales (2006), the Total Economic Value (TEV) of the damaged area resulting from grounding accidents can be estimated by considering both the value of resource use and the value of conservation. The study incorporates various economic values, including recreational value, research value, and fish production value. It concludes that an average fee of PHP 12,000 per square meter of affected area is applicable to grounded ships.

This valuation was later confirmed and incorporated in the 2012 *Park Rules and Regulation* for Tubbataha National Marine Park in The Philippines, where a grounding fine of PHP 12,000 per square meter was mandated (TPAMB (2012)). After adjusting for inflation from 2012 to 2023 and converting the amount to US dollars, this fine equates to approximately USD 300 per square meter of damaged area.

Rosales (2006) also draws attention to specific instances of fines that have been imposed on ships involved in grounding incidents within protected marine parks. These fines, showcased in Table 2.6, offer a practical illustration of the financial implications that such accidents can incur.

The table displays data from four different marine parks, detailing the size of the affected area and the total fine assessed. Additionally, it breaks down these fines to a per square meter basis, offering a direct comparison between the different incidents and locations.

For example, at the Apo Reef Marine Park in Mindoro Oriental, Philippines, a grounding incident affecting an area of 2,910 square meters resulted in a fine of approximately PhP 13,148, equivalent to around USD 235 per square meter. In contrast, two separate incidents within the Florida Keys National Marine Sanctuary in the USA incurred fines of approximately USD 482 and USD 7,490 per square meter. Lastly, in the Great Barrier Reef Marine Park in Australia, a grounding accident impacting a 1,500 square meter area was penalized with a fine of roughly AUD 733 per square meter, equivalent to approximately USD 491. The study did not provide specific dates for these groundings.

These case studies serve to underscore the significant economic consequences that grounding incidents can pose, especially within protected marine environments. They also highlight the variability of fines across different regions, reflecting the diverse local considerations in assessing the financial impact of such environmental damages.

Egypt has been at the forefront in advancing methodologies to value environmental damages and seeking legal measures to ensure appropriate compensation for harms done to their coral reefs. This leadership is particularly reflected in their development and implementation of a unique model, widely acknowledged and utilized across the Middle East (Kotb and Zeid (2009)).

This model, as shown in Equation (2.11), has been designed to provide a quantitative estimate of the environmental damage, specifically targeting coral reefs:

$$A \cdot LC \cdot D \cdot RP \cdot V \tag{2.11}$$

Here, A is a measure of the affected area in square meters, LC is the percentage of living

Table 2.6: Ship grounding fines in designated marine parks. Extracted from Rosales (2006)

Marine Park	Location	Size of Area Affected (m^2)	Total Fine Assessed	Fine Assessed (per m^2)
Apo Reef Marine Park	Mindoro Oriental, Philippines	2,910	PhP 38,260,521	PhP 13,148
Florida Keys National Marine Sanctuary	Florida, USA	1,175	USD 565,796	USD 482
Florida Keys National Marine Sanctuary	Florida, USA	502	USD 3,760,000	USD 7490
Great Barrier Reef Marine Park	Great Barrier Reef, Australia	1500	AUD 1,100,000	AUD 733

coral, D is the percent of damage in the area, RP is the number of years required for recovery and V is a given valuation of one square metre. In 2009, the valuation (V) was set at USD 300 for areas designated as national parks, and USD 120 for other regions. However, taking into account inflation over the years, these values translate to USD 423 and USD 169 respectively, as of 2023.

Consequence of Chemicals Spilling

When we shift our focus to the environmental damage caused by the spilling of dangerous chemicals, we enter a particularly concerning aspect of marine accidents. Chemical spills pose a unique set of threats to the environment and biodiversity, often having lasting and severe impacts. In the context of this thesis, we utilize an oil tanker to illustrate this scenario.

Chemicals that enter the marine environment can have diverse and severe effects depending on their nature. For instance, oil spills are one of the most recognized forms of chemical pollution, largely due to high-profile incidents like the Exxon Valdez and Deepwater Horizon oil spills(Peterson et al. (2003)). Oil spills can cause immediate and long-term damage to marine ecosystems. They harm wildlife, disrupt food chains, and can lead to substantial loss of biodiversity. Moreover, they contaminate the marine environment for years, even decades, as complete oil degradation is a slow process Appolinario et al. (2020).

The potential environmental and economic consequences of a chemical spill at sea are significant, and numerous studies, such as Liu and Frangopol (2018), have approached the quantification of these impacts. A common method of assessing these impacts is by calculating the comprehensive cleanup cost of the spilled chemicals. This approach is

demonstrated in Equation (2.12).

$$C_{spill} = c_{spill}(Q_{spill}) \tag{2.12}$$

In this equation, C_{spill} represents the total cleanup cost, while c_{spill} is a function that takes the tonnage of the spilled chemicals, denoted as Q_{spill}, as an argument. This function is designed to estimate the cleanup cost for a given grounding accident based on the volume of the spill.

Liu and Frangopol (2018) provide an implementation of this function, as shown in Equation (2.13). Here, $x = Q_{spill}$ represents the tonnage of the chemical spill.

$$C_{spill}(x) = 24020x^{0.8447} \tag{2.13}$$

The calculation of the total quantity of chemicals spilled (Q_{spill}) due to a grounding incident is outlined in Equation (2.14). This estimation is made under the assumption that a tank penetration results in the spillage of all the chemicals contained within. The equation, which is derived from Liu and Frangopol (2018), multiplies the number of tanks penetrated (N_{DS_i}) by the size of each tank (Q_i), providing an estimate of the total volume of the spill.

$$Q_{spill} = Q_i N_{DS_i} \tag{2.14}$$

The number of tanks penetrated (N_{DS_i}) can be estimated based on the damage state of the ship following a grounding incident. These equations enable the cost and potential volume of a chemical spill to be integrated into an risk assessment for a given grounding.

Typical sizes for tanks carrying oil on various ship types are provided in Table 2.7. The values represent typical tank capacities and offer a baseline for estimating the potential scale of a spill in the event of a grounding incident.

Table 2.7: Standard tank configurations for oil tankers. Extracted from Konovessis (2012)

Ship type	Cargo tank configuration	Total capacity (t)	Typical tank size (t)
AFRAMAX	6 x 2	80 000-120 000	8 333
SUEZMAX	6 x 2	120 000-200 000	13 333
VLCC	5 x 3	200 000-320 000	17 333

2.5.2 Social Consequences

Grounding incidents not only cause environmental damage, but they can also have severe social implications. The human cost associated with these accidents is significant. The social impact following a grounding incident is measured by considering the potential loss

of life and non-fatal injuries among crew members. Historical data suggests that grounding incidents have profound social consequences. According to an analysis of 826 passenger ship accidents, grounding incidents were associated with a higher likelihood of fatalities than other incidents, accounting for 17% of the total fatalities Vanem and Ellis (2010).

Fatalities

The fatality rate is calculated based on the previously discussed damage state of the ship. COWI (2008) refers to an analysis that showed that the expected number of fatalities in the case of an oil spillage is 0.01 persons. In our case, this corresponds to damage state larger or equal to 3. For minor damage states 1 and 2, no loss of life is expected.

COWI (2008) converts loss of life into monetary units by using the so-called value of a statistical life(VSL). This is based on the assumption that "every person has a limited willingness to pay for a possible prolongation of his own life or that of a fellow member of society by a small time span. Extrapolating the willingness to pay from this time span to the duration of an average life yields the VSL." (COWI (2008)). Skjong et al. (2005) estimates the VSL to USD 3 million.

In this context, the financial consequence of the loss of life, denoted as C_{LL}, from a specific grounding incident can be approximated using the formula presented in Equation (3.4.2). Here, N_{ll} represents the expected number of fatalities and V_{ll} denotes the Value of a Statistical Life. Thus, the overall monetary consequence from loss of life in a grounding accident is estimated to be the product of the expected number of fatalities and the Value of a Statistical Life.

$$\begin{gathered} C_{LL} = N_{ll} V_{ll} \\ E[N_{ll}|oil\ spillage] = E[N_{ll}|DS_i; i >= 3] = 0.01 \\ V_{ll} = USD\ 3\ mill \end{gathered} \tag{2.15}$$

Non-fatal Injuries

Non-fatal injuries are also important to remember when considering the social consequence of a grounding incident.

The data collected by the United States Coast Guard from 1992-2008, as presented by US Coast Guard (2009), offers valuable insights into ship collision incidents. According to their findings, the expected number of crew injuries per incident was estimated to be 2.0. While this metric is specifically derived from ship collision data, both this study and Liu and Frangopol (2018) suggest its applicability to ship grounding incidents as well, given the similar risks and impacts associated with both types of accidents.

A further dimension to consider in estimating the overall cost of these incidents is the financial implication of non-fatal injuries to crew members. Liu and Frangopol (2018) proposes a cost estimate of USD 60,000 per injured crew member. With this, we can formulate a monetary representation of the cost of non-fatal injuries resulting from a grounding accident as presented in Equation (2.5.2). In this equation, N_{inj} is the expected number

of non-fatal injuries, while c_{inj} denotes the estimated cost per injured crew member. By multiplying these two factors, we can obtain an estimated cost, C_{Inj}, of non-fatal injuries sustained in a grounding incident.

$$\begin{aligned} C_{Inj} &= N_{inj} c_{inj} \\ E[N_{inj}] &= 2.0 \\ c_{inj} &= USD\ 60,000 \end{aligned} \tag{2.16}$$

2.5.3 Economic Consequences

Assessing the economic impact of a ship grounding incident requires a detailed evaluation of the damage incurred. Direct economic losses from such incidents can be extensive, encompassing several elements such as repair costs, lost revenue due to operational downtime during repairs, and the loss of cargo particularly when cargo compartments are compromised.

In 2011, The Swedish Club, a Swedish insurance company, published a paper detailing recorded collisions and groundings for vessels insured under their Hull and Machinery (HM) policy The Swedish Club (2011). As per The Swedish Club (2023), the H&M policy "protects the insured's financial interest in the vessel and its equipment and provides coverage for total and partial losses of the insured property."

The document is of particular interest to this thesis as it provides detailed data on the average claim cost and frequency, focusing specifically on grounding incidents, as depicted in Figure 2.5. The data, covering the period from 2001 to 2011, reveals that the average claim costs oscillated between USD 250,000 and USD 2,100,000. The average cost, derived from the entire period under study, equates to slightly above USD 900,000.

It may seems fruitful to diversify the economic consequence estimates based on the damage state of the grounded vessel. Specifically, Liu and Frangopol (2018) provide a framework for estimating repair time and associated costs across varying damage states, as illustrated in Table 2.8. This includes a measure of damage relative to the ship's value, denoted as RD_{DS_i}, and the estimated repair time represented as t_{DS_i}.

Table 2.8: Estimated costs of damage and repair durations corresponding to the damage state of the vessel. Sourced from Liu and Frangopol (2018)

Damage state	Damage relative to ship value (RD_{DS_i})	Repair time (t_{DS_i})
1	0.01	7 days
2	0.02	14 days
3	0.025	21 days
4	0.04	30 days
5	0.1	40 days
6	0.2	50 days

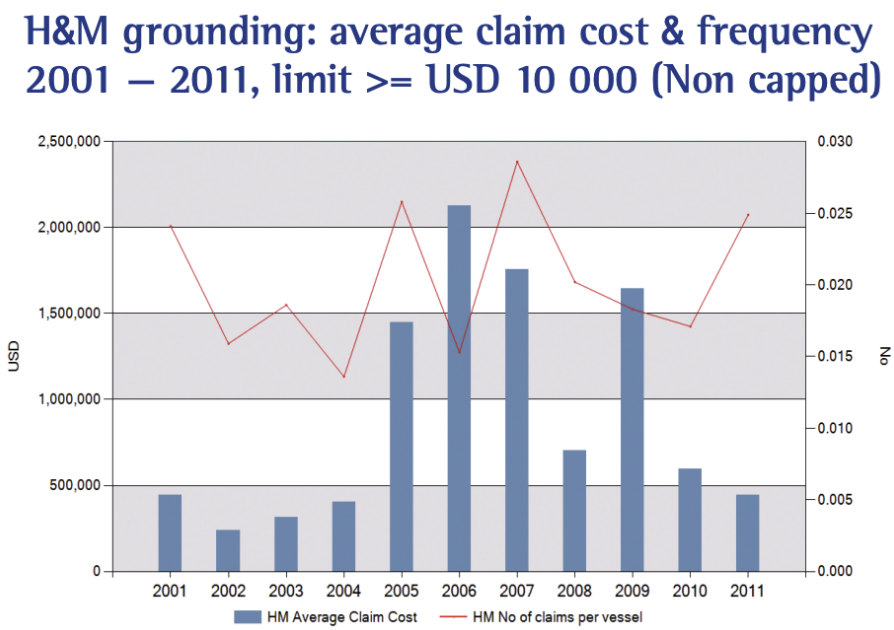

Figure 2.5: Average cost and frequency for HM insurance claims between the years of 2001 and 2011. Retrieved from The Swedish Club (2011)

Repair Cost

The cost of repairing a grounded ship is a significant factor to consider when evaluating the overall impact of a grounding incident. The repair cost can vary significantly based on the extent of the damage, which can range from minor cosmetic fixes to extensive structural repairs.

According to Liu and Frangopol (2018), the repair cost (C_{RC}) for a grounded ship can be estimated using the formula shown in Equation (2.17).

$$C_{RC} = RD_{DS_i} V_{ship} \tag{2.17}$$

In this equation, RD_{DS_i} represents the relative damage as a proportion of the ship's value (V_{ship}). The determination of this ratio is based on the damage state of the vessel, as depicted in Table 2.8.

Loss of Potential Earnings

The concept of loss of potential earnings due to repair time involves the key principle of opportunity cost. When a vessel is taken out of operation for repairs, it isn't able to

generate revenue during that period. This absence of revenue generation is an indirect cost and is an important part of the total economic loss.

The duration of ship repairs can vary significantly depending on the severity of the damage sustained. Typically, more severe damage leads to a longer repair period, resulting in increased lost potential earnings. This relationship is represented by Equation (2.18), where t_{DS_i} represents the repair duration associated with the damage severity, and c_{day} denotes the daily potential earnings.

$$C_{LE} = t_{DS_i} c_{day} \tag{2.18}$$

Estimates for repair durations t_{DS_i} can be obtained from Table 2.8, which is sourced from Liu and Frangopol (2018). However, it is important to note that these values should be treated as broad approximations rather than absolute figures. This is primarily due to the multitude of factors that can influence the timeline for ship repair. While the damage state categorization provides a broad framework, actual damages could range from relatively simple issues such as minor hull breaches to complex problems like damage to the ship's internal systems or machinery. Each type of damage would require different expertise and equipment to repair, influencing the repair duration. Nonetheless, the framework offered by Liu and Frangopol (2018) affords a convenient and straightforward methodology for implementation, despite its potential limitations.

Calculating the parameter c_{day}, representing the daily indirect cost of lost earnings, requires a careful approach. One potential method involves determining the net daily earnings, which is obtained by subtracting variable operating costs from gross earnings. It should be noted that fixed costs such as loan repayments and insurance continue to accrue even when the ship is non-operational and are not included in the subtracted costs. Due to competitive reasons, shipping companies typically do not disclose their net daily earnings. One could argue that, as an estimation, average daily bareboat charter rates can be considered. As delineated by Dalgic et al. (2013), a "bareboat charterer leases the ship devoid of crew or any operational responsibilities, thereby being accountable for daily running costs, voyage expenses, and costs related to cargo handling and claims." Referring to data from HandyBulk (2023), the daily charter rate for Handysize bulk carriers was approximately USD 10,000 as of May 13, 2023.

Loss of Cargo

This section research the financial implications associated with the loss of cargo in the event of a grounding incident. When a ship grounds, there is a significant risk that the cargo onboard may be damaged or entirely lost. Liu and Frangopol (2018) describes the cost of loss of cargo intuitively as shown in Equation (2.19). Here, Q_{loss} represents the quantity of the lost cargo and c_{cargo} is the unit cost of the cargo. Essentially, the equation multiplies the volume of the lost cargo by its unit cost to compute the overall cost of cargo loss.

$$C_{LC} = Q_{loss} c_{cargo} \tag{2.19}$$

In the specific scenario of oil tankers, the calculation of cargo loss is slightly adjusted to take into account the spilled oil. The oil spillage quantity (Q_{spill}) and the price of crude oil per ton (c_{oil}) are used, as shown in Equation (2.20).

$$C_{LC} = Q_{spill} c_{oil} \tag{2.20}$$

2.6 Consequence Associated with Time Usage

In marine transportation, time is a valuable resource. Any additional time spent during a voyage, whether caused by inefficient route planning, mechanical failures, or adverse environmental conditions, can have a negative impact on a shipping company's financial performance.

One perspective to consider is the potential loss of earnings. The shorter the duration of the voyage, the sooner the vessel can commence its next journey, resulting in increased earnings. This concept is aligned with the Time Charter Equivalent (TCE) principle, which measures income generation per unit of time Rygaard (2009). However, in this thesis, we assume that the additional time usage is minimal and does not enable the vessel to undertake any additional voyages. Therefore, the concept of potential loss of earnings based on additional time usage is not further considered.

Another approach to assessing the cost of additional time usage is to estimate the extra operating expenses incurred by the vessel. According to (Počuča (2006)), obtaining accurate data on a ship's operating costs from shipowners is challenging as this information is often treated as a proprietary trade secret. Owners may argue that costs can vary widely for vessels of the same type and size due to factors such as crew expenses, maintenance costs influenced by the vessel's age and past maintenance quality.

The publication titled "OPCOST-Benchmarking vessel running cost" by Moore Stephens Chartered Accountants, as cited in Počuča (2006), provides factual information on the operating costs of specific types of ships. This publication represents the average costs of the vessels for which Moore Stephens Chartered Accountants perform their accounting. One notable finding is that crew wages account for the largest share of costs, approximately 37%, and this can vary significantly based on the nationalities of the crews.

In their study, Počuča (2006) examined data from the aforementioned source, focusing on a sample of 89 ships with an average Dead Weight Tonnage (DWT) of 28,909. The study revealed that the average daily total operating cost for these ships in 2003 was USD 3,284. Adjusting for inflation, this corresponds to a daily cost of USD 5,378. This translates to a cost per second of approximately USD 0.06.

2.7 Consequence Associated with Fuel Consumption

Fuel consumption is a significant consideration in marine operations, affecting financial expenses and overall operational efficiency. Various factors influence the amount of fuel a ship consumes, including the design of the hull and engine, as well as the speed at which the vessel operates.

The work of Rokseth and Utne (2023) illustrates a method to compute the fuel consumption of a ship, utilizing specific fuel consumption curves. These curves are employed to translate the loads on each power source into a rate of fuel consumption. In essence, the specific fuel consumption curves delineate how much fuel is used per unit of power produced. To create these specific fuel consumption curves, a second-order polynomial is fitted to fuel consumption data. The data used for the main engine (ME) pertains to the *Wärtsilä 6L26* and includes fuel consumption measurements at 100%, 85%, 75%, and 50% load.

The calculation for the fuel consumption rate of the main engine (ME) is given by Equation (2.21):

$$\dot{\chi}_{ME} = S_{ME}(x_{ME})P_{ME} \tag{2.21}$$

In this equation, S_{ME} represents the specific fuel consumption curves, x_{ME} denotes the load fractions, and P_{ME} corresponds to the power generated by the main engine.

2.8 Mathematical Modeling of Marine Vessels and Environmental Forces

This subsection aims to provide the necessary mathematical foundation for the ship simulator used in this report, presented in Section 3.2.

According to Fossen (2011), the study of dynamics can be divided into two parts: kinematics, which treats only geometrical aspects of motion, and kinetics, which is the analysis of the forces causing the motion. The two parts will be treated in sections 2.8.1 and 2.8.2, respectively.

2.8.1 Kinematics

It is necessary to establish four reference frames for later reference. They are illustrated in Figure 2.6, and the definitions are retrieved from Fossen (2011).

- **ECI:** The Earth-centered inertial (ECI) frame $\{i\} = (x_i, y_i, z_i)$ is an intertial, nonaccelerating reference frame in which Newton's laws of motion apply. The origin of i is located at the center o_i of the Earth with axes as shown in Figure 2.6.

- **ECEF:** The Earth-centered Earth-fixed (ECEF) reference frame $\{e\} = (x_e, y_e, z_e)$ has its origin o_e fixed to the center of the Earth, but the axes rotate with the Earth, relative to the interial frame ECI.
- **NED:** The North-East-Down (NED) coordinate system $\{n\} = (x_n, y_n, z_n)$ is defined relative to the Earth's reference ellipsiod (World Geodetic System (1984)). It is usually defined as a tangent plane moving with the vessel, but with the *x* axis pointing towards true *North*, the *y* axis pointing towards *East* and the *z* axis pointing downwards normal to the Earth's surface. For marine vessels operating in a local area where one can approximate constant longitude and latitude, an Earth-fixed tangent plane is used for navigation. In the local area, the earth is assumed as flat and that the frame is inertial such that Newton's laws still apply (Fossen (2011)).
- **BODY:** The body-fixed reference frame $\{b\} = (x_b, y_b, z_b)$ is fixed to the vessel. The position and orientation of the vessel is often defined relative to NED, while the linear and angular velocities are defined in the body-fixed coordinate system (Fossen (2011)).

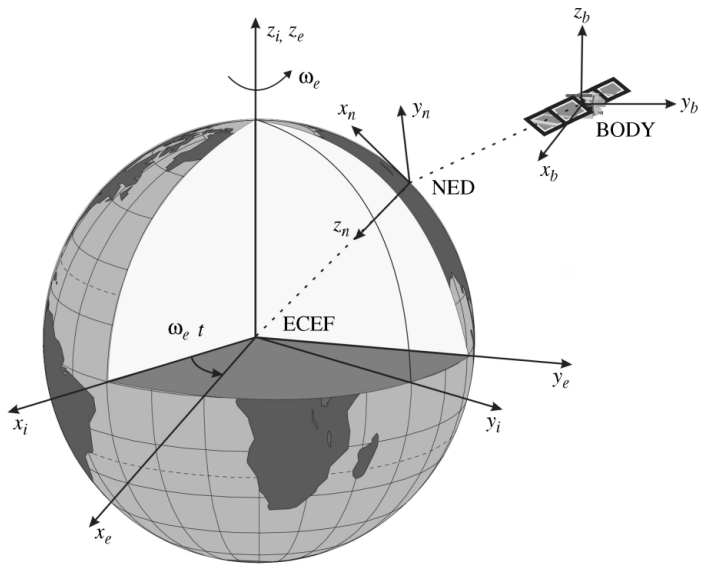

Figure 2.6: The ECEF frame $x_e y_e z_e$ is rotating with angular rate ω_e with respect to an ECI frame $x_i y_i z_i$ fixed in space. NED and BODY frames are also illustrated. Retrieved from Fossen (2011).

As marine vessels are moving in six degrees of freedom (DOFs), we need six independent coordinates to determine the position and orientation. The first three coordinates correspond to the position of the vessel, and the last three coordinates are used to describe orientation. In the notation of SNAME (1950), the positions and Euler angles are noted as x, y, z, ϕ, θ and ψ. The corresponding linear and angular velocities are defined as

surge(u), sway(v), heave(w), roll(p), pitch(q) and yaw(r), respectively. See Figure 2.7 for reference.

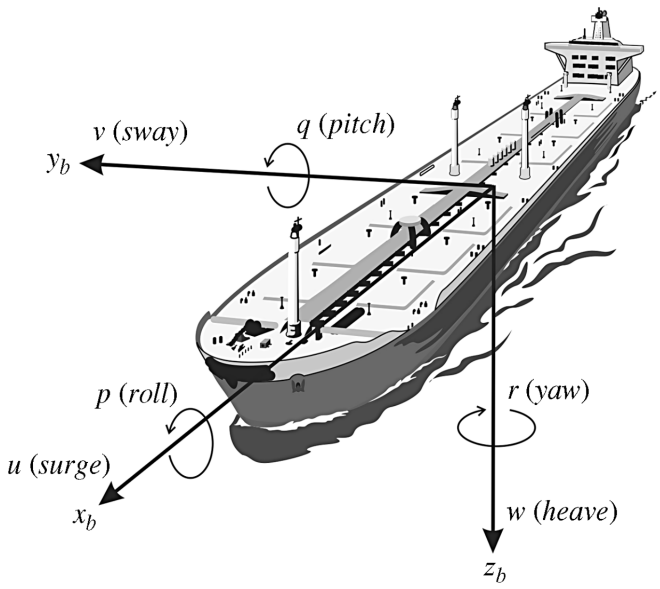

Figure 2.7: The 6 DOF velocities u, v, w, p, q and r in the body-fixed reference frame $\{b\} = (x_b, y_b, z_b)$. Retrieved from Fossen (2011).

Position and orientation of a vessel in $\{\mathrm{b}\}$ is often defined relative to $\{\mathrm{n}\}$. We need to establish the transformations between the two frames. The notation from Fossen (2011) is used:

$p^n_{b/n}$ Position of $\{\mathrm{b}\}$ with respect to $\{\mathrm{n}\}$ expressed in $\{\mathrm{n}\}$

Θ_{nb} Euler angles between $\{\mathrm{n}\}$ and $\{\mathrm{b}\}$

The position and orientation vectors in the NED frame are defined as

$$p^n_{b/n} := \begin{bmatrix} N \\ E \\ D \end{bmatrix} \in \mathbb{R}^3 \qquad \Theta_{nb} := \begin{bmatrix} \phi \\ \theta \\ \psi \end{bmatrix} \in \mathcal{S}^3 \tag{2.22}$$

where $\mathbb{R}^3$ is the three dimensional Eucledian space and $\mathcal{S}^3$ is a sphere with the three Euler angles defined in the range [0, 2π].

The body fixed velocities are defined as

$$v_{b/n}^{n} := \begin{bmatrix} u \\ v \\ w \end{bmatrix} \in \mathbb{R}^3 \qquad \omega_{b/n}^{n} := \begin{bmatrix} p \\ q \\ r \end{bmatrix} \in \mathbb{R}^3 \tag{2.23}$$

To transform the body velocities of the vessel into the NED frame, this transformation, retrieved from Fossen (2011), can be used:

$$R_b^n(\Theta_{nb}) := R_{z,\psi} R_{y,\theta} R_{x,\phi} \tag{2.24}$$

where

$$R_{x,\phi} = \begin{bmatrix} 1 & 0 & 0 \\ 0 & cos(\phi) & -sin(\phi) \\ 0 & sin(\phi) & cos(\phi) \end{bmatrix} \tag{2.25}$$

$$R_{y,\theta} = \begin{bmatrix} cos(\theta) & 0 & sin(\theta) \\ 0 & 1 & 0 \\ -sin(\theta) & 0 & cos(\theta) \end{bmatrix} \tag{2.26}$$

$$R_{z,\psi} = \begin{bmatrix} cos(\psi) & -sin(\psi) & 0 \\ sin(\psi) & cos(\psi) & 0 \\ 0 & 0 & 1 \end{bmatrix} \tag{2.27}$$

We can now express the body velocities in NED as

$$\dot{p}_{b/n}^{n} = R_b^n(\Theta_{nb}) v_{b/n}^{b} \tag{2.28}$$

To transform the body angular velocities of the vessel into the NED frame, this transformation, retrieved from Fossen (2011), can be used:

$$T_\Theta(\Theta_{nb}) = \begin{bmatrix} 1 & sin(\phi)tan(\theta) & cos(\phi)tan(\theta) \\ 0 & cos(\phi) & -sin(\phi) \\ 0 & sin(\phi)/cos(\theta) & cos(\phi)/cos(\theta) \end{bmatrix} \tag{2.29}$$

.

One important note is that Equation (2.29) is not defined for $\theta \pm 90°$. The body angular velocity in terms of NED can now be expressed as

$$\dot{\Theta} = T_\Theta(\Theta_{nb}) \omega_{b/n}^{b} \tag{2.30}$$

Combining Equations (2.28) and (2.30), we get

$$\begin{bmatrix} \dot{p}^n_{b/n} \\ \dot{\Theta} \end{bmatrix} = \begin{bmatrix} R^n_b(\Theta_{nb}) & 0_{3x3} \\ 0_{3x3} & T_\Theta(\Theta_{nb}) \end{bmatrix} \begin{bmatrix} v^b_{b/n} \\ \omega^b_{b/n} \end{bmatrix} \tag{2.31}$$

.

If we now rewrite Equations (2.22) and (2.23) as

$$\eta := \begin{bmatrix} p^n_{b/n} \\ \Theta_{nb} \end{bmatrix} \qquad \nu := \begin{bmatrix} v^n_{b/n} \\ \omega^n_{b/n} \end{bmatrix} \tag{2.32}$$

we can represent the transformations with the following notation from Fossen (2011):

$$\dot{\eta} = J_\Theta(\eta)\nu \tag{2.33}$$

2.8.2 Rigid-Body Kinetics

Kinetics is the analysis of the forces causing a craft to move (Fossen (2011)). Marine vessels described in this report can be defined as rigid-body and this section will therefore describe rigid-body kinetics, which can be expressed according to Fossen (2011):

$$M\dot{\nu} + C(\nu)\nu + D(\nu)\nu + g(\eta) + g_0 = \tau + \tau_{wind} + \tau_{wave} \tag{2.34}$$

The terms of equation (2.34) represents:

- $M = M_{RB} + M_A$. M_{RB} is the vessel's rigid body inertia matrix. M_A is the added mass intertia matrix, included due to the inertia of the surrounding fluid (Alme (2008)).
- $C(\nu) = C_{RB}(\nu) + C_A(\nu)$. Coriolis-centripetal matrices. They describe the rotational motion in the reference frame not fixed to the intertial body frame (Alme (2008))
- $D(\nu) = D_N(\nu) + D_{NL}(\nu)$. Linear and nonlinear damping matrices. Mainly caused by potential damping, hull skin friction, wave drift damping and vortex shredding (Alme (2008)).
- $g(\eta)$. Vector of gravitational and buoyancy forces and moments. Called restoring forces and moments in hydrodynamic terminology (Fossen (2011).
- g_0 is used for pretrimming and ballast control.
- τ is the vector of control inputs, representing the thrust forces.
- τ_{wind} and τ_{wave} describes the environmental disturbance forces from wind and waves, respectively.

2.8.3 Simplified 3 DOF Model

By doing some assumptions, the 6 DOF model described earlier can be reduced to the 3 DOF horizontal model used in the simulator, presented in Section 3.2. Alme (2008) includes the following assumptions

1. The origin of the BODY frame is assumed to be at the geometric center point(CP) of the vessel structure
2. $y_g = 0$: A surface vessel is normally designed with a port-starboard symmetry. This will place the center of gravity along the x-axis. Hence $y_g = 0$.
3. Roll and pitch angles neglected: By assuming the vessel is longitudinally and laterally meta-centrically stable with small amplitudes $\phi \approx \theta \approx \dot{\phi} \approx \dot{\theta} \approx 0$, the dynamics in roll and pitch can be neglected. This implies that the rotation matrix $J_\Theta(\eta)$ in Equation (2.33) can be reduced to only a rotation along the z-axis $R_{z,\psi}$. The restoring forces and moments in surge will be a function of $sin\theta$. Sway and yaw will be a function of $cos\phi$. Since $sin\theta \approx cos\phi \approx 0$, $g(\eta) \approx 0$ for the 3 DOF model.
4. $z = 0$: For a surface vessel the mean heave position is $z = 0$, the the heave dynamics can be neglected.

Employing these assumptions leads to the following ship kinematics, used in the simulator (Rokseth (2022)):

$$\dot{\eta} = R_z(\psi)\nu \tag{2.35}$$

where

$$\eta = \begin{bmatrix} N \\ E \\ \psi \end{bmatrix} \qquad \nu = \begin{bmatrix} u \\ v \\ r \end{bmatrix} \tag{2.36}$$

and $R_z(\psi)$ is given by 2.27

The ship kinetics is simplified to

$$M\dot{\nu} + C_{RB}(\nu)\nu - C_A(\nu_r)\nu_r + D_L\nu_R + D_{NL}(\nu_R)\nu_r = \tau_w + \tau_r + \tau_p \tag{2.37}$$

where

$$M = M_{RB} + M_A = \begin{bmatrix} m - X_{\dot{u}} & 0 & 0 \\ 0 & m - Y_{\dot{v}} & mx_g \\ 0 & mx_g & I_z - N_{\dot{r}} \end{bmatrix} \tag{2.38}$$

is the ships mass matrix,

$$C_{RB}(\nu) = \begin{bmatrix} 0 & 0 & -m(x_g r + v) \\ 0 & 0 & mu \\ m(x_g r + v) & -mu & 0 \end{bmatrix} \tag{2.39}$$

is the Coriolis matrix,

$$C_A(\nu_r) = \begin{bmatrix} 0 & 0 & Y_{\dot{v}v_r} \\ 0 & 0 & -X_{\dot{u}u_r} \\ -Y_{\dot{v}v_r} & X_{\dot{u}u_r} & 0 \end{bmatrix} \tag{2.40}$$

is the Coriolis added mass matrix, and

$$D_L = \begin{bmatrix} m/T_N & 0 & 0 \\ 0 & m/T_E & 0 \\ 0 & 0 & m/t_\psi \end{bmatrix} \qquad D_{NL} = \begin{bmatrix} K_u u & 0 & 0 \\ 0 & K_v v & 0 \\ 0 & 0 & K_r r \end{bmatrix} \tag{2.41}$$

are the linear and non-linear damping matrices, where $T_N, T_E, T_\psi, K_u, K_v, K_r$ are coefficients.

τ_w are the wind forces calculated based on the ship's projected area towards the wind:

$$F = 0.5\rho_a v_w^2 c_d A_p \tag{2.42}$$

where ρ_a is the density of the air, v_w is the relative wind speed in the direction of F, c_d is the drag coefficient in air and A_p is the projected are of the ship in the wind direction.

$\tau_r = [0, F_v, F_r]^T$ are the rudder forces acting in sway and yaw according to

$$F_v = c_v \delta (u - u_c) \qquad F_r = c_r \delta (u - u_c) \tag{2.43}$$

where c_v and c_u are coefficients, $u - u_c$ is the velocity of a water particle in the direction of the longitudinal axis relative to the surge speed, and δ is the rudder angle.

$\tau_p = [F_p, 0, 0]^T$ is the propulsion force acting in surge. This is modelled using the following shaft dynamics

$$J_p \dot{\omega}_p = \frac{1}{\tau_{ME}}(\tau_{ME} - d_{ME}\omega_p) + \frac{1}{r_{HSG}}(\tau_{HSG} - d_{HSG}\omega_p) - k_p \omega_p^2 \tag{2.44}$$

The trust force F_p is given by

$$F_p = D_p^4 K_T \omega_p |\omega_p| \tag{2.45}$$

where D_p is the diameter of the propeller, K_T is a constant, and ω_p is the propeller rotation speed.

2.8.4 LOS Guidance

To be able to navigate through a predefined set of waypoints, the simulator use lookahead-based Line-of-Sight(LOS) guidance. This is a navigation strategy where the simulated vessel follows a predetermined set of waypoints. If the next waypoint is within a specified distance, the vessel will head directly towards it. If the waypoint is farther away, the vessel will instead head towards the straight line between the previous and next waypoints. This principle is illustrated in Figure 2.8, and further explained in Lekkas and Fossen (2013), Breivik and Fossen (2009), Breivik (2010), Fossen (2011).

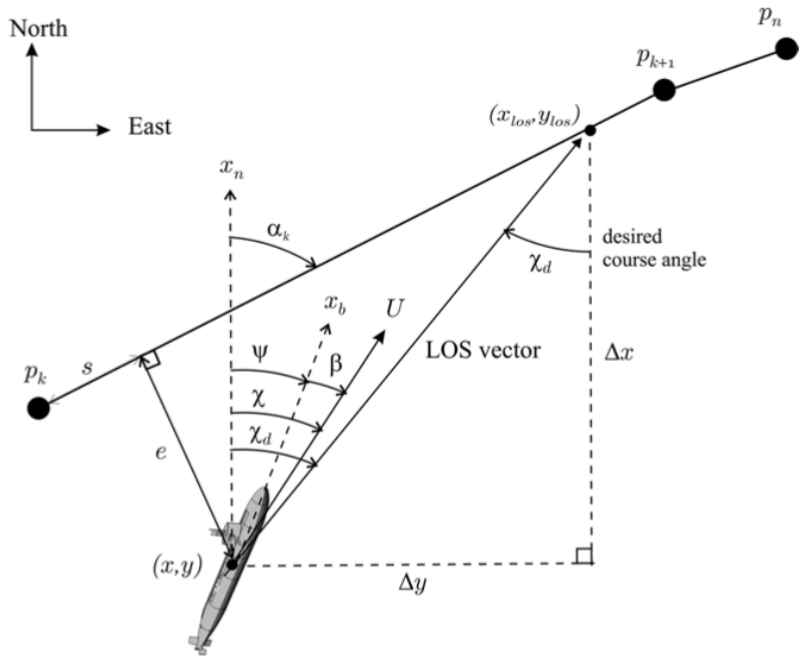

Figure 2.8: Figure explaining LOS guidance, with relevant variables. Retrieved from Fossen (2011)

The desired course angle, $\chi_d(e)$, is given by

$$\chi_d(e) = \chi_p + \chi_r(e) \tag{2.46}$$

where χ_p is the path-tangential angle and χ_r is the velocity-path relative angle. Consider a straight line path shown in Figure 2.8, implicitly defined by the two waypoints $p_k^n = [k_x, y_k]^T$ and $p_k^n = [k_{x+1}, y_{k+1}]^T$. Then

$$\chi_p = \alpha_k = atan2(y_{k+1} - y_k, x_{k+1} - x_k) \tag{2.47}$$
$$\tag{2.48}$$

χ_r is defined as

$$\chi_r(e) := arctan\left(\frac{-e}{\Delta}\right) \tag{2.49}$$

where

$$e(t) = [y(t) - y_k]cos(\chi_p) - [x(t) - x_k]sin(\chi_p) \tag{2.50}$$
$$\Delta(t) = \sqrt{R_{LOS}^2 - e(t)^2} \tag{2.51}$$

e is the crosstrack error and R_{LOS} is the pre-defined lookahead radius.

The vessel has a radius of acceptance, R_a, around each waypoint. If the vessel is positioned inside this radius of acceptance, the waypoint is considered reached. Mathematically expressed, the waypoint is considered reached if and only if

$$[x_{k+1} - x(t)]^2 + [y_{k+1} - y(t)]^2 \leq R_a^2 \tag{2.52}$$

3

Simulation-Based, Risk-Influenced Path Planning Framework

This chapter presents the proposed framework for the simulation based optimization of path based on grounding risk analysis. The framework is further developed in several case studies in Chapter 4.

The chapter begins a brief introduction to the framework by illustrating its application through an example. Then, in Section 3.1, failure modes are discussed. The proposed framework is simulation-based, and in Section 3.2, we present the simulator that has been developed as an integral part of this framework.

To assess the risk associated with grounding, we establish metrics for both the likelihood of a vessel's loss of propulsion (Section 3.3) and the potential consequences of such an event (Section 3.4). These metrics are then combined in Section 3.5 to form a risk assessment for a given route. Finally, in Section 3.8, we discuss the expression and minimization of a cost function to identify the optimal path from a set of predefined routes.

The essence of the method proposed by the framework presented in this report are the following steps:

1. Identify a set of possible failure modes. This is discussed in Section 3.1.
2. Identify critical sections of the route. This might for example be sections where islands or reefs are directly in, or close to, the suggested route.
3. For each critical section, identify a set of suitable paths to follow in order to avoid the obstacles.
4. Estimate the grounding risk associated with each of the paths. The risk is determined by simulating all failure modes with a given frequency, calculating the consequence

(Section 3.4). Thereafter, the probabilities for each failure mode are taken into account (Section 3.3). This forms a risk metric for each path.

5. Optimize the choice of path based on the estimated risk, as well as fuel consumption and time usage.

Figure 3.1 shows the path of a vessel navigating through a set of obstacles. This figure is used as an example to further explain the proposed framework. The sections of the route that are close to the objects O1, O2 and O3 may be considered critical sections. Lets further focus on the critical section around object O3. The illustration shows two separate paths, labeled I and II, that the vessel can follow to avoid the obstacle.

The grounding risk associated with each route is evaluated by simulating all potential failure modes at each point along the route. For example, if we consider the north route and a loss of propulsion occurs early on, it is likely to result in the vessel grounding, which would have a high consequence. We will then estimate the probability of each failure mode occurring. A loss of propulsion might for example be predicted to occur once every year. Finally, the risk metric will be calculated by combining the consequence of each failure mode with the probability of that failure mode occurring. The final step is the optimization of the choice of path. With the environmental forces working in the eastwards direction, the result would likely be that route II involves less risk, as the vessel is drifting away from the obstacle in the case of loss of propulsion. Path I is, however, faster and more fuel effective. The optimal path therefore depends on the optimization algorithms implemented and the priorities of the ship operator.

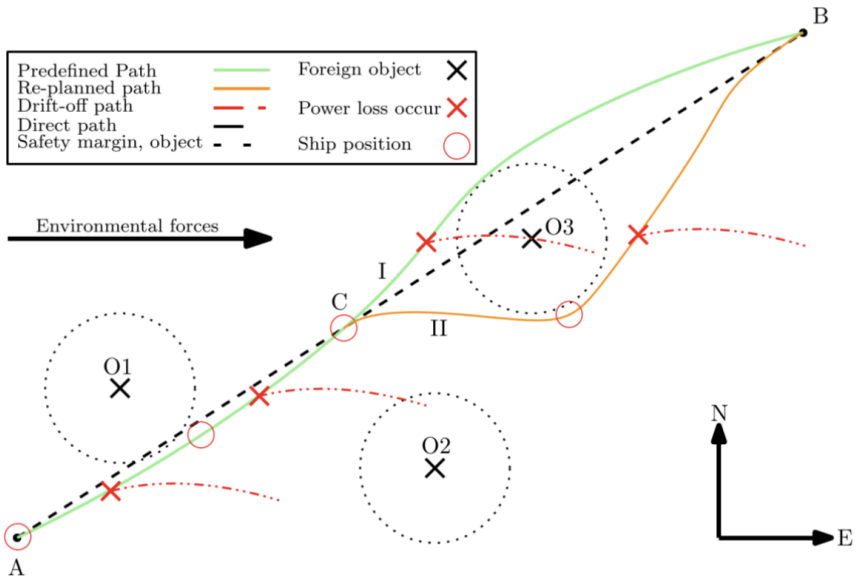

Figure 3.1: Illustration of a ship following a given path. Loss of propulsion incur at different points in time. Retrieved from Fossdal (2018)

In the case of manual operation, the framework would be implemented in the following way: Before the sailing mission, a human operator would manually go through the route, identifying critical sections. Then, the operator would manually identify the possible paths the vessel can travel in order to avoid the obstacles in that area. Based on the weather forecast, the paths can now be simulated to obtain the estimated risks of sailing the paths. At the day of the sailing mission, the vessel can use its own sensors and updated information about environmental factors to update the estimated risk. This risk is combined with the simulated fuel consumption and time usage to estimate the optimal path.

3.1 Failure Modes

The development of a robust risk model necessitates an understanding of the ways in which a vessel can fail. According to Friis-Hansen et al. (2008), the primary causes for a ship losing command control are 'rudder stuck' and 'blackout of the main engine'. These failure modes have been incorporated into the risk analyses of multiple studies, such as Fossdal (2018) and Løite (2022).

However, a critical evaluation of the risk assessment framework presented in Løite (2022) revealed certain limitations with rudder freeze simulations. The simulation attempted to direct the ship towards the next waypoint, which could potentially lead to grounding. However, in reality, a more strategic response would be to maintain the vessel's current position while initiating emergency procedures. This aspect of decision-making is not accounted for in the simulation.

Moreover, the simulation's outcomes are highly sensitive to the specific circumstances of rudder freezing. A slight alteration in the rudder's position could drastically change the simulation results, adding a layer of complexity to its effective representation.

Considering the aforementioned complexities, this thesis specifically concentrates on the loss of propulsion as the sole failure mode. It is worth noting that throughout this thesis, the term 'blackout' is used interchangeably with the concept of a loss of propulsion. Implementing loss of propulsion as the sole failure mode simplifies the risk analysis while still providing substantial insights into the risk landscape of marine navigation. Yet, it is important to recognize that the risk model's scope could be extended to include additional failure modes if necessary. This adaptability is integral to the model's design, ensuring that it can evolve in response to the growing understanding of risks in marine navigation.

Establishing the duration of the propulsion loss is a critical aspect of our risk analysis, with the parameters needing to be tailored according to the individual vessel and its capacity for recovery post-failure. As a guiding principle, we turn to *The Rules for Classification of Ships - Dynamic Positioning Systems* (DNV GL (2014)), which stipulate that Dynamic Positioning (DP) vessels should be capable of regaining thrust within a 45-second window following a blackout.

The established recovery time for DP vessels can be used as a reference point for estimating recovery times for other vessel types. However, it should be acknowledged that vessels in transit may not be as constrained by strict recovery timings as DP vessels. Con-

sequently, one could argue that transit vessels might endure propulsion losses extending over a more extended period.

That said, the exact duration of failure modes remains an important and complex parameter that warrants further exploration. It will be a subject of in-depth discussion in subsequent chapters, specifically in Chapters 4 and 5.

3.2 Simulator

To develop the simulation-based path-planning framework, it is crucial to establish a comprehensive simulation framework for surface vessels. This framework should fulfill the following criteria:

1. **Degree of Freedom:** It should model the vessel with at least 3 degrees of freedom, utilizing the theoretical groundwork discussed in Section 2.8.
2. **Environmental Model:** It should incorporate an environmental model accounting for wind and current conditions.
3. **Guidance System:** It should possess a competent guidance law capable of adhering to a predetermined route composed of waypoints.
4. **Failure Mode Simulation:** It should be able to simulate the failure modes as outlined in Section 3.1.
5. **Programming Language:** Python should be the chosen language for the simulator's implementation due to its open-source nature, free accessibility, and wider usage compared to MATLAB.
6. **Sea Depth Mapping:** It should be capable of implementing and visualizing map data concerning sea depths.
7. **Grounding Risk Estimation:** The simulator should be capable of estimating the risk of grounding accidents, including the usage of Bayesian Networks.
8. **Ecologically Sensitive Areas:** Finally, the simulator should have the capacity to implement special treatment for areas that are deemed ecologically sensitive.

Bø et al. (2015) discuss a number of possible simulators for marine vessels. However, none of these appear to satisfy the comprehensive list of requirements stipulated. The marine vessel simulators detailed in Fossdal (2018) and Rasmussen (2019) also do not seem to meet the requirements in their entirety. Additionally, the full implementation details for these simulators are not readily accessible, and both are designed using MATLAB, rather than the desired Python.

The Open Simulation Platform (OSP), an "open-source initiative for co-simulation of maritime equipment and entire ships" (Open Simulation Platform (2023)), was another potential choice. OSP's simulation library and associated tools are primarily based in C++, without Python wrappers to support compatibility with the current study's requirements.

Despite its capabilities, OSP's complexity and focus on extensive maritime systems exceeds the specific needs of this project. Moreover, the challenge of integrating OSP with methodologies like Bayesian Networks for risk estimation could pose significant difficulties. Furthermore, OSP's flexibility in accommodating custom requirements, such as unique treatments for ecologically sensitive areas, is uncertain.

Thus, despite its strengths, OSP's compatibility issues, integration challenges, and potential limitations in customization rendered it unsuitable for this project.

The simulator presented by Rokseth (2022) proved to be a promising foundation for the current study due to its close alignment with the established requirements. This Python-based simulator models marine surface vessels in 3 DOF and integrates models for both wind and current, utilizing Line of Sight (LOS) guidance for navigation through predefined waypoints. However, it lacked certain functionalities, such as simulating the failure modes specified in Section 3.1, integrating real-life depth data, defining ecologically sensitive areas, and supporting Bayesian Networks.

To address these gaps, a customized version of the Rokseth (2022) was developed. Modifications included the introduction of a framework to simulate the aforementioned failure modes and an API to incorporate real-life depth data, enhancing the simulator's visualization capabilities. Additionally, the capacity to define ecologically sensitive areas was integrated, contributing to a more accurate risk assessment. To facilitate Bayesian Networks, the SMILE library from BayesFusion (BayesFusion LLC (2023)) was incorporated.

The developed simulator encapsulates the ship's motion in three degrees of freedom (DOFs): surge, sway, and yaw. The six states represented are:

- North position (meters)
- East position (meters)
- Yaw angle (radians)
- Surge speed (meters per second)
- Sway speed (meters per second)
- Turn rate (radians per second)

The ship model features a single propeller shaft and a solitary rudder. The propeller shaft can be energized either by the main power source, typically a diesel engine, or a hybrid shaft generator. This hybrid shaft generator, when operating as a motor, is powered by an electrical distribution system typically backed by a set of diesel generators (Rokseth (2022)). However, for the purpose of this study, only the main power source is utilized in the simulations. The inclusion of the hybrid shaft generator presents a compelling approach for future work.

The employed equations of motion encompass inertial forces, forces induced by the added mass effect, Coriolis forces, linear and non-linear friction forces, environmental forces, and control forces originating from the main propeller and rudder (Rokseth (2022)). Further details regarding the mathematical modeling applied within the simulator can be found

in Section 2.8.

The simulator subjects the ship to constant environmental forces, specifically those derived from wind and current.

Accompanying the simulator is a controller capable of navigating through a series of waypoints utilizing Line of Sight (LOS) guidance, elaborated on in Section 2.8.4.

It is important to note that the simulator does not include any collision avoidance mechanism. Its singular objective is to traverse the predetermined waypoints, and it is fundamentally oblivious to potential obstructions. This lack of situational awareness may result in unexpected outcomes, further discussed in Section 5.1.

To simulate blackout scenarios, the maximum shaft speed of the throttle controller was decreased to zero. It is possible to initiate this blackout at any point along the pre-defined route and also to observe the vessel's behavior post-recovery. However, given the absence of a collision avoidance system, the vessel's response may lack realism. For instance, in an effort to rejoin the original route, it might head directly towards an obstacle. Consequently, the utility of these post-recovery simulations may be limited due to these potential inaccuracies.

3.2.1 Integration of Electronic Navigational Charts

The Python API, *Seacharts* (Blindheim (2021)), is designed to read and process spatial depth data from FileGDB files, transform them into shapefiles, and present the resultant data in an easily comprehensible format.

Integration of this API into the simulator serves two principal objectives:

1. Incorporation of authentic depth data from the Norwegian coast into the simulations.
2. Visualization of simulation results in a clear and informative manner.

The Seacharts API utilizes an FGDB file populated with depth data to execute simulations. The depth data for the *Møre og Romsdal* county, sourced from Norwegian Mapping Authority (2023), is utilized as an example in this case. Figure 3.2 presents the corresponding data, while Table 3.1 provides a description of each included element. The vessel's position and direction are recorded at 30-second intervals and portrayed on the map. The depicted vessel sizes are accurate, though they may appear small and could potentially be mistaken for minor line segments.

3.3 Likelihood of Blackout

In order to establish the risk metric presented in Section 3.5, it is necessary to assess a metric that can estimate the probability of a blackout occurrence in a specific scenario. In this thesis, this probability is determined through a two-step procedure.

The first component of this methodology involves developing a Bayesian Network, inspired by Rasmussen (2019), to calculate a blackout utility metric for a ship. This prob-

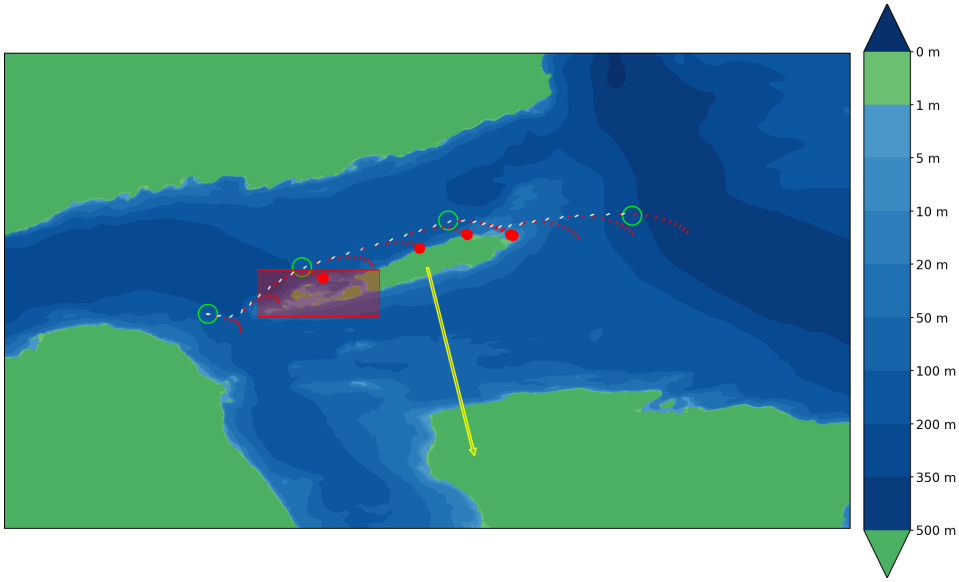

Figure 3.2: Example of *Seacharts*-implementation. The elements are described in Table 3.1

Table 3.1: Explanation of components depicted in the Seachart example implementation displayed in Figure 3.2

Yellow arrow	Direction and speed of current
Green circle	Waypoint
Red circle	Grounded vessel
Red rectangle	Ecologically sensitive area
White vessel	Original route without failures
Red vessel	Blackout simulation

abilistic model incorporates various inputs such as site-specific wind and current conditions, Flag of Registry, Vessel Age, and Vessel Type. The latter three parameters utilize data from Cariou et al. (2008) to estimate a deficiency metric. These combined inputs result in the calculation of a blackout metric, which represents the blackout probability and ranges between 0.598 and 1.273.

Figure 3.3 illustrates the Bayesian Network, with the joint probability tables constructed to the best of the author's ability using data from Section 2.4. It is important to note that the Bayesian Network does not precisely mirror real-world blackout likelihood for a specific vessel in a specific environment.

In the second step of the process, the contextual background for the blackout probabilities is explored, as discussed in Section 2.4. Two studies are reviewed to provide insights into the blackout frequencies.

Friis-Hansen et al. (2008) indicates an annual blackout frequency of 0.75 for non-passenger

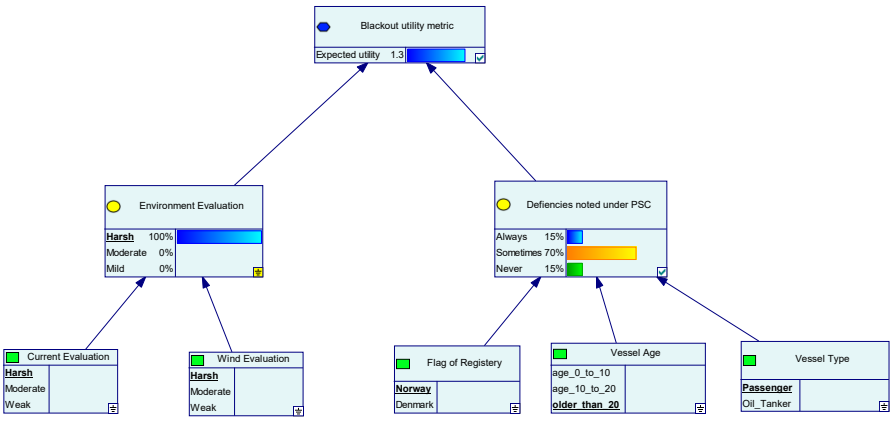

Figure 3.3: Bayesian Network for estimation of blackout utility. Displayed using the Genie Modeller (BayesFusion LLC (2023))

vessels and 0.1 for passenger vessels. Bolbot et al. (2021) provides a broader perspective, reporting a frequency of approximately 1.4 blackouts per ship annually during the harbor phase and a significantly lower rate of 0.003 during sailing. This suggests the potential for differentiating blackout frequencies based on vessel type and operational phase, which could be a focus for future research. However, for the purposes of this thesis, the general blackout frequency of 0.4 per ship annually, as found by Bolbot et al. (2021), is adopted.

To convert the annual blackout frequency of 0.4 per ship into a per-second metric, Equation (3.1) is applied, assuming continuous ship operation throughout the year. This assumption aligns with the concepts endorsed by Friis-Hansen et al. (2008) and Bolbot et al. (2021). Adjustments to account for different operational levels can be made with minimal effort.

$$\frac{0.4 \frac{blackouts}{ship \cdot year}}{365 \text{ days} \cdot 24 \text{ hours} \cdot 3600 \text{ seconds}} = 1.3 \cdot 10^{-8} \frac{blackouts}{ship \cdot seconds} \tag{3.1}$$

The thesis assumes that the probability of a blackout under specific circumstances is obtained by multiplying the blackout metric with the base blackout probability, as shown in (3.2). This approach allows for the assessment of blackout risk under different conditions, providing nuanced insights into the ship's reliability in the face of varying operational and environmental factors.

$$P = U_{blackout} \cdot 1.3 \cdot 10^{-8} \frac{blackouts}{ship \cdot seconds} \tag{3.2}$$

3.4 Consequence Analysis

In order to evaluate the grounding risk a vessel incurs on a specific route, it is necessary to determine the consequences of possible scenarios. One approach to achieving this, as described by Rasmussen (2019), involves calculating the vessel's distance to the nearest obstacle at each time step throughout the simulation. The smallest distance over the entire simulation is then compared to three pre-determined consequence level radii, which determines the overall consequence level of the simulation. Alternative methods for assessing consequence are proposed by Bø et al. (2016) and Fossdal (2018).

This thesis introduces a more refined approach to consequence analysis, drawing from the concepts proposed by Dong and Frangopol (2015) and Liu and Frangopol (2018). Here, the ultimate consequence of an incident is determined considering the environmental, economic, and social implications of the event.

The consequence analysis starts by evaluating the structural damage to the ship, which serves as the foundation for assessing the environmental, economic, and social consequences. In contrast to the approach used by Liu and Frangopol (2018) that incorporates the geometric characteristics of the damage to estimate damage states, this thesis takes a different approach. The complexity of simulating the geometric characteristics of damage is considered outside the scope of this thesis. Instead, a Bayesian Network has been developed to predict the resulting damage state based on various factors related to the accident. These factors include vessel type, vessel speed, and the material of the surface with which the vessel collides. By considering these factors, the Bayesian Network provides a probabilistic prediction of the damage state resulting from the accident. This alternative approach allows for a more practical and manageable methodology to assess the consequences of ship grounding incidents.

The Bayesian Network is shown in Figure 3.4. It is used to estimate the damage state of a grounded vessel and incorporates different variables that influence the extent of damage during a grounding incident. In this thesis, these variables are chosen:

- **Speed of the Vessel:** The higher the speed at the time of grounding, the more energy the vessel has, which can cause more severe structural damage.
- **Ground Material:** The material of the ground on which the vessel grounds can significantly affect the extent of damage. For instance, grounding on a rocky area may cause more damage than grounding on a sandy or muddy seabed.
- **Environmental Conditions on the Grounding Site:** Weather and environmental conditions on the grounding site, including factors like wave height, wind speed, and current, can significantly influence the grounding impact. For instance, rough weather might exacerbate the grounding damage by causing the vessel to repeatedly slam against rocks or impede timely rescue and towing operations, leading to extended periods of hazardous exposure.

Although these variables offer a solid foundation for estimating grounding damage, additional parameters could be incorporated for a more nuanced and accurate analysis. This, however, extends beyond the scope of this thesis and is suggested as a topic for further

research.

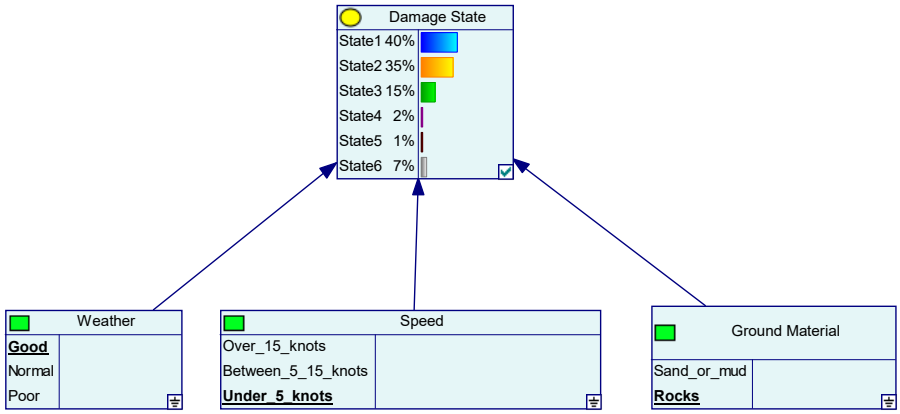

Figure 3.4: Bayesian Network for determining Damage State

The damage states derived from the Bayesian Network form the basis for assessing the environmental, economic, and social consequences resulting from a grounding event. Each damage state has distinct implications across these three domains. In the environmental perspective, the severity of the damage state informs the potential ecological damage, ranging from minor disturbances to severe contaminations that threaten marine ecosystems. In the economic sphere, both direct and indirect costs are considered, with damage states influencing the potential financial impact from repairs and compensation to broader trade disruptions. The social assessment finally contemplates potential fatilities and injuries. Here too, the severity of the grounding event, as described by the damage state, directly impacts the magnitude and nature of social consequences.

The total consequence of a particular grounding incident can be quantified using Equation (3.3). In this equation, C_{env}, C_{soc}, and C_{eco} correspond to the environmental, social, and economic consequences, respectively. The weighting parameters u, v, and w provide flexibility for operators to adjust according to their specific priorities.

$$C_{grounding} = uC_{env} \cdot vC_{soc} \cdot wC_{eco} \tag{3.3}$$

3.4.1 Environmental Consequence

In this thesis, environmental consequence is evaluated in two key dimensions: the physical impact of the ship and the consequences arising from chemical spills. The physical impact of a ship grounding can cause direct harm to marine ecosystems, while chemical spills, particularly of oil or other harmful substances, can have more far-reaching, long-term effects. Both aspects of environmental consequence are vital in assessing the broader ecological implications of a grounding incident.

In the assessment of environmental consequences, we begin by examining the impact of the physical interaction between the ship and the environment. Drawing on the background theory presented in Section 2.5.1, the estimated consequence resulting from the ship's impact on the environment can be calculated based on the extent of the damaged area and a prescribed environmental fine. This relationship is shown in Equation (3.4).

$$C_{impact} = c_{env} \cdot Q_{area} \tag{3.4}$$

Here, c_{env} represents the assumed fine in USD per square meter of damaged area, while Q_{area} refers to the area affected, measured in square meters. The value of c_{env} is set to USD 300 for ecologically sensitive areas and USD 120 for other areas. The determination of Q_{area} is based on the values provided in Table 3.2.

Table 3.2: Affected area of grounding given damage state of the vessel.

Damage state (DS_i)	1	2	3	4	5	6
Affected area (m^2)	100	200	300	400	500	600

In the case of vessels transporting hazardous chemical cargo, it is important to consider the environmental consequences that arise from the potential spillage of chemicals. Evaluating these consequences involves quantifying the cost associated with the cleanup of any spilled substances, as detailed in Section 2.5.1. Equation (3.5) presents a mathematical representation of this calculation:

$$C_{spill} = c_{spill}(Q_{spill}) \tag{3.5}$$

where c_{spill} is the cleanup cost of the spilled chemical per ton and Q_{spill} is the tonnage of spilled chemical.

In the context of this thesis, we utilize an oil tanker as a case study to illustrate this scenario. The quantity of oil spilled as a result of a grounding incident can be estimated based on the method suggested by Liu and Frangopol (2018), encapsulated by Equation (3.6). This accounts for both the size of the tanker's tank and the number of tanks breached in a given damage state.

$$Q_{spill} = Q_i N_{DS_i} \tag{3.6}$$

where Q_i is the size of one tank and N_{DS_i} is the number of tanks penetrated in the given damage state.

The subsequent cleanup cost due to the oil spill is then calculated using Equation (3.7), which is obtained from Liu and Frangopol (2018). This equation provides an estimate of the cost based on the tonnage of oil spilled.

$$C_{spill}(x) = 24020x^{0.8447} \tag{3.7}$$

Here, $x = Q_{spill}$ represents the tonnage of oil spillage, calculated using Equation (3.6).

Ultimately, the total environmental consequence can be expressed as the sum of the impact of the ship on the environment and the cleanup cost of the oil spill, as shown in Equation (3.8):

$$C_{env} = c_{env}Q_{area} + c_{spill}(Q_{spill}) \tag{3.8}$$

3.4.2 Social Consequence

After exploring the environmental consequences of a grounding incident, the attention turns to its social implications. Central to these social consequences is the potential impact on human life, particularly that of the ship's crew. The magnitude of these consequences can be assessed by examining the occurrence of crew fatalities and non-fatal injuries resulting from such incidents, as discussed in Section 2.5.2. To evaluate the overall social consequences, a general equation capturing the combined impact of crew fatalities and non-fatal injuries can be expressed as Equation (3.9)

$$C_{soc} = C_{LL} + C_{inj} \tag{3.9}$$

We first discuss the estimated consequences of crew fatalities in a given grounding scenario. The rate of fatalities is determined based on the severity of the ship's damage state, denoted as DS_i. To quantify the consequences resulting from the loss of life, denoted as C_{LL}, Equation (3.4.2) is utilized, sourced from COWI (2008). In this equation, N_{ll} represents the number of fatalities, while V_{ll} represents the monetary value assigned to a statistical life. For a grounding incident, we anticipate the average number of fatalities, denoted as $E[N_{ll}|oil\ spillage]$, to be 0.01 for damage states $i \geq 3$. Furthermore, based on the findings in Skjong et al. (2005), the value of a statistical life, V_{ll}, is set at USD 3 million for the purpose of this thesis.

$$\begin{gathered} C_{LL} = N_{ll}V_{ll} \\ E[N_{ll}|oil\ spillage] = E[N_{ll}|DS_i; i >= 3] = 0.01 \\ V_{ll} = USD\ 3\ mill \end{gathered} \tag{3.10}$$

Furthermore, the social consequences of grounding extend to non-fatal injuries suffered by the crew. As elaborated in Section 2.5.2, estimates from US Coast Guard (2009) suggest an average of 2.0 crew injuries per incident. The associated cost per injury is placed at

USD 60,000, based on the study by Liu and Frangopol (2018). This allows us to quantify the consequence of non-fatal injuries, C_{Inj}, as given in Equation (3.4.2). Here, N_{inj} represents the number of injured crew members and c_{inj} is the cost per injured individual.

$$\begin{aligned} C_{Inj} &= N_{inj} c_{inj} \\ E[N_{inj}] &= 2.0 \\ c_{inj} &= USD\ 60,000 \end{aligned} \tag{3.11}$$

Combining the consequences from fatalities and non-fatal injuries results in the total social consequence, C_{soc}, of a grounding incident, as shown in Equation (3.12). This summation embodies the societal impact, offering a more comprehensive understanding of the potential human toll in a grounding event.

$$C_{soc} = N_{ll} V_{ll} + N_{inj} c_{inj} \tag{3.12}$$

3.4.3 Economical Consequence

Moving beyond the social impact, a grounding event also has substantial economic implications. The assessment of economic consequences in this thesis is based on the damage state of the ship, and revolves around three major factors: repair costs, lost revenue during the repair period, and loss of cargo. These factors are important in evaluating the financial viability of marine operations and contribute significantly to the overall risk assessment. To quantify the overall economic consequence, Equation (3.13) is employed and will be further expanded in this section. The theory utilized in this section is derived from Section 2.5.3, where the assessment of economic consequences is discussed in detail.

$$C_{eco} = C_{RC} + C_{LE} + C_{LC} \tag{3.13}$$

Repair costs form a major component of the economic consequences, encompassing the expenses associated with restoring the ship to its pre-incident condition. Additionally, the lost revenue during the repair period due to the ship's downtime disrupts operations and leads to a loss of income. Furthermore, the loss of cargo resulting from the grounding event adds to the financial implications, requiring additional costs for cargo handling and potential financial losses for shipping companies or cargo owners.

To estimate repair costs, a modified version of the formula employed in Liu and Frangopol (2018) is utilized, as depicted in Equation (3.14):

$$C_{RC} = RD_{DS_i} \cdot V_{ship} \tag{3.14}$$

In this equation, RD_{DS_i} represents the damage relative to the ship value, which can be found in Table 3.3. Meanwhile, V_{ship} denotes the value of the ship itself. By applying this equation, an estimation of the repair costs associated with the grounding incident can be obtained.

To estimate the economic loss resulting from the potential earning during the repair period, Equation (3.15) is employed, which is sourced from Liu and Frangopol (2018):

$$C_{LE} = t_{DS_i} \cdot c_{day} \tag{3.15}$$

In this equation, t_{DS_i} represents the repair days corresponding to the damage state of the ship, as provided in Table 3.3.

To determine the parameter c_{day}, this framework use the net daily earnings of the vessel, discussed in Section 2.5.3.

Table 3.3: Damage costs and repair times based on the damage state of the vessel

Damage state	Damage relative to ship value (RD_{DS_i})	Repair time (t_{DS_i})
1	0.01	7 days
2	0.02	14 days
3	0.025	21 days
4	0.04	30 days
5	0.1	40 days
6	0.2	50 days

The economic loss resulting from the loss of cargo can be calculated using Equation (3.16). In this equation, C_{LC} represents the cost of lost cargo, which is determined by multiplying the quantity of the lost cargo, denoted as Q_{loss}, by the price of the cargo per unit, represented by c_{cargo}.

$$C_{LC} = Q_{loss} c_{cargo} \tag{3.16}$$

For the specific case of oil tankers, the cost of lost cargo can be specifically calculated using Equation (3.17). In this equation, C_{LC} denotes the cost of the lost oil cargo, which is determined by multiplying the tonnage of spilled oil, denoted as Q_{spill}, by the price of crude oil per tonnage, represented by c_{oil}.

$$C_{LC} = Q_{spill} c_{oil} \tag{3.17}$$

The total economic loss of a grounding accident can then be expressed as

$$C_{eco} = RD_{DS_i} \cdot V_{ship} + t_{DS_i} \cdot c_{day} + Q_{loss} c_{cargo} \tag{3.18}$$

3.5 Risk Associated with Sailing a Specific Path

In this section, the risk associated with sailing a particular path is examined. The concept of risk, which is defined in Section 2.1, serves as the foundation for this analysis. In this thesis, for a given grounding incident, the risk is understood as the combination of the consequence of the incident and the probability of its occurrence.

The total simulated risk of a vessel traveling a particular path at a given time t along the original route, is calculated by simulating all failure modes. If the simulation leads to a grounding incident, the likelihood of that failure mode happening is multiplied by the estimated grounding consequence. In the specific case considered in this thesis where the sole failure mode considered is blackout, the estimation is expressed in Equation (3.19). Here, $P(Blackout_t)$ is the likelihood of a blackout happening at the time t and $C(Grounding_t)$ is the consequence of the corresponding grounding.

$$R_t := P(Blackout_t) \cdot C(Grounding_t) \tag{3.19}$$

In order to estimate the overall risk for a specific path, we evaluate the risk at each time step and sum these individual risks. This calculation is expressed in Equation (3.20). It's worth noting that a more comprehensive risk calculation would consider the dependency of events, namely, the likelihood of an event at a given time is affected if an event has already occurred at a previous time step. However, for simplicity, this report assumes that all events are independent.

$$R_{\text{total}} := \sum_{t}^{T} R_t \tag{3.20}$$

3.6 Cost Associated with Time Usage

In Section 2.6, the cost of additional time usage is examined from two perspectives. The first perspective focuses on the potential loss of earnings resulting from extended voyage duration. In the case studies presented in this thesis, the additional time usage is on a small scale, measured in seconds. It is assumed that saving this amount of time would not provide the vessel with enough time to undertake another journey. Therefore, the macro perspective of loss earnings due to time usage is not considered in the cost analysis, as discussed further in Chapter 5.

The micro perspective of the cost of additional time usage focuses on estimating the extra operating expenses that the vessel incurs during the extended time period. Based on data from Počuča (2006), which analyzed ships with an average Dead Weight Tonnage of 28,909, the average total daily operating cost was USD 5,378. This translates to an approximate cost per second of USD 0.06.

To calculate the cost of additional time usage, the operating cost per second (OC) is multiplied by the duration of the additional time usage (t), as shown in Equation (3.21).

$$C_{time} = OC \cdot t \tag{3.21}$$

3.7 Cost Associated with Fuel Consumption

To calculate the fuel consumption of the ship in the proposed framework, the approach presented by Rokseth and Utne (2023) was adopted. This method utilizes specific fuel consumption curves and has already been integrated into the simulator developed by Rokseth (2022). Fuel consumption theory is further discussed in Section 2.7.

3.8 Optimization of Path

In the context of marine navigation, the notion of the optimal path takes on a multidimensional meaning. It is not simply a question of the shortest or the fastest route but is an interplay between different, often competing, considerations. Specifically, in this thesis, we consider the risk of grounding, the fuel consumption, and the time spent on a given path as our primary metrics for evaluating a path's optimality. Each of these factors is integrated into a cost function that seeks to minimize the overall cost associated with a given navigation route.

The cost function is defined as:

$$C_{total} = \alpha C_{risk} + \beta C_{fuel} + \gamma C_{time} \tag{3.22}$$

where C_{total} is the total cost, C_{risk} is the cost associated with the risk of grounding, C_{fuel} is the cost associated with fuel consumption, and C_{time} is the cost associated with time usage. α, β, and γ are weighting parameters set by the operator. They reflect the relative importance assigned to risk, fuel, and time respectively in the decision-making process.

The objective of the optimization process is to find the path that minimizes C_{total}. In essence, the optimal path is the one that provides the best trade-off between minimizing risk, conserving fuel, and reducing time spent, given the operator's preferences. By adjusting the weighting parameters, the operator can prioritize certain aspects according to their needs and operational constraints. For instance, in situations where safety is paramount, a higher weight can be assigned to α, emphasizing the minimization of C_{risk}.

It is essential to clearly define the limitations of this thesis. The optimization process discussed in this thesis is limited to selecting the best path from a predetermined set of options. The exploration for new routes that may offer even greater efficiencies is beyond the scope of this work.

This exploration of uncharted paths, involving the application of optimization algorithms that can adjust the route in the direction of the lowest cost, is beyond the scope of this thesis. It presents an opportunity for future research, leading to more dynamic and adaptable navigation strategies. While the current methodology offers a practical solution for

selecting among the defined paths, there is considerable potential for more sophisticated route optimization in the future.

4

Case Studies

To better illustrate the proposed framework for the grounding risk model presented in Chapter 3, two case studies was conducted.

The first case study concerns a passenger ferry passing near two islands that are wildlife sanctuaries. This scenario presents an opportunity to explore the application of the grounding risk model and the path-planning optimization in a context characterized by tight navigation spaces and high environmental risk due to potential grounding incidents.

The second case study shifts focus to an oil tanker navigating around a nature reserve. This case allows for an examination of the model's capacity to evaluate and mitigate the increased risks associated with oil spills.

4.1 Case Study 1 - Passenger ferry passing two islands and wildlife sanctuary

The first case study situates us in Norway's *Møre og Romsdal* county, examining a passenger ferry's operation. This case assumes the ferry's journey begins at *Dryna ferjekai*, with its intended destination being *Åfarnes ferjekai*. The ferry's route is depicted in Figure 4.1. The vessel's course requires careful navigation around two islands, *Tautra* and *Sekken*, to reach its final docking point.

Table 4.1 presents the vessel properties and environmental conditions employed in the case study. The vessel properties are derived from the Norwegian Ro-ro passenger vessel *M/F Veøy* (Norwegian Environment Agency (2023)), which operates primarily in the waters surrounding Tautra and Sekken, with *Molde* serving as its home port. Figure 4.2 showcases an image of the passenger vessel.

Due to the unavailability of the exact monetary value of the ship, an assumption was made based on a similar Norwegian passenger ship that was listed for sale at the time of writing

Figure 4.1: The route of the vessel in the first case study, traveling from *Dryna* to *Åfarnes*. The red and blue pins represent the prominent obstacles along the route, namely *Tautra* island and *Sekken* island. The image is retrieved from Gule sider (2023)

(Shipselector.com (2023)).

Net daily earnings for a passenger ferry in Norway can vary significantly based on several factors such as the number of passengers, the length of the route, ticket price, time of year, and whether it is publicly subsidized. In the context of this case study, net daily earnings were arbitrarily set to USD 1000.

Figure 4.2: Image of M/F Veøy, retrieved from Fjord1 (2023)

In the conducted case study, Figure 4.3 depicts the wildlife sanctuaries in the area. Situated on the western side of Tautra Island, there exists a sanctuary that supports a diverse range of sea bird species. On the eastern side of Sekken, a landscape protection area is

Table 4.1: Summary of vessel properties and environmental conditions utilized in the first case study.

Property	Value
Type	Passenger
Production year	1974
Value	USD 2 000 000
Net Daily Earnings	USD 1000
Length	75 m
Width	12 m
Draft	4.5 m
Deadweight tonnage	467
Max rudder angle	30°
Current velocity	4.12 m/s in south-eastern direction

present. Its primary objective is to safeguard the historically significant cultural landscape and the distinctive natural surroundings encompassing the old *Veøy* church (Norwegian Environment Agency (2023)).

Grounding accidents in these areas represent catastrophic risk. Such an incident could lead to extensive environmental damage, disrupting the delicate balance of these habitats and posing a significant threat to the wildlife that calls these areas home. The highest consequence would come from chemicals spilling in these areas, but grounding with a passenger ship could also cause huge damage.

Figure 4.3: The wildlife sanctuaries in the area where the case study is conducted are highlighted in red and green areas. The red area represents a wildlife sanctuary, while the green area represents a protected landscape region. Notably, there is a sea bird wildlife refuge located on the western side of Tautra Island, and a protected landscape region situated to the east of Sekken. The image is retrieved from Norwegian Directorate of Fisheries (2023)

To determine the optimal path for the ferry's journey, we employ the step-by-step frame-

work presented in Chapter 3.

4.1.1 Step 1 - Identify Failure Modes

As mentioned in Section 3.1, the sole failure mode simulated in this study was loss of propulsion. To ensure that the framework considers a wide range of scenarios, also grounding with small objects, it was deemed necessary to simulate a loss of propulsion at least once every 20 meters. Based on a desired forward speed of 8.5 m/s, this translates to simulating failures every two seconds. At maximum speed, the vessel experiences simulated blackouts approximately every 17 meters. The interval between blackouts decreases when the vessel operates at lower speeds. Each simulated blackout lasts for 300 seconds, equivalent to five minutes.

4.1.2 Step 2 - Identify Critical Sections of the Route

Step two of the proposed framework is to identify the critical sections of the route.

The route from Dryna to Åfarnes, as illustrated in Figure 4.1, passes near the islands of Tautra and Sekken. To ensure a safe passage to the destination, the vessel must navigate around these islands. Given their potential to complicate the journey, these islands are identified as critical sections. Figures 4.4 and 4.5 indicate the starting and ending points of these critical sections. Notably, the red rectangles shown in these figures denote ecologically sensitive areas. This identification of ecological sensitivity is informed by protected area data provided by Norwegian Directorate of Fisheries (2023).

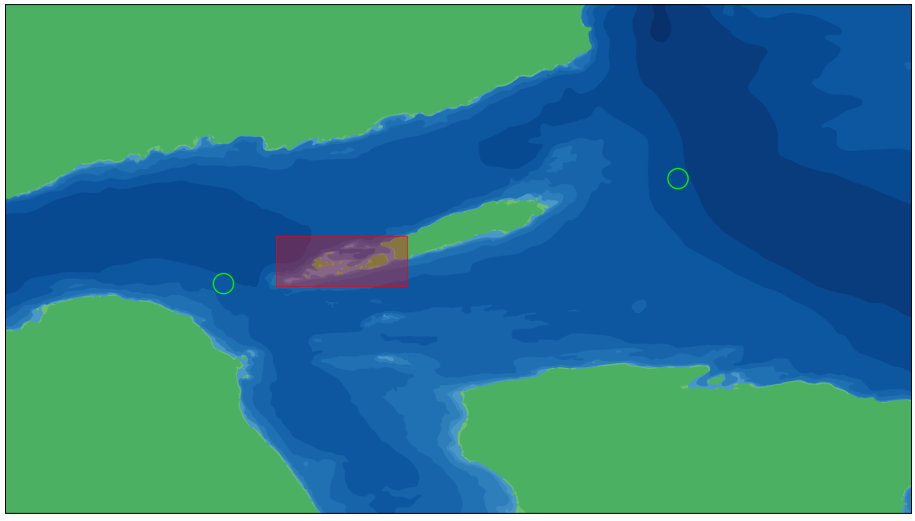

Figure 4.4: This map depicts the critical section around Tautra, with the starting and ending points indicated by green circles. Additionally, the red rectangle marks an ecologically sensitive area

Figure 4.5: This map depicts the critical section around Sekken, with the starting and ending points indicated by green circles. Additionally, the red rectangle marks an ecologically sensitive area

4.1.3 Step 3 - Identify Suitable Paths

The third step of the proposed framework is to identify a set of suitable paths for the vessel to follow in order to avoid the obstacles.

The first critical section to be addressed is the area around Tautra. It is evident that the vessel must navigate either to the north or south of the island to avoid grounding. In theory, numerous viable routes could be established. However, due to limitations in computational resources, three northern and three southern routes have been identified. These selected paths are assumed to adequately represent the plausible and manageable routes to a satisfactory extent. The six paths can be observed in Figure 4.6.

Concerning the critical section around Sekken, a total of four potential paths have been determined. One path is situated north of the island, while the remaining three paths are located on the southern side. Due to the relatively narrow nature of the north passage, it was deemed sufficient to consider only a single northern path. Figure 4.7 illustrates the defined paths for navigation around Sekken.

4.1.4 Step 4 - Determine Grounding Risk Associated with the Identified Paths

The fourth stage in the proposed methodology requires an evaluation of the grounding risk associated with each potential path. This evaluation was conducted by initially performing simulations in which the vessel successfully navigated the paths without any system failures. Once these baseline simulations were completed, additional simulations were run that introduced loss of propulsion into the vessel's operation along the same routes.

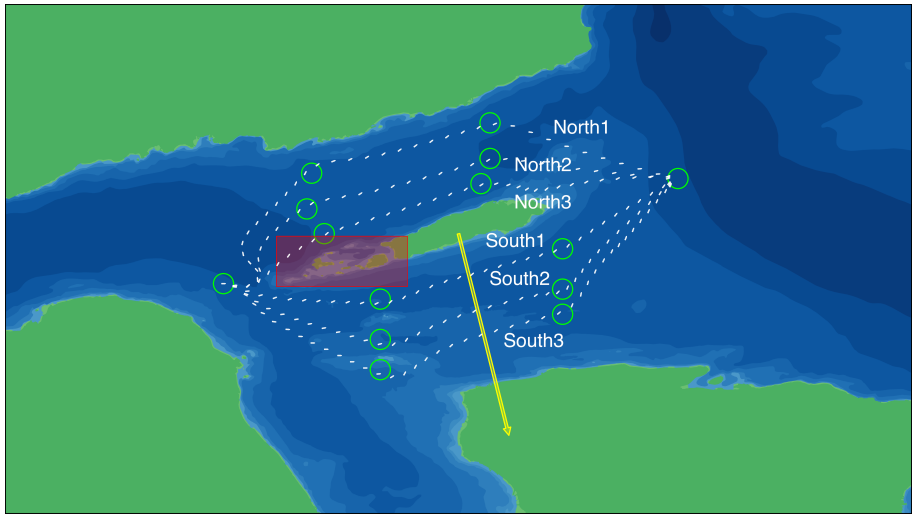

Figure 4.6: The figure illustrates the six designated paths for the vessel to navigate through the critical area around Tautra. The yellow arrow indicates the direction and magnitude of the environmental forces. The white text denotes the path names, which are utilized throughout this thesis

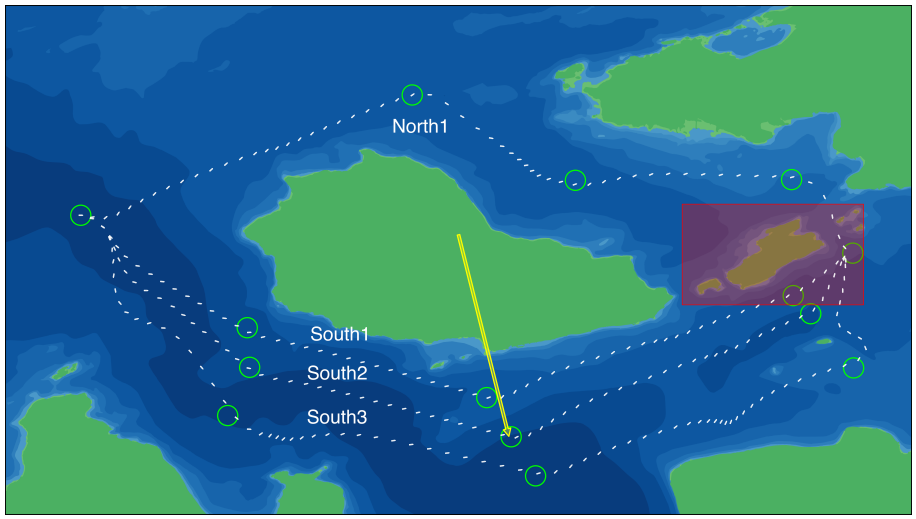

Figure 4.7: The figure illustrates the six designated paths for the vessel to navigate through the critical area around Sekken. The yellow arrow indicates the direction and magnitude of the environmental forces. The white text denotes the path names, which are utilized throughout this thesis

As mentioned, this case study is simulated with the technical data of M/F Veøy (Sjøhistorie (2023)). The passenger vessel travels under the Norwegian flag, and was build in 1974, making it more than 20 years old. In the simulations, it is assumed that the weather on site can be characterized as 'harsh'. By employing the Bayesian Network depicted in

Figure 4.8, we estimate a blackout utility metric of 1.3. This metric is multiplied with the base probability of $1.3 \cdot 10^{-8}$ blackouts per seconds, discussed in Section 3.3. Loss of propulsion are induced in the simulation every two seconds, with the assumption that any blackout occurring within this time period will yield the same risk metric. Consequently, the probability of blackout during each simulation can be articulated as

$$P_{blackout} = 1.3 \cdot 2 \cdot 1.3 \cdot 10^{-8} = 3.38 \cdot 10^{-8} \tag{4.1}$$

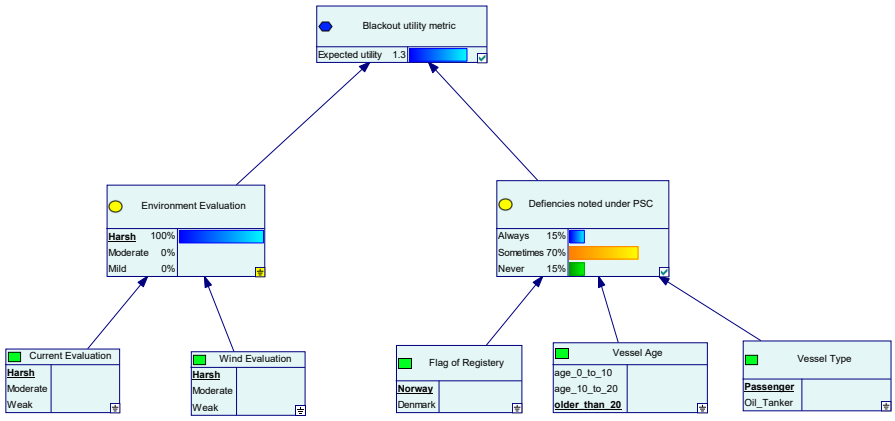

Figure 4.8: The Bayesian Network employed to estimate the blackout utility metric for the first case study.

The analysis begins with the examination of potential routes skirting the first obstacle, the island of Tautra. Upon simulating loss of propulsion on both the two northernmost paths and the southernmost path, no grounding incidents were recorded. As a result, according to the proposed framework, these routes are assessed to carry no associated risk of grounding.

Contrarily, the simulations involving failures on the northern route situated closest to the island led to groundings in 117 instances. A significant share of these groundings took place within the bird sanctuary located on the western section of the island. The corresponding simulation results are illustrated in Figure 4.9, where the red circles signify the grounding sites resulting from the simulated blackouts.

The 117 grounding instances led to a total environmental consequence amounting to USD 4,558,500, a social consequence totaling USD 15,277,800, and an economic consequence of USD 13,258,037. The relatively low environmental consequence, accounting for only 11% of the total consequence, may be due to the fact that the simulated vessel was a passenger ferry, and thus grounding incidents did not result in any chemical leakage. To provide a risk estimate, the total consequence was combined with the probability of each grounding scenario occurring. Using Equation (3.20), the resulting estimated total risk was a sum of USD 1.12.

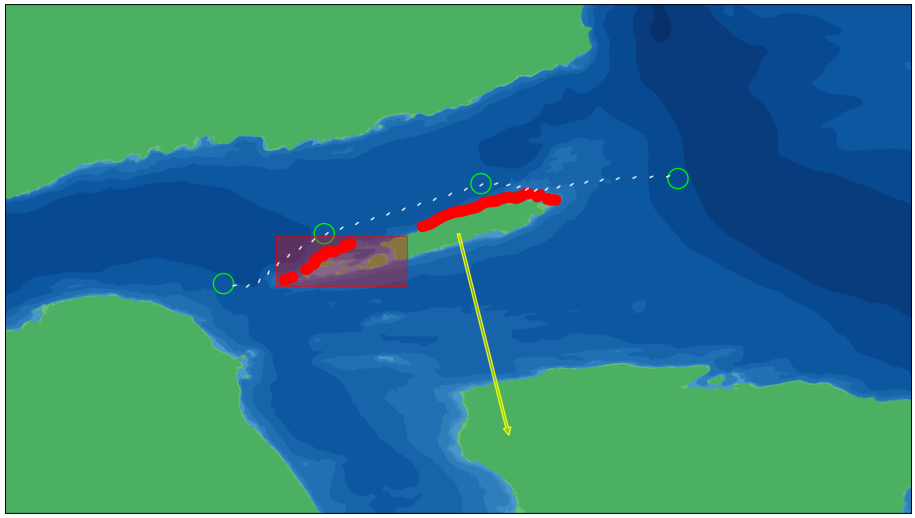

Figure 4.9: Blackout simulations on the northern path closest to the island

Figure 4.10 depicts the simulated failures that occurred on the southern path closest to Tautra. A total of 4 groundings were recorded, resulting in a cumulative consequence of USD 1,151,970. Interestingly, only 11% of the cost can be attributed to environmental consequences, which is lower compared to the previously discussed path. This discrepancy is likely due to a significant portion of the grounding incidents in the first path occurring in an ecologically sensitive area. The estimated total risk for this path was USD 0.04.

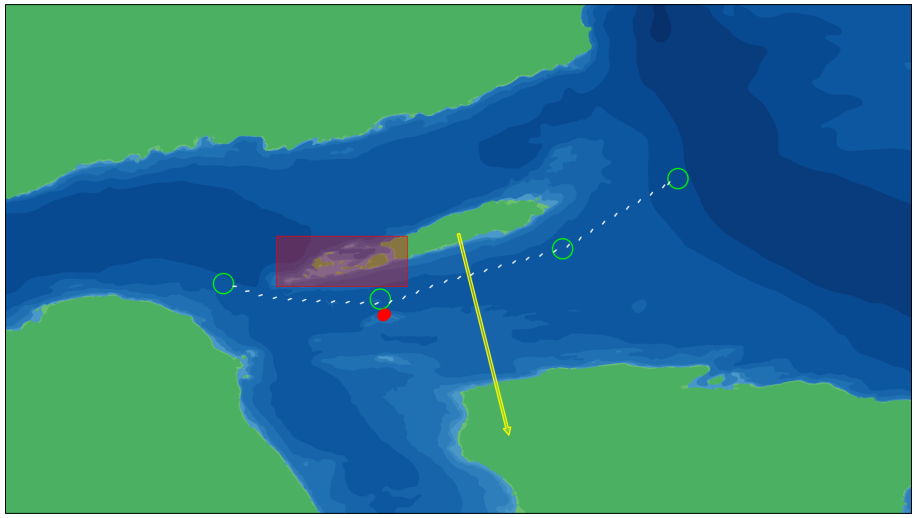

Figure 4.10: Blackout simulations on the sourthern path closest to the island

Figure 4.11 illustrates the simulated failures that occurred on the middle section of the

southern paths. A total of 12 groundings were recorded, resulting in a cumulative consequence of USD 3,428,725. Of this total, approximately 11% was attributed to environmental consequences, while the remaining 89% was nearly evenly split between social and economic consequences. The estimated total risk for this route was calculated to be USD 0.12.

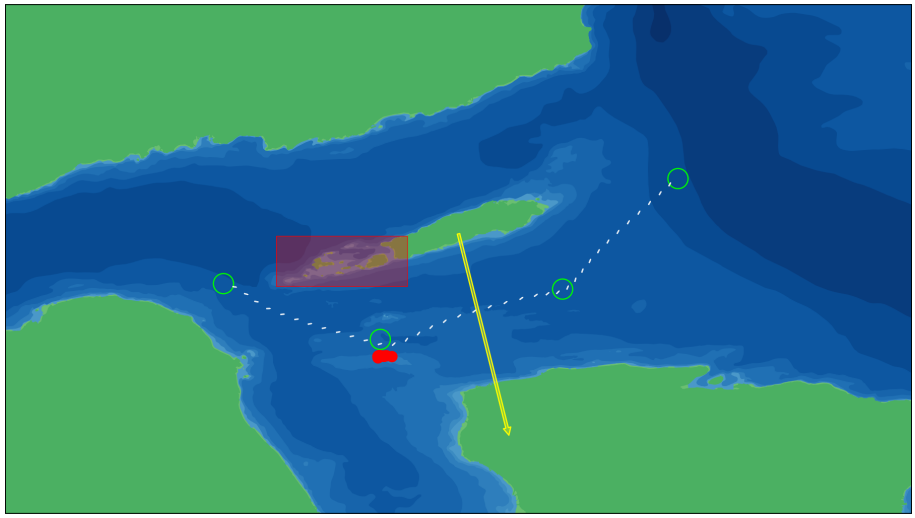

Figure 4.11: Blackout simulations on the middle southern path

Table 4.2 presents the mean damage states derived from the groundings for each navigational path being considered. It was consistently found across all paths that damage state 2 had the highest probability. This finding is consistent with the results of Liu and Frangopol (2018), which conducted an analysis of the likelihood of various damage states for AFRAMAX vessels in a comparable study. A comparative review between the damage states from the AFRAMAX study and those reported in our case studies is conducted in Chapter 5.

Table 4.2: The average damage states probabilities for the Tautra simulations are presented. It is worth noting that the three other paths did not encounter any simulated groundings.

Damage state (DS_i)	1	2	3	4	5	6
Tautra North 3	32.1%	32.6%	17.9%	2.5%	1.0%	13.9%
Tautra South 1	29.0%	30.0%	21.0%	3.0%	1.0%	16.0%
Tautra South 2	29.5%	30.4%	20.5%	2.9%	1.0%	15.7%

Figure 4.12a shows the total consequence metric for each of the proposed paths. Upon incorporating the probabilities associated with each failure event, we arrive at the risk metrics portrayed in Figure 4.12b. These figures collectively reveal that, under the prescribed conditions, the northern path situated nearest to the island incurs the highest risk. The mid-southern path emerges as the second riskiest, followed by the southern path in

close proximity to the island. Blackout simulations on the remaining three paths did not lead to any grounding incidents, thus their associated risk is regarded as zero.

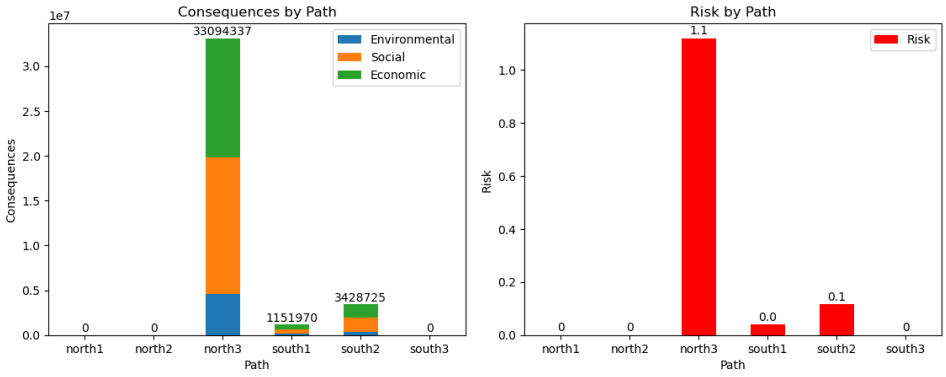

(a) Consequences **(b)** Risks

Figure 4.12: Figures displaying the consequences and risk associated with sailing the six paths around Tautra

We will now turn our attention to the voyage's second obstacle, specifically, the Sekken island. Analysis of the blackout simulations revealed that only the southernmost route encountered any groundings, with the remaining three paths showing no signs of simulated groundings. Visual representations of these paths are available in Figure 4.13, where the 19 grounding sites resulting from the simulation of the southernmost path are indicated by red circles. The average damage states resulting from these groundings are displayed in Table 4.3.

Table 4.3: The average damage state probabilities for the Sekken simulations are presented. It is worth noting that the three other paths did not encounter any simulated groundings.

Damage state (DS_i)	1	2	3	4	5	6
Sekken South	29.0%	30.0%	21.0%	3.0%	1.0%	16.0%

Figure 4.14 provides an overview of the total consequences and risks associated with the paths around Sekken. It is clear that travelling the southernmost path involves the most risk, as the other paths does not involve any risk. The southernmost path resulted in a total consequence of USD 5,471,857, leading to a total risk of USD 0.2.

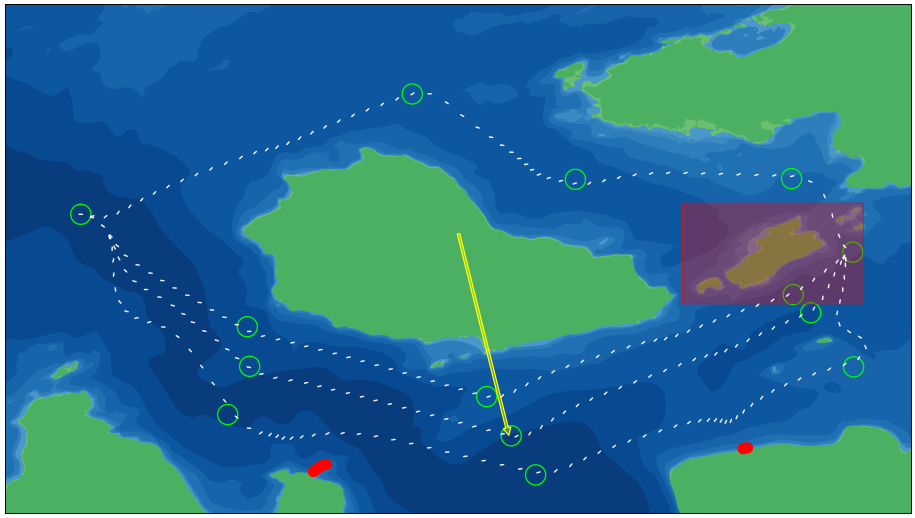

Figure 4.13: Blackout simulations were conducted on the paths around Sekken, with only the southernmost path resulting in simulated groundings. The red circles represent the 19 grounding sites resulting from the blackout simulations of this path.

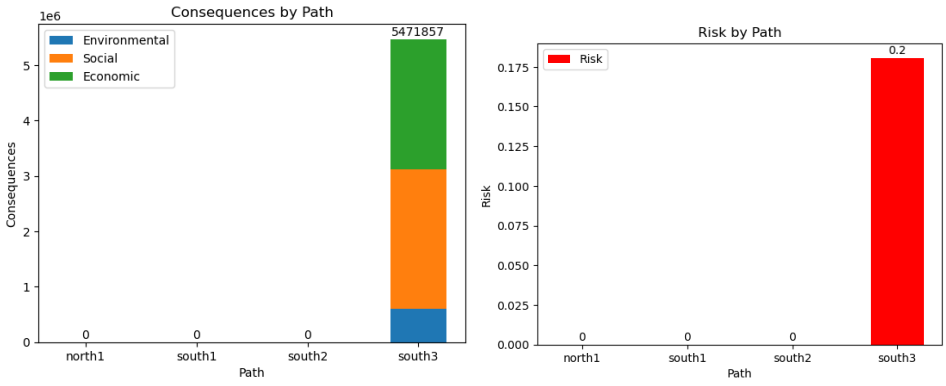

(a) Consequences **(b)** Risks

Figure 4.14: Figures displaying the consequences and risk associated with sailing the six paths around Sekken

4.1.5 Step 5 - Optimization

The fifth step of the proposed framework focuses on optimizing the selection of path based on risk, fuel consumption, and time usage. The cost function to be optimized is presented in Equation (3.22).

We first consider the optimal path around Tautra. The individual metrics in this case, with $\alpha = \beta = \gamma = 1$, are illustrated in Figure 4.15.

Using this Figure, it is apparent that the optimal path is the southern route that hugs the coastline of the island. While this path isn't devoid of potential hazards, it stands out due to its superior speed and fuel efficiency—attributes that seem to weigh heavily in the cost function.

The difference between the two extreme scenarios in terms of time usage is approximately USD 15. Similarly, the variance in fuel consumption reaches around USD 50, while the difference in risk is approximately USD 1.75. These differences between the extremes suggest that adjustments may be needed in the weighting parameters. Further discussion on this topic can be found in Chapter 5.

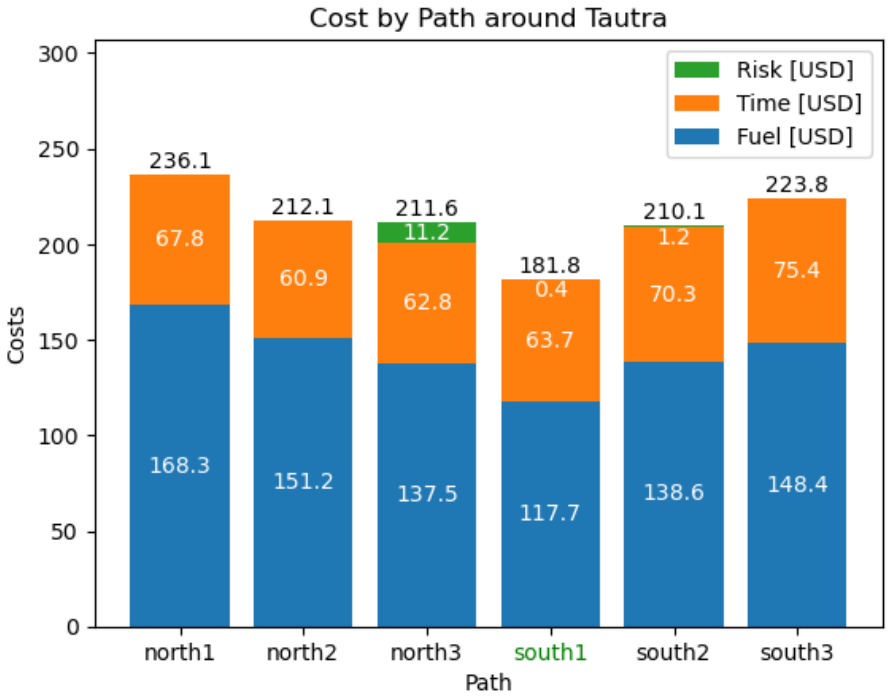

Figure 4.15: Cost function parameters for the six paths around Tautra

Among the paths surrounding Sekken, the southern path closest to the island was identified as the optimal choice based on the provided metrics. None of the three northernmost routes experienced any groundings. Interestingly, the fastest and most fuel-efficient path among these routes, which happened to be the northernmost path among the southern routes, emerged as the optimal path in this scenario. A visualization of the metrics used in the cost function can be seen in Figure 4.16.

The optimal route for the first case study is a combination of the two optimal paths, as shown in Figure 4.17. However, it should be noted that this route is not entirely optimal, as there may be potential for further optimization. For example, a direct navigation from

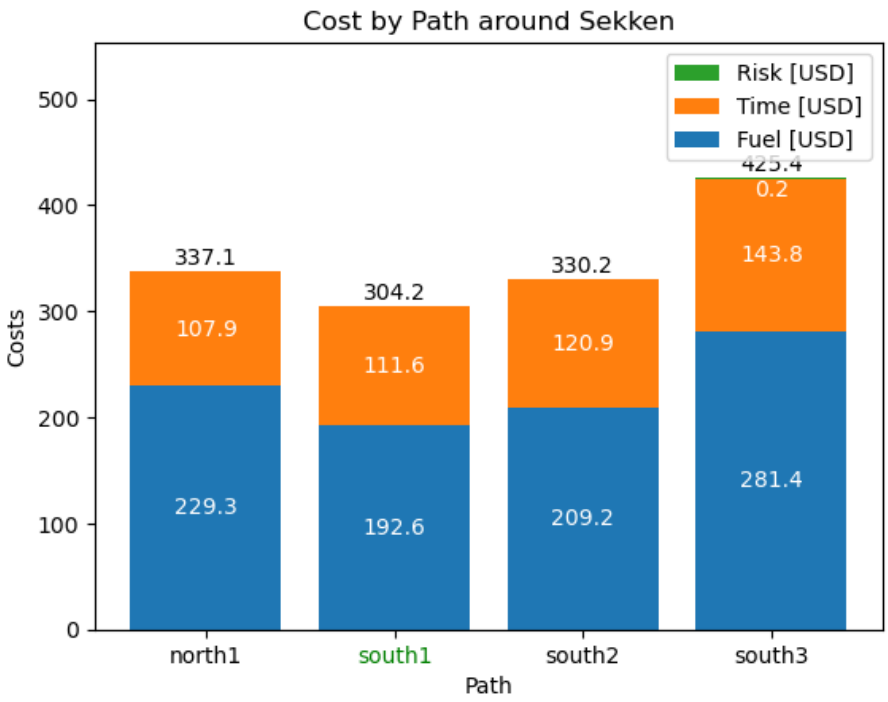

Figure 4.16: Cost function parameters for the six paths around Sekken

waypoint three to waypoint five could potentially result in a faster and more optimal route. This aspect is discussed further in Section 5.

Figure 4.17: The optimal paths around the islands Tautra and Sekken are merged to create the overall optimal path for the first case study.

4.2 Case Study 2 - Oil Tanker in Nature Sanctuary

The voyage of the oil tanker *Hordafor VI* (Marine Traffic (2023)) was monitored using the Marine Traffic platform as it traveled from *Bergneset* to *Salthella*. Figure 4.18 shows an image of the tanker. Along a specific segment of this route, the tanker navigated around the *Sandøya-Vattøya Nature Sanctuary*, located near *Ulsteinvik*.

The specific information about the vessel is summarized in Table 4.4, which is sourced from Marine Traffic (2023). While it was difficult to retrieve the precise number of oil tanks on the vessel, an estimate of eight cargo tanks was deemed reasonable and consistent with the available data by referencing other vessels of similar dead-weight tonnage shipsforsale.eu (2023).

The net daily earnings for the oil tanker is derived from ship charter rates reported by HandyBulk (2023). As of May 13, 2023, this charter rate was approximately USD 10,000.

Table 4.4: Vessel properties and environmental conditions used in the second case study

Property	Value
Type	Oil Tanker
Production year	1991
Value	USD 2 150 000
Net Daily Earnings	USD 10,000
Length	83 m
Width	13 m
Draft	6.6 m
Dead-weight tonnage	3 232
Number of tanks	8
Tonnage in each tank	375
Max rudder angle	30°
Current velocity	4 m/s in eastern direction
Environment Evaluation	Moderate

This case study focuses on a specific scenario wherein an oil tanker is at risk of grounding within a nature sanctuary. Nature sanctuaries are designated areas of utmost ecological importance, harboring diverse and delicate ecosystems. The objective of this case study is to assess the potential consequences and risks associated with a grounding incident, particularly the potential for chemical spills, within this environmentally sensitive area.

The planned route, as outlined in Marine Traffic (2023), involved traveling along the eastern side of the island, as depicted in Figure 4.19. Figure 4.20 displays ecologically sensitive areas in the vicinity. The red zone situated in the center is a bird sanctuary, requiring special precautions and protective measures. The pink area has the sole restriction of prohibiting bird and mammal hunting, and it is not considered an ecologically sensitive area in the context of this particular study.

To validate whether the typical route taken by the vessel Hordafor VI is indeed the optimal path around the wildlife sanctuary, the methodical approach outlined in Chapter 3 will be

Figure 4.18: Image of Hordafor VI, retrieved from Marine Traffic (2023)

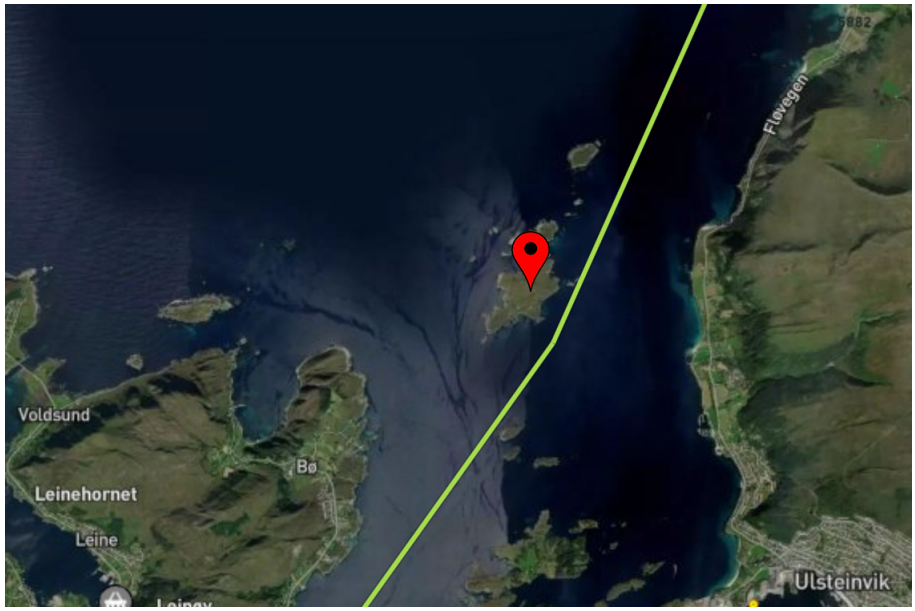

Figure 4.19: The yellow line shows the planned route of the Oil Tanker Hordafor VI. The red pin marks the Sandøya-Vattøya Nature Sanctuary. Retrieved from Marine Traffic (2023)

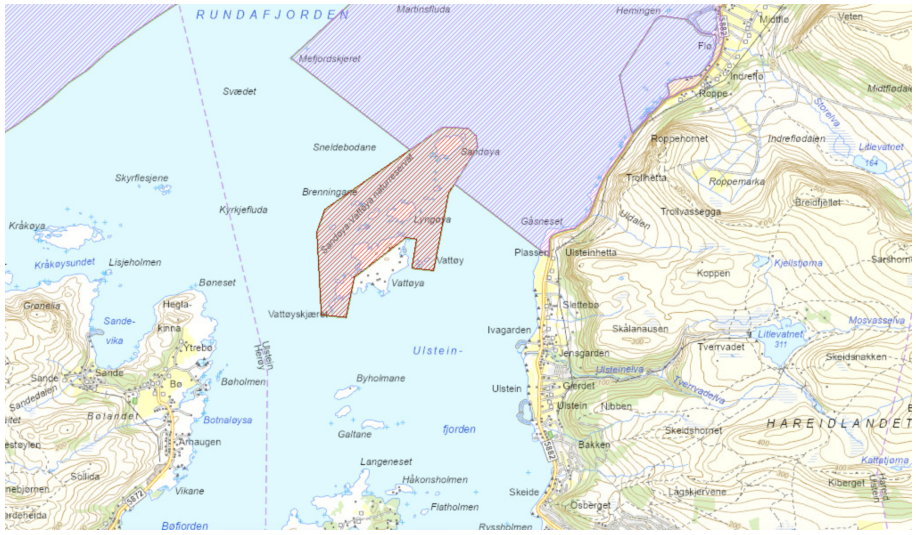

Figure 4.20: The figure depicts the presence of wildlife sanctuaries in the study area, highlighted in red. The pink area, on the other hand, imposes restrictions on hunting activities but is not classified as an ecologically sensitive area within the scope of this study. The image source is Norwegian Directorate of Fisheries (2023).

utilized. This will involve following the step-by-step framework to assess and analyze the risks associated with different navigation options.

4.2.1 Step 1 - Identify Failure Modes

For the second case study, the methodology outlined in Section 4.1.1 regarding the simulation of failure modes remains unchanged. Specifically, only the loss of propulsion failure mode is simulated at a frequency of every two seconds, with each blackout lasting for 300 seconds.

4.2.2 Step 2 - Identify Critical Sections of the Route

Step two of the proposed framework is to identify the critical sections of the route.

The journey of Hordafor VI from Bergeneset to Salthella involves multiple significant sections. However, for this case study, the focus will be solely on the critical portion encompassing the Sandøya and Vattøya islands. The starting and ending points of this critical section are highlighted in Figure 4.21.

4.2.3 Step 3 - Identify Suitable Paths

The third step in the proposed framework entails identifying a set of feasible paths that the vessel can follow to successfully navigate around the obstacles.

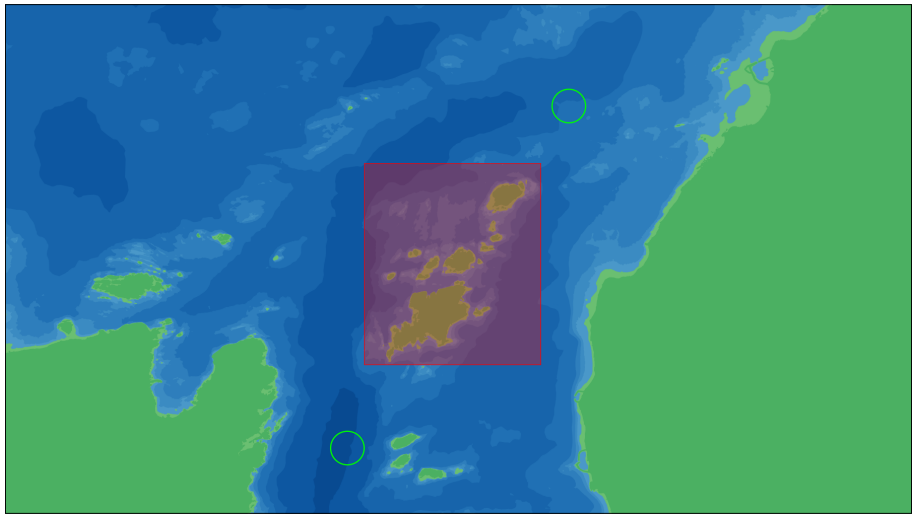

Figure 4.21: This map depicts the critical section around the Sandøya-Vattøya Nature Sanctuary, with the starting and ending points indicated by green circles. Additionally, the red rectangle marks an ecologically sensitive area

For this particular case study, two routes have been identified: the east route and the west route. These routes are located on opposite sides of the Nature Sanctuary, as shown in Figure 4.22. The main objective of this study was to determine the optimal selection between the east and west paths. Consequently, the exploration of additional routes was not a primary focus within the scope of this investigation.

4.2.4 Step 4 - Determine Grounding Risk Associated with the Identified Paths

In step four of the proposed framework, the risk of grounding for each potential path is evaluated.

The oil tanker, constructed in 1991 and originating from Norway, has been operational for more than 20 years. In the context of this study, the environmental conditions are classified as 'moderate'. According to the Bayesian Network depicted in Figure 4.23, under these conditions, the estimated blackout utility for the vessel is 0.973. The blackout utility serves as an indication of the likelihood of the ship experiencing a loss of propulsion. This metric is multiplied by the base probability of $1.3 \cdot 10^{-8}$, discussed in Section 3.3. During the simulations, failures occur every two seconds, and it is assumed that any blackout within these two-second intervals would result in the same risk metric. Hence, the blackout probability for each simulation can be expressed as follows:

$$P_{blackout} = 0.973 \cdot 2 \cdot 1.3 \cdot 10^{-8} = 2.53 \cdot 10^{-8} \tag{4.2}$$

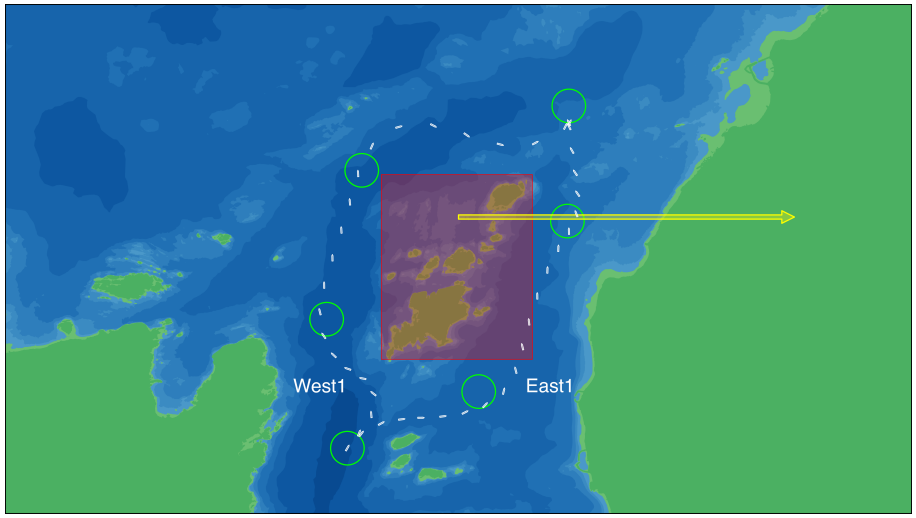

Figure 4.22: The figure illustrates the two designated paths for the vessel to navigate through the critical area around Sandøya-Vattøya Nature Sanctuary. The yellow arrow indicates the direction and magnitude of the environmental forces. The white text denotes the path names, which are utilized throughout this thesis

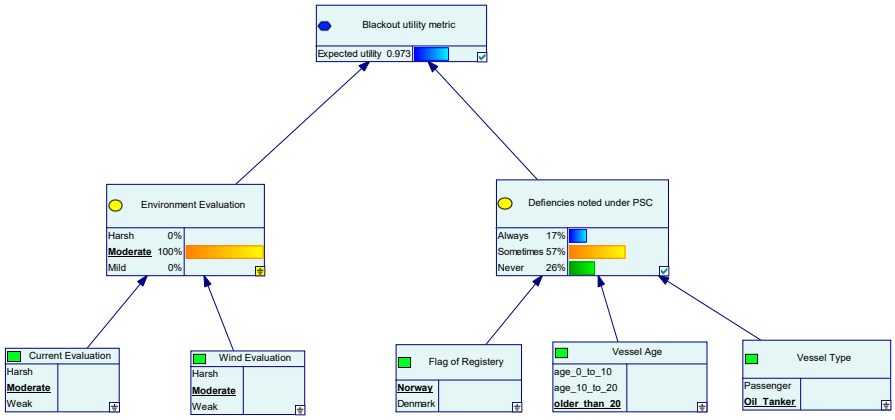

Figure 4.23: The Bayesian Network employed to estimate the blackout utility metric for the second case study

The simulations of blackouts are showed in Figures 4.24 and 4.25, where the red circles indicate the locations of grounding incidents. The eastern path experienced 29 simulated groundings, while the western path had 10 simulated groundings. It should be noted that only one of the grounding incidents occurred within the nature sanctuary.

From the simulated groundings, the average damage states for the two paths can be seen in Table 4.5. In comparison to the paths illustrated in the first case study, the simulated

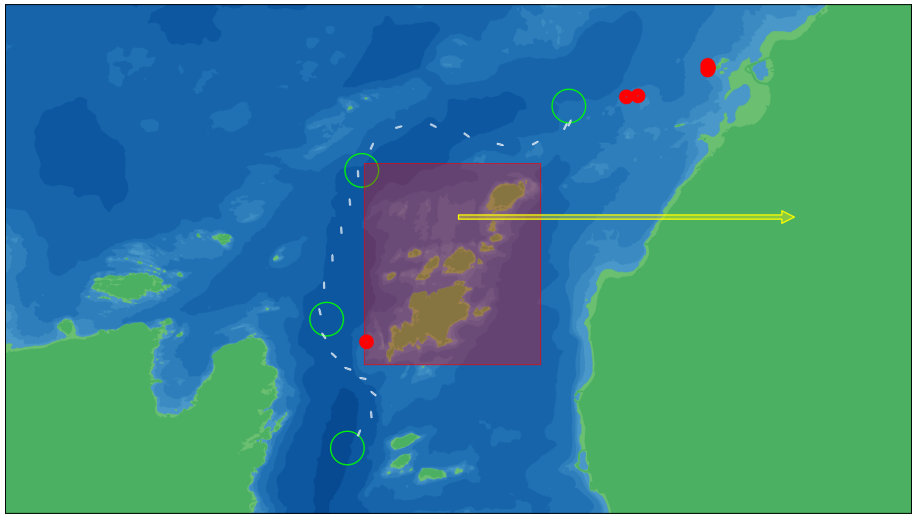

Figure 4.24: Blackout simulations on the western path

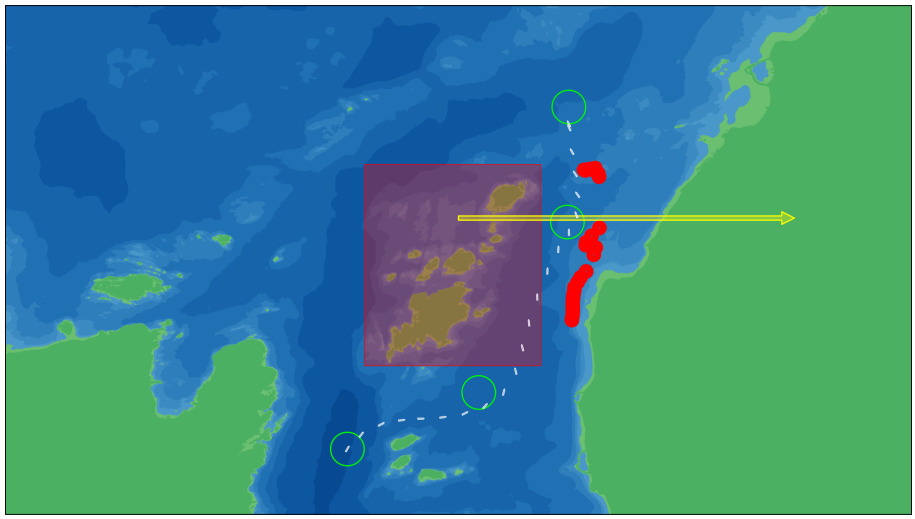

Figure 4.25: Blackout simulations on the eastern path

groundings for the two paths result in an average damage state that is slightly lower. This difference can be attributed to the environmental conditions taken into consideration during the simulations. In the first case study, the weather was described as 'poor', potentially contributing to higher severity accidents and thus, higher average damage states. In contrast, the weather conditions were described as 'normal' in the second case study, which may result in lesser severity of accidents and correspondingly lower average damage states.

The eastern route resulted in a significant total estimated consequence of USD 762,302,236,

Table 4.5: Average damage state probabilities for the second case study

Damage state (DS_i)	1	2	3	4	5	6
Sandøya-Vattøya East	32.7%	30.7%	20.2%	2.9%	1.0%	12.6%
Sandøya-Vattøya West	32.5%	30.5%	20.4%	2.9%	1.0%	12.7%

corresponding to a calculated risk value of USD 19.3. The environmental consequence accounted for over 83% or USD 635,853,036 of this total. This substantial environmental consequence can be attributed to the high potential impact of an oil spill, which is a significant risk associated with the operation of an oil tanker.

The comparatively high total risk associated with this case, relative to the previous passenger ferry scenario, can also be explained by the inherent attributes of the vessel involved. The vessel under consideration here is an oil tanker – a class of ship that generally possesses a higher value and generates greater net daily earnings. The associated potential economic loss in the event of an accident or grounding incident is thus inherently higher.

The social consequence component contributes less to the total risk profile in this case. This might appear counterintuitive, considering the larger scale and potential for greater human impact with such a vessel. However, the model assumes a constant estimation of injuries and fatalities, regardless of the ship's size or the number of people on board. This element of the model, arguably not capturing the full scope of potential social consequences in cases like this, warrants further discussion, which is addressed in Section 88.

The consequence of taking the western path amounted to USD 265,417,814, resulting in a risk value of USD 6.7. Similar to the eastern path, the majority of the consequence was attributed to environmental factors, while the social consequence was negligible.

Figure 4.26 shows the consequence and risk of the two paths. This figure suggests that under the environmental conditions used in the case study, the eastern path, typically used by the oil tanker, exhibits a lower risk metric compared to the western path.

4.2.5 Step 5 - Optimization

The fifth step of the proposed framework focuses on optimizing the selection of path based on risk, fuel consumption, and time usage. The cost function, as presented in Equation (3.22), captures these metrics. In this particular scenario, where $\alpha = \beta = \gamma = 1$ and considering the prevailing environmental forces, the individual metrics are depicted in Figure 4.27. Analysis of this figure reveals that the eastern route offers the lowest overall cost. This discrepancy can be attributed to the higher fuel consumption associated with the western route, despite both routes having comparable travel times. It is plausible that the vessel navigating the western route encounters more challenging conditions, such as adverse winds and currents, compared to the eastern route. Interestingly, the influence of the risk factor on the total cost appears to be minimal.

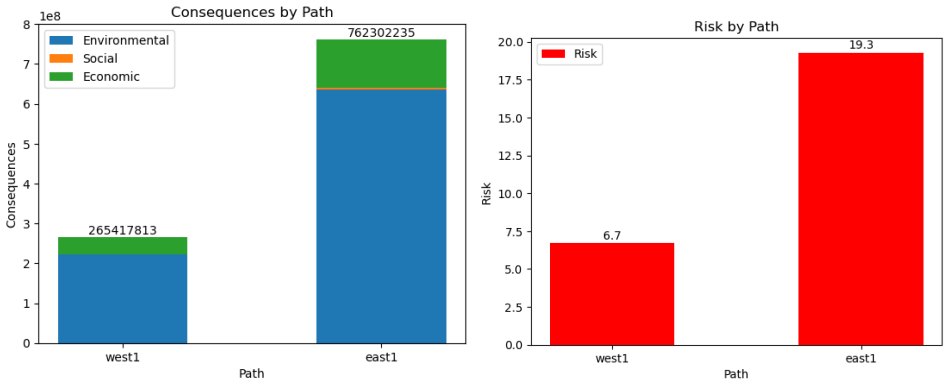

(a) Consequences **(b)** Risks

Figure 4.26: Consequences and Risks for the paths around the Sandøya-Vattøya

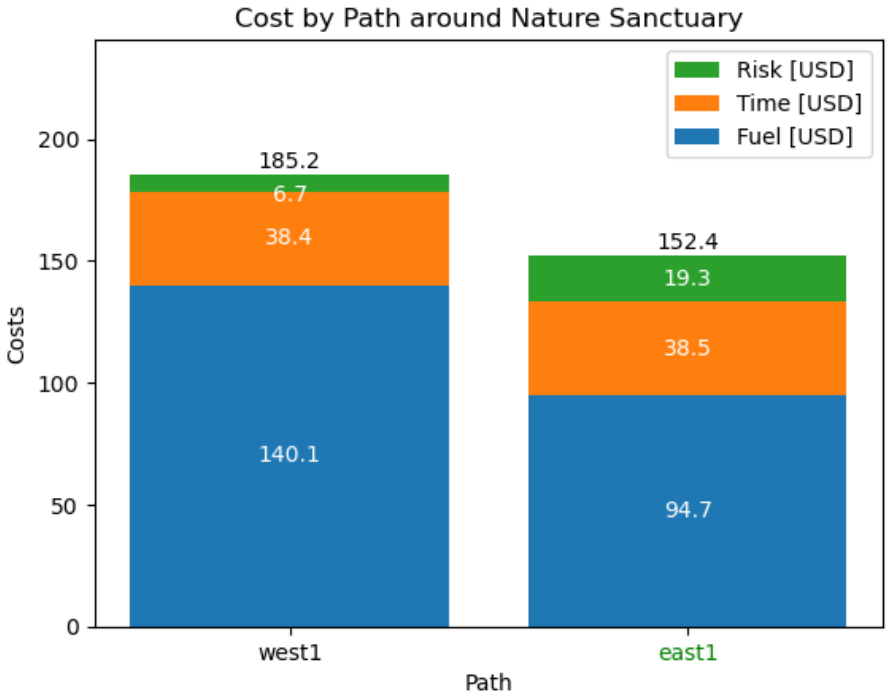

Figure 4.27: Cost function parameters for the paths around Sandøya-Vattøya

5

Discussion

This chapter embarks on an in-depth discussion and analysis of the central elements and outcomes of this thesis. It opens with an exploration of the main contributions, emphasizing on the proposed path-planning framework and its grounding risk model. It then navigates towards the validation of the framework, which involves a detailed examination of the simulator, grounding risk analysis, and the cost function.

The chapter then delves further into various dimensions of the proposed framework. It includes a comprehensive examination of elements such as the impact of environmental forces on route optimization, the potential evolution of the framework into a real-time path planner, and a deeper understanding of propulsion loss duration before grounding. To conclude, the chapter contemplate potential future advancements that could refine and enhance the framework.

5.1 Main Contributions

The main contributions of this thesis revolve around the development of the proposed path-planning framework aimed at enhancing the operational efficiency of both manned and autonomous marine surface vessels.

While significant attention has been given to collision and obstacle avoidance in the context of autonomous navigation and guidance, the issue of reliable grounding prevention has received limited consideration. Existing literature on grounding risk often lacks comprehensive analysis and instead relies on arbitrarily chosen consequence levels. In contrast, this thesis addresses this gap by proposing a framework that incorporates a detailed estimation of grounding consequences for specific grounding incidents.

A fundamental focus of this research has been the emphasis on creating a universally applicable framework. The goal was to establish a grounding risk model and path-planning tool that easily could be adapted and utilized by ship operators worldwide, regardless of the

unique characteristics of the vessel or the prevailing operating conditions. The framework should let ship operators input their own ship data, prioritize consequences, and provide route information to simulate voyages and dynamically calculate optimal routes.

5.2 Validation

5.2.1 Simulation

The utilized simulation model demonstrates a realistic representation of the vessel dynamics; however, there are some notable remarks:

Firstly, the model's lack of a collision avoidance system can lead to unexpected behavior, especially during the path identification phase. If a path is defined to traverse an obstacle directly, the vessel will proceed without attempting to avoid a collision. Although this limitation is less problematic when simulating total loss of propulsion, as ship operators have limited options to avoid grounding in such scenarios, it could become a greater concern if future simulations incorporate additional failure modes, particularly partial loss of propulsion. In these cases, the simulated vessel would still aim to reach the next waypoint without considering obstacles, while a human operator would likely prioritize keeping the ship stationary and contacting emergency services.

Another noteworthy aspect is observed in the simulations that simulate propulsion loss, where the ship is depicted as taking no action. In reality, a human operator would typically respond to such a situation by employing strategies like deploying an anchor or adjusting the rudder to prevent grounding. However, these proactive measures are not implemented within the model. This limitation is noteworthy because what might be simulated as a grounding incident could potentially be a minor issue that could be successfully mitigated by a human operator's prompt actions.

An important caveat to consider about the framework illustrated in this report is that it does not account for any COLREG rules. This oversight could potentially lead to the recommendation of routes that infringe these maritime regulations. This aspect is discussed as further work in Section 5.9.

5.2.2 Likelihood of Propulsion Loss

The likelihood of propulsion loss is a key parameter in our risk model. To model this parameter, a Bayesian network was constructed, utilizing data from Section 2.4. However, it is essential to acknowledge that the available research did not provide direct values that could be directly inputted into the Bayesian Network. Consequently, the specific values used in the Bayesian Network were determined based on the author's informed judgment, considering the underlying theory. While this approach does provide a reasonable approximation, it inherently carries a degree of uncertainty. It should be noted that the reliability and accuracy of the propulsion loss prediction are strongly dependent on the quality and relevance of the underlying data. Thus, refining these estimates as more data becomes available, or utilizing domain experts' knowledge for parameter estimation, would enhance

the precision of the model. This, in turn, would improve the risk assessments, aiding in more robust and informed decision-making for path planning.

5.2.3 Consequence of Grounding

The estimation of the consequence of a grounding incident is based on the classification of the damage state of the grounded vessel. Liu and Frangopol (2018) introduced a method for determining the damage state by assessing the geometrical damage to the ship, which is then used to estimate the consequence of the grounding incident. In this thesis, we extend this framework.

Implementing metrics for geometrical damage of a simulated grounded vessel has been deemed impractical. Instead, a Bayesian Network has been implemented to classify groundings into damage states, using vessel speed, weather conditions, and the ground material involved in the specific grounding incident. In order for the consequence model developed in this thesis to effectively utilize the insights provided by Liu and Frangopol (2018), it is crucial that the damage state classification yields results that are within the same order of magnitude.

Table 5.1 presents a comparison of the damage states classified using geometrical damage from Liu and Frangopol (2018) and the Bayesian Network in the case studies conducted in this thesis. The 'AFRAMAX Average' row represents data obtained from a Monte Carlo simulation presented in Liu and Frangopol (2018), which collected and classified a significant number of damage samples. The other rows indicate the damage states from the case studies in this thesis. The first case study, involving Tautra and Sekken, had a classified weather condition of 'harsh', while the Sandøya-Vattøya case study had a classified weather condition of 'normal'. All groundings in the case studies were simulated to occur on rocks, with none on sand or mud.

The damage state classifications using the Damage State Bayesian Network generally fell within the same order of magnitude as the samples from Liu and Frangopol (2018). However, they appear to demonstrate a higher probability for more severe damage states. Notably, there is a significant probability for Damage state 6, where Liu and Frangopol (2018) reported a probability of 2.2 %, whereas the case studies in this thesis portray probabilities ranging from 12.6 % to 16 %. This discrepancy may be attributed to the fact that all simulated groundings occurred on rocks, with none on sand or mud. Additionally, the weather conditions were simulated as harsh. It is plausible that groundings on sand or mud and in better weather conditions would yield damage state probabilities closer to the samples provided in Liu and Frangopol (2018).

Environmental Consequences

The environmental consequences arising from grounding incidents are of paramount importance and have been taken into serious consideration in this thesis. In our framework, we have chosen to estimate these consequences by the fines imposed by authorities for the direct impact of the ship and the potential cleanup costs related to chemical spills. This approach provides a quantifiable method for assessing the environmental impact, linking

Table 5.1: Average probabilities of damage states in various scenarios. Damage states represent the severity of grounding incidents, with 6 indicating the highest severity. The AFRAMAX Average is determined through a Monte Carlo simulation outlined in Liu and Frangopol (2018), which involved the collection and classification of numerous damage samples. The remaining rows present damage state averages estimated in this thesis's case studies, utilizing the Bayesian Network explained in detail in Section 3.4.

Damage state (DS_i)	1	2	3	4	5	6
AFRAMAX Average	40.8%	37%	11.5%	7.6%	0.9%	2.2%
Tautra North 3	32.1%	32.6%	17.9%	2.5%	1.0%	13.9%
Tautra South 1	29.0%	30.0%	21.0%	3.0%	1.0%	16.0%
Tautra South 2	29.5%	30.4%	20.5%	2.9%	1.0%	15.7%
Sekken South	29.0%	30.0%	21.0%	3.0%	1.0%	16.0%
Sandøya-Vattøya East	32.7%	30.7%	20.2%	2.9%	1.0%	12.6%
Sandøya-Vattøya West	32.5%	30.5%	20.4%	2.9%	1.0%	12.7%

it directly to the economic implications. While the nature and extent of environmental damage can be subject to intense debate and an array of estimation methodologies, the adopted approach provides a balanced and reasonably accurate representation within the boundaries of our model. It gives a clear, quantifiable measure while capturing the essential aspects of environmental impacts, providing a sound basis for decision-making within the proposed framework. Yet, it should be acknowledged that this is a complex and multifaceted issue, and alternative methods of assessment may provide additional insights and refinements.

Social Consequences

This thesis incorporates the social consequence assessment of grounding incidents, following the approach laid out by Liu and Frangopol (2018). The evaluation of social consequences involves the estimation of potential fatalities and injuries. Research by Liu and Frangopol (2018) estimates the fatality rate at 0.01 for all groundings with a damage state of 3 or higher, and it also considers that each grounding incident results in two injuries. This thesis has adopted these values, leading to an assumption that any incident with a damage state above 2 yields the same social consequences.

However, a more nuanced approach could be beneficial in future developments of this model. For example, an incident resulting in a Damage State of 6, indicating that more than four tanks have been penetrated, is likely to result in more injuries than an incident that merely causes limited plane damage and yields a Damage State of 1. This level of differentiation is currently absent in the model, leading to potential misrepresentation of the social consequences depending on the severity of the incident.

Moreover, attributing a monetary value to a human life and to injuries involves ethical considerations and can vary considerably. Liu and Frangopol (2018) estimate the monetary value of a life at USD 3,000,000 and the value of an injury at USD 60,000. Although these values have been adopted in this thesis, it's important to acknowledge that they are con-

troversial and difficult to universally agree upon. Future enhancements to the framework could explore alternative methods for quantifying social consequences, possibly including non-monetary assessments.

Economic Consequences

The economic consequence of a grounding incident was estimated in this study based on repair cost, loss of potential earnings, and loss of cargo. The repair cost and loss of potential earnings were determined considering the damage state of the vessel, its value, and its net daily earnings. It is important to note that while these estimations provide valuable insights, they may not perfectly replicate the complexities and variations encountered in real-world scenarios. The calculation of the monetary consequence for loss of cargo involved multiplying the amount of lost cargo by its corresponding value. This estimation is, on the other hand, expected to be fairly accurate, assuming that realistic values for cargo quantity and cargo worth are utilized

To validate the total economic consequence estimations, a paper issued by the insurance company The Swedish Club (2011) was utilized. This paper, presented in Section 2.5.3, provides empirical data about the average insurance claims resulting from grounding incidents. According to this data, the average cost derived from grounding incidents between 2001 and 2011 amounted to slightly above USD 900,000.

The framework's assessments for the case studies revealed distinctive differences in economic consequences. For the passenger ferry maneuvering around Tautra, the framework calculated an average economic cost of USD 119,803 per grounding incident. Conversely, the oil tanker's navigation around the nature reserve projected a significantly higher average cost per grounding incident, reaching up to USD 3,381,937. This discrepancy in cost can primarily be attributed to the estimated values and net daily earnings of the vessels involved.

Although there are some discrepancies between the economic consequences estimated by the proposed framework and the average insurance claims presented in The Swedish Club (2011), it is noteworthy that the values obtained are still within the same order of magnitude. This indicates a reasonable level of validity and reliability in the economic consequences estimated by the framework.

5.2.4 Cost of Time Usage

In this thesis, the cost associated with time usage is computed based on the additional operating expenses of the vessel. This approach does not account for the potential profit that could be lost because the ship could have embarked on another voyage, essentially overlooking the opportunity cost of the time spent. Likewise, the calculation does not reflect the value of time when the vessel has a narrow docking window. In these scenarios, a delay of just a few minutes could result in the vessel having to wait for hours or even days for the next available slot, incurring significant financial and operational implications.

Given that the difference in time between various routes is assumed to be in the order of seconds, the possibility of garnering additional profit from undertaking an extra job due to

time savings is not considered. While this may hold true in the context of this study, it is important to acknowledge that in a real-world scenario, even marginal time savings could culminate in significant economic benefits over the long term.

Furthermore, it is important to highlight that there are no limitations preventing the framework from being applied to determine the optimal route around larger islands. In such cases, the framework can be adapted to incorporate the potential financial losses incurred due to missed opportunities for the vessel to undertake alternative voyages.

5.2.5 Cost of Fuel Consumption

The estimation of fuel consumption is predicated on the utilization of specific fuel consumption curves, as elucidated in the work of Rokseth and Utne (2023). These curves are derived from fuel consumption data generously provided by the engine manufacturers. Although this approach provides an approximation that is far from perfect, it serves as a fairly reliable estimate for the purposes of this study.

Moreover, the dynamic nature of fuel prices presents another layer of complexity. Fuel prices are subject to constant fluctuations due to a multitude of factors, such as changes in crude oil prices, geopolitical events, and even shifts in global economic trends. This makes the precise prediction of fuel costs for future journeys a challenging endeavor. The model in this thesis uses a fixed fuel price for simplicity, but it should be noted that in a practical application, this price should be updated regularly to reflect current market conditions.

5.2.6 Path Planning

In this Master's thesis, a path-planning framework has been developed that is designed to identify the optimal path for a marine surface vessel. The framework functions by minimizing a cost function that encompasses risk, fuel consumption, and time spent on the journey.

However, it's important to underline that the framework provides the best path only within the confines of the given scenario, including the present environmental conditions and forces. The optimal path is thus highly scenario-specific and might require adjustments in real-time due to the dynamic and sometimes unpredictable nature of marine operations. These considerations will be discussed in more detail in the following sections.

5.3 Choosing Weighting Parameters

The framework formulated in this thesis aims to yield a realistic monetary assessment of a grounding incident. However, it is recognized that vessel operators might have different priorities, which can range from immediate operational considerations to broader strategic or ethical concerns. To account for this, the framework incorporates two sets of weighting parameters that offer flexibility in various operational contexts.

The first set of weighting parameters pertains to the consequence metrics, encompassing the environmental, social, and economic impacts of grounding incidents, as delineated by

Equation (3.3). For example, a vessel operator in a sensitive marine ecosystem might prioritize minimizing environmental impacts over other factors. Such an operator could adjust these parameters to assign greater weight to environmental consequences, thus reflecting a commitment to environmental stewardship.

The second set of parameters allows operators to balance the weighting of risk, fuel consumption, and time usage in the cost function, as represented in Equation (3.22). This can be a great tool in different operational scenarios. For instance, in the case of a vessel facing stringent time constraints due to fixed docking schedules or contractual obligations, the operator may increase the weight for time usage, emphasizing efficient path planning that minimizes time delays. In another scenario, for a company committed to reducing its carbon footprint, the operator might adjust the parameters to give greater importance to fuel efficiency.

Autonomous vessels are still in the early phases of operation and are therefore under close scrutiny from the public and regulatory authorities. Public trust in these new technologies is not yet fully established and can be rather fragile. Any significant mishap, such as a grounding incident, can severely undermine this trust and impede the wider adoption of autonomous vessels.

In this context, ensuring safe navigation becomes paramount not only for operational reasons but also from a societal acceptance perspective. It is not just about avoiding financial costs of a potential accident, but also about preventing harm to the reputation of the industry and the specific image of the operator. Thus, during these early operational phases, it might be prudent for operators of autonomous vessels to assign a higher weight to risk in the cost function. By doing this, the path planning framework would be more risk-averse, favoring routes with lower grounding risk, even if they might be less fuel-efficient or take slightly longer.

5.4 Risk of Grounding versus Operational Costs

One notable aspect of the grounding risk model developed in this thesis is that even with a fairly high incidence of grounding in simulations, the overall risk estimate remains relatively low compared to the cost of fuel consumption and time usage. This is primarily due to the extremely low probability of a loss of propulsion. Even in a case of travelling the northern path closest to the island Tautra, which resulted in grounding in 117 out of 502 loss of propulsion simulations, the risk does not significantly influence the outcome of the path planning framework.

The low risk assessment can therefore lead to routes with frequent groundings in simulations being selected as optimal. This is because the cost of time and fuel consumption tends to overshadow the risk cost in the cost function, given their relatively high operational impact. The immediate operational expenses of fuel usage and the significant costs related to time delays at the destination port often outweigh the predicted costs associated with a grounding incident.

Therefore, the fastest and most fuel-efficient paths tend to be optimal, regardless of the

grounding risk associated with them. It illustrates a kind of imbalance within the current path planning framework, with the grounding risk being underrepresented compared to time and fuel costs.

Considering the second case study, described in Section 4.2, involving the oil tanker traversing the Sandøya-Vattøya Nature Reserve, an analysis on the grounding risk is performed.

Figure 5.1 illustrates the behavior of the cost function parameters in two scenarios: one where all parameters are set to 1, representing an equal consideration of risk, fuel consumption, and time; and the second one where the α-value, corresponding to risk, is accentuated by setting it to 5. This adjustment in the α-value implies that more importance is given to minimizing the risk, which is particularly relevant in sensitive areas such as the Sandøya-Vattøya Nature Reserve.

In the first scenario where all parameters are equally weighted, the cost function determines the eastern path as optimal. This result is due to the combined assessment of risk, time usage, and fuel consumption. However, with an increase in α, the scenario changes dramatically. In the case where α is set to 5, thus prioritizing the minimization of risk, the western path is selected as the optimal route.

This shift in the choice of optimal path showcases the significance of the operator's ability to adjust the weights in the cost function according to the vessel's operation. For instance, in ecologically sensitive areas or regions with high marine traffic, the operator might choose to prioritize the minimization of risk over other factors, leading to the selection of a different, safer route. This adaptability of the framework enables it to cater to various operational preferences and situational requirements, making it a versatile tool for marine navigation.

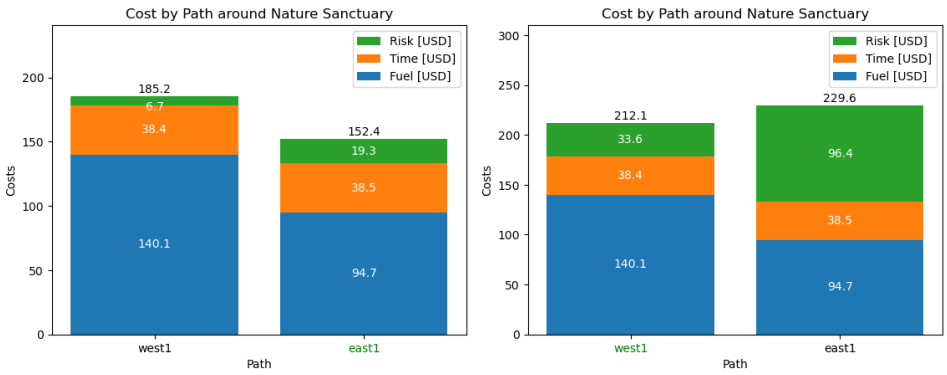

(a) All weighting parameters equal to 1 **(b)** Parameter corresponding to to risk, $\alpha = 5$

Figure 5.1: Cost function parameters for the second case study

5.5 Influence of Environmental Forces on Path Planning

It is essential to consider the impact of environmental forces on the determination of optimal paths within the framework. The framework does not identify a universally optimal path, as environmental conditions such as wind and currents can significantly influence the route selection. These forces can alter a ship's course, affect its speed, and add complexity to maintaining a predefined path. Therefore, an optimal path under specific environmental conditions may no longer be optimal or even feasible if these conditions change.

In the case studies conducted, the optimal routes were identified based on the specified environmental conditions. However, it is important to acknowledge that even slight changes in these environmental forces can have significant implications for blackout scenarios. For instance, if the environmental forces in the Tautra case study were oriented in the opposite direction, the optimal path would be the northern route closest to the island, as shown in Figure 5.2. The associated cost function for this route is presented in Figure 5.3.

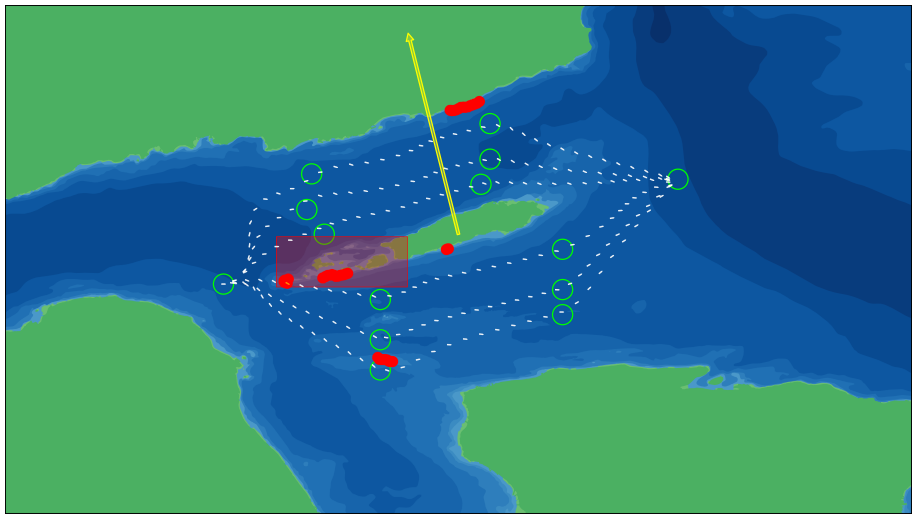

Figure 5.2: Simulation results of blackout occurrences on the paths around Tautra under northwestern environmental forces

The influence of environmental forces on optimal path planning around the nature reserve discussed in Section 4.2 has been investigated. The simulated voyages of the oil tanker within this area are analyzed under different environmental force scenarios, including currents in the north, east, south, and west directions. Figure 5.5 illustrates the voyages of the oil tanker under these various environmental force conditions, while Figure 5.4 displays the corresponding cost function parameters.

Based on the framework's predictions, it can be observed that the west path is identified as optimal when facing western or southern environmental forces. Conversely, in the presence of eastern or northern environmental forces, the east path is considered optimal. This further emphasizes the significant influence that environmental forces exert on the selec-

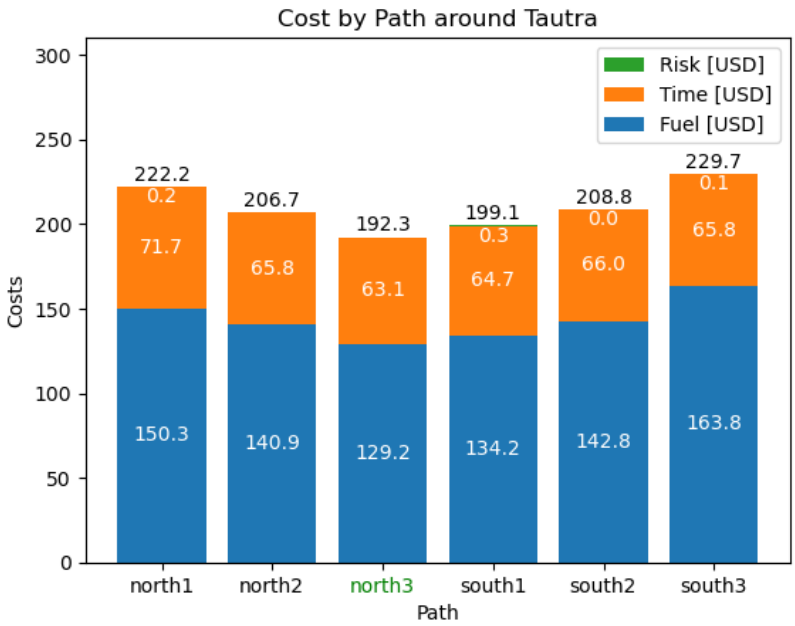

Figure 5.3: Cost function parameters results for the paths around Tautra under northwestern environmental forces

tion of the optimal path within the framework.

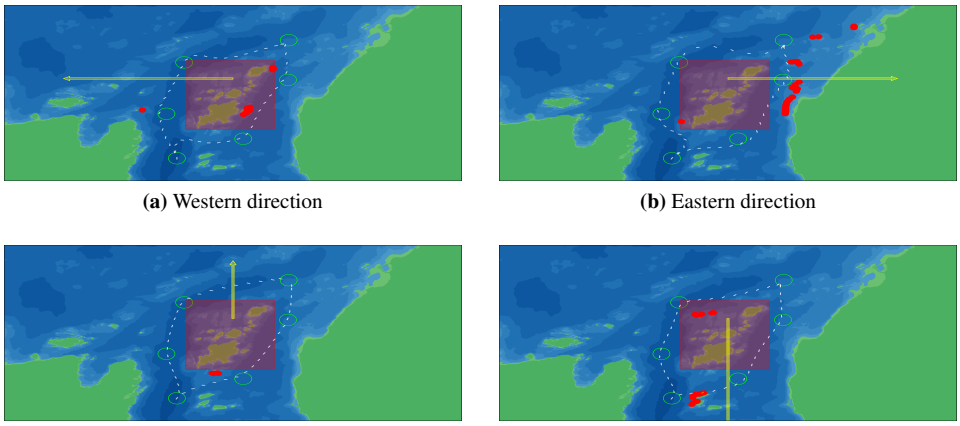

(a) Western direction

(b) Eastern direction

(c) Northern direction

(d) Southern direction

Figure 5.4: Blackout simulations for the paths around Sandøya-Vattøya Nature Sanctuary under varying directions of environmental forces

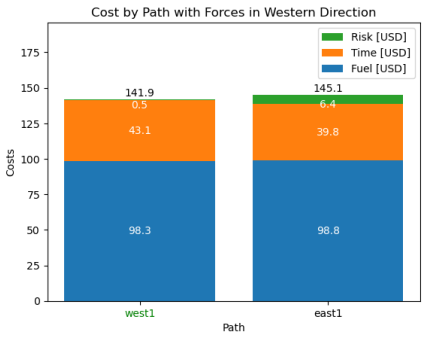

(a) Western direction. West path is optimal

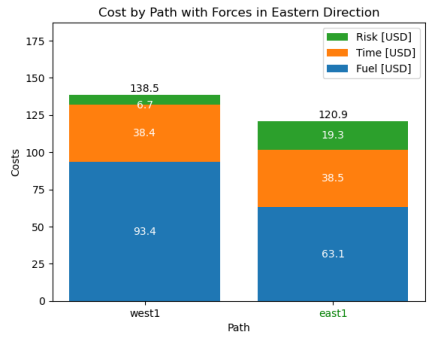

(b) Eastern direction. East path is optimal

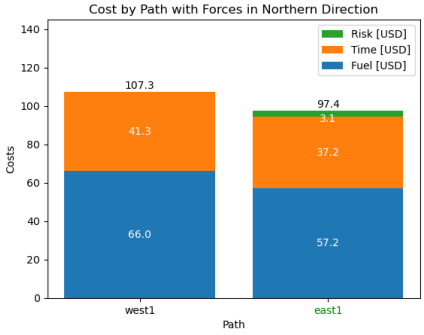

(c) Northern direction. East path is optimal

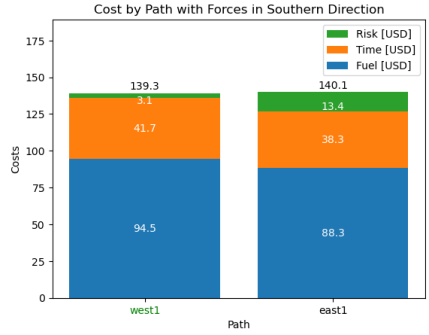

(d) Southern direction. West path is optimal

Figure 5.5: Cost function parameters for the paths around Sandøya-Vattøya Nature Sanctuary under varying directions of environmental forces

5.6 Online Path Planner and Algorithmic Path Identification

The proposed framework has the potential to be used in two phases of a sailing mission. In the planning phase, it can be used to determine the optimal route between two harbors based on a weather forecast, as is done in the case studies. However, since weather conditions and prioritations can change unexpectedly, it may also be beneficial to use the framework in an online mode, in which it continuously reevaluates the route based on the most recent data.

In the simplest case, a human operator would identify critical sections of the route and potential paths to avoid the obstacles. The framework, utilizing real-time risk analysis, can then select the optimal alternative among these operator-defined options.

An exciting area for further research and development is the integration of an algorithm capable of automatic identification of critical sections and potential paths. One poten-

tial approach for defining critical sections is to consider any area where an obstacle is within a certain distance of the original route. For scenarios with multiple obstructions, manual path identification might become a formidable task. To navigate these more complex circumstances, leveraging pathfinding algorithms such as Dijkstra or A* could be a promising approach. These algorithms could determine the most favorable routes based on parameters such as the proximity to obstructions, deviation from the original route, and the vessel's maneuvering capabilities.

Moreover, integrating machine learning techniques could further bolster the efficiency and efficacy of the framework. The utilization of an iterative algorithm that continuously improves the optimal path by learning from previous navigational data and grounding incidents holds great potential. Such a dynamic approach would ensure that the framework continues to evolve with each voyage, consistently improving its ability to anticipate and manage risks.

5.6.1 Frequency of Online Path Planning Initialization

When implementing an online path planning framework, it is an interesting topic to consider how often to initiate simulations and how long to run them. On one hand, it's beneficial to initiate simulations as frequently as possible in order to detect as many obstacles as possible. On the other hand, there is a trade-off between simulation frequency and duration due to limited computational resources.

When navigating through narrow passages, it may be possible to use a high-redundancy engine mode that allows for quicker recovery in the event of a failure. This may enable the use of shorter, higher-resolution simulations in order to more accurately assess the risks. In contrast, in open water, it may be necessary to run longer simulations with lower resolution due to the increased complexity and potential for longer recovery times. In order to find the optimal balance between simulation frequency, duration, and accuracy, it may be helpful to selectively simulate certain failure modes based on the specific needs and resources of the vessel. The most effective approach will depend on the vessel's capabilities and the nature of the voyage.

5.7 Simulated Duration of Propulsion Loss

In order to develop the most realistic framework as possible, it is important to accurately determine the appropriate duration for simulating propulsion loss. The duration of propulsion loss varies a lot across real-life incidents and is influenced by a multitude of factors. In this thesis, propulsion loss was arbitrarily chosen to be simulated for a duration of 300 seconds. However, developing a more accurate estimation of the duration could be an interesting topic for further research.

A key element in determining the duration of a propulsion loss is the condition of the machinery system. This includes not only its overall design and capability but also factors such as its age and the level of maintenance it has received. Moreover, having multiple

functional propulsion systems can further decrease the downtime, reinforcing the operational efficiency.

Crew competence is another vital factor. Crew members with advanced training and practice dealing with propulsion losses can significantly reduce the duration of such an event. In particular, the ability of the crew to diagnose and troubleshoot the issue swiftly plays a major role in restoring propulsion. Furthermore, the number of crew members on duty at the time of propulsion loss can affect how quickly the problem can be addressed. Larger crews can divide tasks and work simultaneously, potentially leading to faster resolution times.

Given these considerations, it becomes evident that accurate estimation of propulsion loss duration in simulations demands a nuanced approach. One such method could be the implementation of a Bayesian Network. Bayesian Networks provide a robust probabilistic graphical model that can take into account multiple variables and their relationships.

For estimating the duration of propulsion loss, a Bayesian Network can incorporate variables such as the condition and age of the machinery system, the maintenance history, crew competence, and crew size. By incorporating these factors and their complex interrelationships, the Bayesian Network can provide a more realistic estimation of the duration of propulsion loss, enhancing the accuracy of the simulations and making the path-planning framework more effective.

5.8 Assessing Recovery Time to Prevent Grounding

The durations of the simulated loss of propulsion in the case studies can be used to determine the minimum recovery time needed to avoid a grounding under the specific conditions considered. This information, in theory, could be employed to set recovery time standards for vessels with the goal of preventing grounding accidents. This also poses an economic question, as it may be more cost-effective to invest in systems to restore power following a blackout, rather than to expend additional fuel by sailing a longer, safer route.

The ability to rebound after a failure is a characteristic that needs to be determined on a case-by-case basis for each vessel. For example, according to industry standards, Dynamic Positioning (DP) vessels are required to regain thrust within 45 seconds of a blackout (DNV GL (2014)). Given their highly reliable nature and redundancy levels, DP vessels are generally able to meet this standard. However, it is unrealistic to expect all transit vessels to meet this same standard.

In the first case study, the shortest observed recovery time was 125 seconds, occurring 696 seconds into the journey on the northern path closest to the island Tautra. In essence, this means that in the most challenging circumstances, the vessel's propulsion system would need to be restored in just over two minutes after a blackout to prevent a grounding incident.

On the paths around Sekken, the most critical scenario was on the southern route, where the vessel grounded after a minimum drifting period of 270 seconds, starting 1640 seconds

into the voyage. This indicates that, under the most adverse conditions, the vessel would have approximately 4.5 minutes to recover its propulsion system to avoid grounding.

In the second case study, the worst-case scenario was on the eastern path, with a grounding occurring only 99.5 seconds after a loss of propulsion, which happened 492 seconds into the voyage. In this most demanding situation, the vessel would have less than 1.7 minutes to recover from a blackout to avoid grounding.

These observations underscore the fact that the required recovery time from a blackout varies substantially based on the specific route and environmental conditions. It suggests that in certain high-risk areas, where the window of time between loss of propulsion and grounding is critically short, opting for a more reliable engine mode could potentially be a cost-effective strategy. The expenditure incurred by using a more reliable but perhaps more expensive engine mode could be justified when considering the potential cost savings associated with avoiding grounding incidents or bypassing a longer, more time-intensive route.

5.9 Further work

The proposed framework presented in this report should by no means be regarded as finalized. The purpose is that the framework will serve as a building block for further work.

Online Path Planning Framework

As discussed in Section 5.6, the proposed framework has the potential to be extended to an online use case. One should consider eliminating the role of the human operator by implementing algorithms for identifying critical sections and possible paths. A thorough investigation with regards to the duration and initialization frequency of the online risk analysis is advised.

Simulated Duration of Propulsion Loss

In order to develop the most realistic framework as possible, it is important to accurately determine the appropriate duration for simulating propulsion loss. As discussed in Section 5.7, this could for example be estimated using a Bayesian Network that incorporates variables such as the condition and age of the machinery system, the maintenance history, crew competence, and crew size.

Including Other Sources of Risk

The framework presented in this report only considers drifting grounding. Other types of risk, such as fire, capsizing, collision with other vessels and damage to the cargo should be included in the model.

Including Moving Obstacles

As part of including risk modelling of collision with other vessels, the framework should be extended to incorporate moving obstacles in the form of other vessels. These new vessels could either be commanded to sail a given route, or they could all use the proposed framework.

Implementing Grounding and Collision Avoidance System

The simulator used in this report does not include any grounding or collision avoidance system. The simulator is therefore practically unaware of any obstacles, both moving and stationary. In the event that an obstacle obstructs the path between two waypoints, the simulated vessel will navigate directly towards it. This results in unexpected behaviour, and implementing grounding and collision avoidance systems are advised.

Implementing the Simulated Use of Anchors

On a real ship, the deployment of anchors would be a common safety measure in the event of a failure onboard. The simulation of anchor deployment could provide additional performance to the model.

Implementing the Simulated Use of Multiple Engine Modes

Many marine vessels have the possibility to be powered by multiple power sources, which increases the redundancy of the system. To enhance the realism of the framework, the capability of redundant engine modes should be incorporated.

Refinement of Blackout Likelihood Estimation Method

The Bayesian network implemented to estimate the likelihood of blackout is not an accurate representation of reality. Extending the network to utilize more information could prove to significantly improve the risk analysis. Some information that could be used are whether multiple power sources are active, and the overall maintenance status of the vessel.

Furthermore, introducing dynamic updates to the Bayesian network while the vessel navigates the path could bolster the accuracy of the failure mode probability forecasts. This would ensure the network stays in sync with constantly changing conditions.

Implementing Simulated Behaviour After Recovery

The current framework assumes that the vessel will be able to recover if it does not ground during the blackout simulation. However, a more realistic model of a vessel's behavior could be achieved by simulating the vessel's response to failure modes rather than making this assumption.

Validation of COLREG Rules

It is advised to perform a thorough investigation concerning whether the framework complies with the COLREGs.

6

Conclusion

The main objectives of this report was the following:

- Develop a grounding risk model for marine surface vessels
- Combine this grounding risk model with other relevant metrics to develop a path-planning framework
- Implement the path-planning framework into a simulation environment, allowing for rigorous evaluation and refinement to ensure real-world applicability
- Develop several case studies to demonstrate and evaluate the proposed framework.

A detailed grounding risk model was developed, as outlined in Section 3.5. With intervals of 20 meters or less, a loss of propulsion for the vessel was simulated. The likelihood of propulsion loss occurring under the given conditions was evaluated using a combination of a base probability, derived from literature, and a Bayesian Network.

In cases where the simulated loss of propulsion result in a grounding incident, the model estimates the total consequence of the grounding. Initially, a Bayesian Network was utilized to estimate the structural damage to the ship, which then informed the assessment of the environmental, social, and economic impacts arising from the grounding event. The probability and consequence metrics were combined to derive a risk metric.

This grounding risk model, paired with the consequences of extended time usage and fuel consumption, formed the basis for the development of a path-planning framework. By minimizing a cost function, this framework could identify the optimal path from a predefined selection of paths. The steps of the simulation-based path-planning framework can be summarized as follows:

1. Identify a set of possible failure modes. This is discussed in Section 3.1.

2. Identify critical sections of the route. This might for example be sections where islands or reefs are directly in, or close to, the suggested route.
3. For each critical section, identify a set of suitable paths to follow in order to avoid the obstacles.
4. Estimate the grounding risk associated with each of the paths. The risk is determined by simulating all failure modes with a given frequency, calculating the consequence (Section 3.4). Thereafter, the probabilities for each failure mode are taken into account (Section 3.3). This forms a risk metric for each path.
5. Optimize the choice of path based on the estimated risk, as well as fuel consumption and time usage.

Two case studies was developed to demonstrate and evaluate the given framework. The first case study focused on a passenger ferry traveling from *Dryna ferjekai* to *Åfarnes ferjekai*, which required navigating around the islands of *Tautra* and *Sekken*. Taking into account the south-eastern environmental forces, the framework identified the optimal paths around the islands as being situated to the south, while also being in closest proximity to the islands. This choice minimized the risk of grounding in the event of propulsion loss, as paths north of the islands would expose the vessel to waves and currents pushing it towards land. The paths closest to the islands proved to be faster and more fuel-efficient compared to the other southern paths.

The second case study involved an oil tanker traveling from *Bergneset* to *Salthella*, with a specific segment of the route requiring navigation around the *Sandøya-Vattøya Nature Sanctuary* near *Ulsteinvik*. The simulated environmental forces were oriented towards the east. The framework suggested that the eastern path had the lowest overall cost when the weighting parameters were set to 1, effectively neglecting their influence. However, when the importance of risk was increased by setting the α parameter to 5, the western path was identified as the optimal choice. The eastern path was faster and more fuel efficient. However, it also entailed an increased risk due to the close proximity of the mainland to the east. Therefore, if risk mitigation is prioritized, the western path is considered optimal.

The proposed framework presented in this report should by no means be regarded as finalized. There are several potential avenues for future improvements. These include enhancing the simulator to account for a broader range of risks and expanding the path-planning framework to enable real-time updates and adjustments.

In conclusion, a path-planning framework with a focus on grounding risk analysis has been developed and demonstrated through two case studies. The ultimate aim is to enhance situational awareness for both manned and unmanned vessels, promoting safer and more efficient maritime navigation.

Bibliography

Alme, J., 2008. Autotuned dynamic positioning for marine surface vessels. Master's thesis. Institutt for teknisk kybernetikk.

Appolinario, L.R., Tschoeke, D., Calegario, G., Barbosa, L.H., Moreira, M.A., Albuquerque, A.L.S., Thompson, C.C., Thompson, F.L., 2020. Oil leakage induces changes in microbiomes of deep-sea sediments of campos basin (brazil). Science of The Total Environment 740, 139556.

Aven, T., 2010. On how to define, understand and describe risk. Reliability Engineering & System Safety 95, 623–631.

Aven, T., 2012. The risk concept—historical and recent development trends. Reliability Engineering & System Safety 99, 33–44.

Aven, T., 2013. Practical implications of the new risk perspectives. Reliability Engineering & System Safety 115, 136–145.

BayesFusion LLC, 2023. Genie modeller. URL: `https://www.bayesfusion.com/genie/`.

Blindheim, S., 2021. Seacharts. URL: `https://github.com/simbli/seacharts`.

Bø, T.I., Dahl, A.R., Johansen, T.A., Mathiesen, E., Miyazaki, M.R., Pedersen, E., Skjetne, R., Sørensen, A.J., Thorat, L., Yum, K.K., 2015. Marine vessel and power plant system simulator. IEEE Access 3, 2065–2079.

Bø, T.I., Johansen, T.A., Sørensen, A.J., Mathiesen, E., 2016. Dynamic consequence analysis of marine electric power plant in dynamic positioning. Applied Ocean Research 57, 30–39.

Bolbot, V., Theotokatos, G., Boulougouris, E., Psarros, G., Hamann, R., 2021. A combinatorial safety analysis of cruise ship diesel–electric propulsion plant blackout. Safety 7, 38.

Breivik, M., 2010. Topics in guided motion control of marine vehicles .

Breivik, M., Fossen, T.I., 2009. Guidance laws for autonomous underwater vehicles. Underwater vehicles 4, 51–76.

Bremnes, J.E., Thieme, C.A., Sørensen, A.J., Utne, I.B., Norgren, P., 2020. A bayesian approach to supervisory risk control of auvs applied to under-ice operations. Marine Technology Society Journal 54, 16–39.

Brito, M., Griffiths, G., 2016. A bayesian approach for predicting risk of autonomous underwater vehicle loss during their missions. Reliability Engineering & System Safety 146, 55–67.

Cariou, P., Mejia Jr, M.Q., Wolff, F.C., 2008. On the effectiveness of port state control inspections. Transportation Research Part E: Logistics and Transportation Review 44, 491–503.

COWI, A., 2008. Risk analysis of sea traffic in the area around bornholm. Report# P-65775-002 .

Dalgic, Y., Lazakis, I., Turan, O., 2013. Vessel charter rate estimation for offshore wind o&m activities. International Maritime Association of Mediterranean IMAM 2013 .

DNV GL, 2014. Rules for classification: Dynamic positioning systems .

Dong, Y., Frangopol, D.M., 2015. Probabilistic ship collision risk and sustainability assessment considering risk attitudes. Structural Safety 53, 75–84.

Eide, M.S., Endresen, Ø., Breivik, Ø., Brude, O.W., Ellingsen, I.H., Røang, K., Hauge, J., Brett, P.O., 2007. Prevention of oil spill from shipping by modelling of dynamic risk. Marine Pollution Bulletin 54, 1619–1633.

Eliopoulou, E., Papanikolaou, A., Voulgarellis, M., 2016. Statistical analysis of ship accidents and review of safety level. Safety science 85, 282–292.

Fields, C., 2012. Safety and shipping 1912–2012: from titanic to costa concordia. Allianz Global Corporate and Speciality AG, Munich .

Fjord1, 2023. Våre fartøy. URL: https://www.fjord1.no/Om-Fjord1/Vaare-fartoey.

Fossdal, M., 2018. Online Consequence Analysis of Situational Awareness for Autonomous Vehicles. Master's thesis. NTNU.

Fossen, T.I., 2011. Handbook of marine craft hydrodynamics and motion control. John Wiley & Sons.

Fowler, T.G., Sørgård, E., 2000. Modeling ship transportation risk. Risk Analysis 20, 225–244.

Friis-Hansen, P., Ravn, E., Engberg, P., 2008. Basic modelling principles for prediction of collision and grounding frequencies. IWRAP Mark II Working Document , 1–59.

Fuji, Y., Yamanouchi, H., Mizuki, N., 1974. Some factors affecting the frequency of accidents in marine traffic. Journal of Navigation 27, 239–247.

Gule sider, 2023. Sjøkart. URL: https://kart.gulesider.no/?c=62.756612,7.139740&z=10&l=nautical&som=e.

HandyBulk, 2023. Ship charter rates. URL: https://www.handybulk.com/ship-charter-rates/.

Haribon, 2016. Ship grounding at tubbataha reef: A case of conservation, loss, and cost. URL: https://haribon.org.ph/ship-grounding-at-tubbataha-reef-a-case-of-conservation-loss-and-cost

Hegde, J., Utne, I.B., Schjølberg, I., Thorkildsen, B., 2018. A bayesian approach to risk modeling of autonomous subsea intervention operations. Reliability Engineering & System Safety 175, 142–159.

Huijer, K., 2005. Trends in oil spills from tanker ships 1995-2004. International Tanker Owners Pollution Federation (ITOPF), London 30.

Ibrion, M., Paltrinieri, N., Nejad, A.R., 2021. Learning from failures in cruise ship industry: The blackout of viking sky in hustadvika, norway. Engineering Failure Analysis 125, 105355.

Kaplan, S., Garrick, B.J., 1981. On the quantitative definition of risk. Risk analysis 1, 11–27.

Konovessis, D., 2012. An investigation on cost-effective tanker design configurations for reduced oil outflow. Ocean engineering 49, 16–24.

Kotb, M., Zeid, M., 2009. Guidelines for compensation following damage to coral reefs by ship or boat grounding. .

Lekkas, A.M., Fossen, T.I., 2013. Line-of-sight guidance for path following of marine vehicles. Advanced in marine robotics , 63–92.

Liu, Y., Frangopol, D.M., 2018. Probabilistic risk, sustainability, and utility associated with ship grounding hazard. Ocean Engineering 154, 311–321.

Løite, L.V., 2022. Simulation based grounding risk analysis for marine surface vessels.

Løite, L.V., 2023. Ship Simulator. URL: https://github.com/ludvigloite/shipSimulator.

MacDuff, T., 1974. The probability of vessel collisions. Ocean industry 9.

Marine Traffic, 2023. Hordafor vi. URL: https://www.marinetraffic.com/en/ais/details/ships/shipid:124431/mmsi:257027910/imo:8820286/vessel:HORDAFOR_VI.

Mazaheri, A., Montewka, J., Kujala, P., 2014. Modeling the risk of ship grounding—a literature review from a risk management perspective. WMU journal of maritime affairs 13, 269–297.

Norwegian Directorate for Civil Protection, 2020. Evaluering av viking sky-hendelsen. URL: https://www.dsb.no/globalassets/dokumenter/rapporter/evaluering-viking-sky.pdf.

Norwegian Directorate of Fisheries, 2023. Plan og sjøareal. URL: https://portal.fiskeridir.no/portal/apps/webappviewer/index.html?id=4b22481a36c14dbca4e4def930647924.

Norwegian Environment Agency, 2023. Veøy landskapsvernområde. URL: https://faktaark.naturbase.no/?id=VV00001591.

Norwegian Mapping Authority, 2023. Depth data. URL: https://kartkatalog.geonorge.no/metadata/sjoekart-dybdedata/2751aacf-5472-4850-a208-3532a51c529a.

Norwegian SciTech News, 2022. Ntnu trials world's first urban autonomous passenger ferry. URL: https://norwegianscitechnews.com/2022/09/ntnu-trials-worlds-first-urban-autonomous-passenger-ferry/.

NTNU, 2023. Autonomous all-electric passenger ferries for urban water transport(autoferry). URL: https://www.ntnu.edu/autoferry.

Open Simulation Platform, 2023. Open simuation platform - frontpage. URL: https://opensimulationplatform.com/.

Otto, S., Pedersen, P.T., Samuelides, M., Sames, P.C., 2002. Elements of risk analysis for collision and grounding of a roro passenger ferry. Marine Structures 15, 461–474.

Pedersen, P.T., et al., 1995. Collision and grounding mechanics. Proceedings of WEMT 95, 125–157.

Peterson, C.H., Rice, S.D., Short, J.W., Esler, D., Bodkin, J.L., Ballachey, B.E., Irons, D.B., 2003. Long-term ecosystem response to the exxon valdez oil spill. Science 302, 2082–2086.

Počuča, M., 2006. Methodology of day-to-day ship costs assessment. Promet-Traffic&Transportation 18, 337–345.

Rasmussen, C.E.B., 2019. Risk-Influenced Path Planning based on Online Risk Analysis, Bayesian Networks and the A* Path Planning Algorithm. Master's thesis. NTNU.

Rausand, M., 2013. Risk assessment: theory, methods, and applications. volume 115. John Wiley & Sons.

Rokseth, B., 2022. Ship in transit simulator. URL: https://github.com/BorgeRokseth/ship_in_transit_simulator.

Rokseth, B., Utne, I., 2023. Risk-based mode control system for the hybrid-electric machinery system of an autonomous ship .

Rosales, R.M.P., 2006. Estimating appropriate fines for ship grounding violations in tubbataha reef national marine park. Report of Consultant, Environmental Economics. Conservation International. Phillipines .

Russel, S., Norvig, P., 2012. Artificial intelligence—a modern approach 3rd edition. The Knowledge Engineering Review 11, 78–79.

Rygaard, J.M., 2009. Valuation of time charter contracts for ships. Maritime Policy & Management 36, 525–544.

Sakar, C., Toz, A.C., Buber, M., Koseoglu, B., 2021. Risk analysis of grounding accidents by mapping a fault tree into a bayesian network. Applied Ocean Research 113, 102764.

Shipselector.com, 2023. 87m / 399 pax passenger / roro ship. URL: https://shipselector.com/offers/sale/passenger-vessel/ro-ropassenger-ship/11536-87m-399-pax-passenger-roro-ship.

shipsforsale.eu, 2023. Dwt 3 000-5 000 tons. URL: https://shipsforsale.su/en/catalog/tankers/dwt_3000_5000/.

Simonsen, B.C., 1997. Mechanics of ship grounding. Department of Naval Architecture and Offshore Engineering , 260.

Sjøhistorie, 2023. M/f veøy. URL: https://www.sjohistorie.no/no/skip/31923.

Skjong, R., Vanem, E., Endresen, Ø., 2005. Risk evaluation criteria. SAFEDOR report D 4.

SNAME, T., 1950. Nomenclature for treating the motion of a submerged body through a fluid. The Society of Naval Architects and Marine Engineers, Technical and Research Bulletin , 1–5.

Stornes, P., 2015. Risk influencing factors in maritime accidents: an exploratory statistical analysis of the norwegian maritime authority incident database .

The Atlantic, 2014. Google's self-driving cars: 300,000 miles logged, not a single accident under computer control. URL: https://www.theatlantic.com/technology/archive/2012/08/googles-self-driving-cars-300-000-miles-logged-not-a-single-accident-260926/.

The Swedish Club, 2011. Collisions and groundings .

The Swedish Club, 2023. Hull machinery. URL: https://www.swedishclub.com/insurance/marine/hull-and-machinery.

Thieme, C.A., Rokseth, B., Utne, I.B., 2021. Risk-informed control systems for improved operational performance and decision-making. Proceedings of the Institution of Mechanical Engineers, Part O: Journal of Risk and Reliability , 1748006X211043657.

Thieme, C.A., Utne, I.B., 2017. A risk model for autonomous marine systems and operation focusing on human–autonomy collaboration. Proceedings of the Institution of Mechanical Engineers, Part O: Journal of Risk and Reliability 231, 446–464.

TPAMB, 2012. Rules and regulations for the entry and the conduct of all activities in the tubbataha reefs natural park and world heritage site. URL: http://tubbatahareefs.org/wp-content/uploads/2012/11/Park-Rules-and-Regulations-2008.pdf.

US Coast Guard, 2009. Accident statistics from 1999 to 2008. COMDTPUB P16754 26.

Vanem, E., Ellis, J., 2010. Evaluating the cost-effectiveness of a monitoring system for improved evacuation from passenger ships. Safety science 48, 788–802.

Varde, P.V., Pecht, M.G., et al., 2018. Risk-Based Engineering. Springer.

Wilhelmsen, 2023. Massterly. URL: https://www.wilhelmsen.com/about-wilhelmsen/our-holdings-and-investments/massterly/.

World Geodetic System, 1984. Its definition and relationships with local geodetic systems. DMA TR 8350.2, 2nd ed., Defense Mapping Agency, Fairfax, VA .

Yamada, Y., 2009. The cost of oil spills from tankers in relation to weight of spilled oil. Marine Technology and SNAME News 46, 219–228.

Yara, 2023. Mv yara birkeland. URL: https://www.yara.com/news-and-media/media-library/press-kits/yara-birkeland-press-kit/.

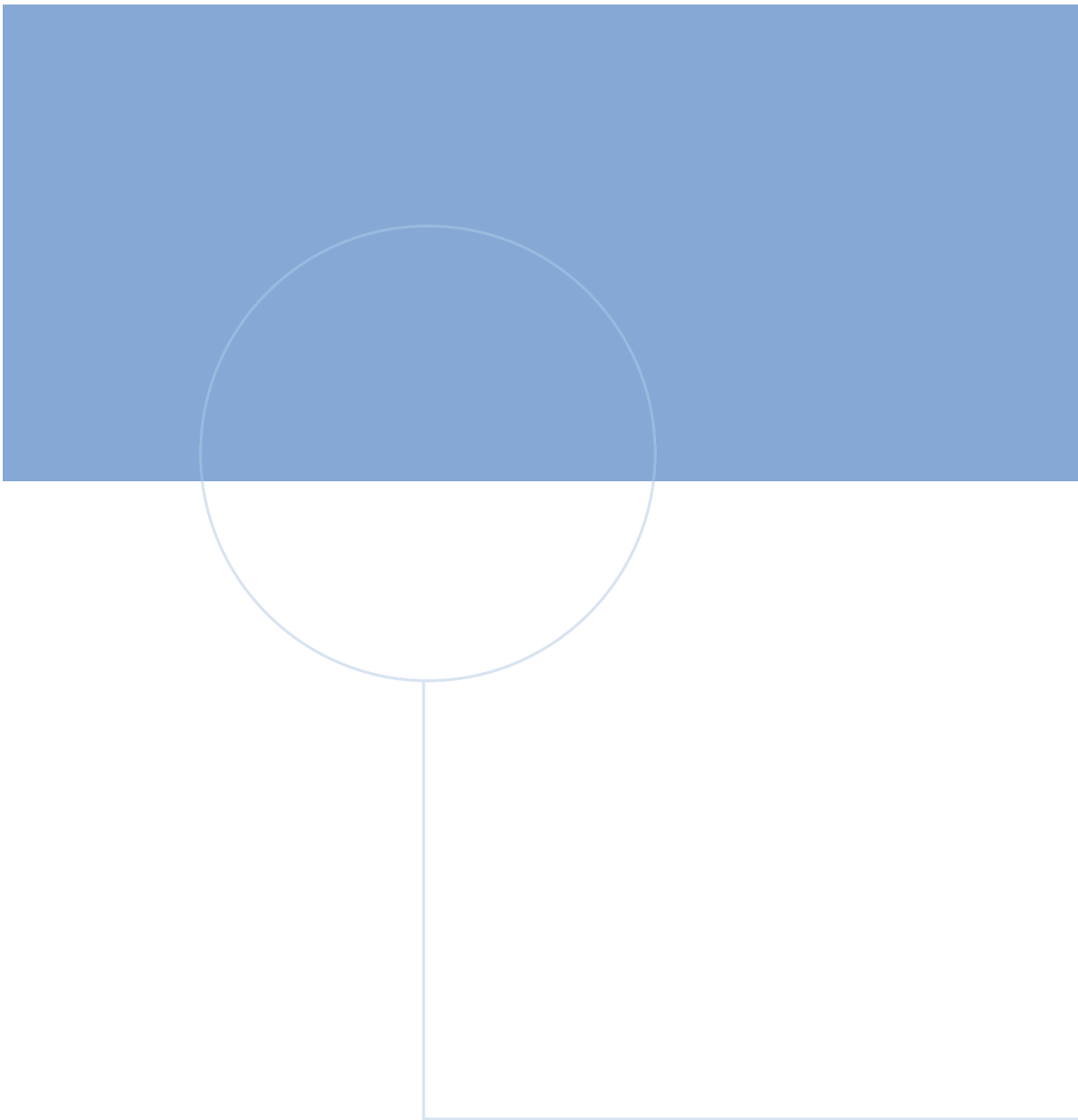

NTNU

Norwegian University of
Science and Technology